AD NUMBER

AD884041

NEW LIMITATION CHANGE

TO

Approved for public release, distribution unlimited

FROM

Distribution authorized to U.S. Gov't. agencies and their contractors; Critical Technology; Mar 1971. Other requests shall be referred to Air Force Materials Laboratory, Wright-Patterson AFB, OH 45433.

AUTHORITY

USAFML ltr, 29 Mar 1972

AFML-TR-71-37

EFFECT OF STRAIN RATE, TEMPERATURE AND MULTIAXIAL STRESS ON THE STRENGTH AND DUCTILITY OF S-200E BERYLLIUM AND 6A1-4V TITANIUM

U. S. LINDHOLM
L. M. YEAKLEY

SOUTHWEST RESEARCH INSTITUTE
8500 CULEBRA ROAD
SAN ANTONIO, TEXAS

TECHNICAL REPORT AFML-TR-71-37

MARCH 1971

AIR FORCE MATERIALS LABORATORY
AIR FORCE SYSTEMS COMMAND
WRIGHT-PATTERSON AIR FORCE BASE, OHIO

NOTICE

When Government drawings, specifications, or other data are used for any purpose other than in connection with a definitely related Government procurement operation, the United States Government thereby incurs no responsibility nor any obligation whatsoever; and the fact that the government may have formulated, furnished, or in any way supplied the said drawings, specifications, or other data, is not to be regarded by implication or otherwise as in any manner licensing the holder or any other person or corporation, or conveying any rights or permission to manufacture, use, or sell any patented invention that may in any way be related thereto.

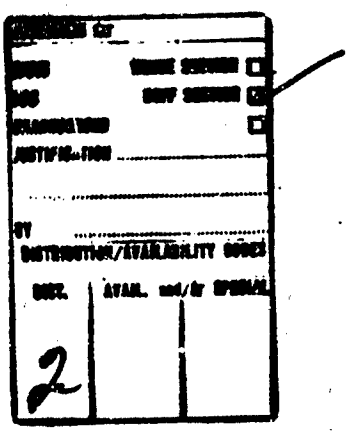

Copies of this report should not be returned unless return is required by security considerations, contractual obligations, or notice on a specific document.

300 - April 1971 - CO305 - 34-71-962

ABSTRACT

The strength properties of S-200E beryllium and 6Al-4V titanium were determined under conditions of combined stress, elevated temperatures and high strain rates. Beryllium specimens were obtained from both extruded rod and hot-pressed block. The range of test conditions included strain rates from 10^{-3} to 1000 sec^{-1}, temperatures from 70 to 1000°F, and both uniaxial and biaxial states of stress. The biaxial stress states were obtained with thin-walled tubular specimens loaded with axial tension or compression, torsion, or internal pressure.

The data presented include the stress-strain curves, yield and failure surfaces in stress space, and the surfaces for total strain to failure. The latter indicate the relative ductility achieved with different applied stress ratios. The effect of temperature and of strain rate on the size and shape of the yield and failure surfaces is determined. In most cases the experimental data correlate well with known yield and failure criteria.

Unclassified

Security Classification

DOCUMENT CONTROL DATA - R&D

(Security classification of title, body of abstract and indexing annotation must be entered when the overall report is classified)

1. ORIGINATING ACTIVITY (Corporate author)	2a. REPORT SECURITY CLASSIFICATION
Department of Mechanical Sciences Southwest Research Institute San Antonio, Texas 78228	Unclassified 2b GROUP

3. REPORT TITLE

Effect of Strain Rate, Temperature and Multiaxial Stress on the Strength and Ductility of S-200E Beryllium and 6Al-4V Titanium

4. DESCRIPTIVE NOTES (Type of report and inclusive dates)

Final Report - December 1968 to September 1970

5. AUTHOR(S) (Last name, first name, initial)

Lindholm, U. S.
Yeakley, L. M.

6. REPORT DATE	7a. TOTAL NO. OF PAGES	7b. NO. OF REFS
March 1971	86	16

8a. CONTRACT OR GRANT NO.	9a. ORIGINATOR'S REPORT NUMBER(S)
F33615-69-C-1248 next b. PROJECT NO. 7351 c. Task No. 735106 d.	9b. OTHER REPORT NO(S) (Any other numbers that may be assigned this report) AFML-TR-71-37

10. AVAILABILITY/LIMITATION NOTICES This document is subject to special export controls and each transmittal to foreign governments or foreign nationals may be made only with prior approval of the Metals and Ceramics Division (AFML/LL), Air Force Materials Laboratory, Wright-Patterson Air Force Base, Ohio 45433.

11. SUPPLEMENTARY NOTES	12. SPONSORING MILITARY ACTIVITY
	Metals and Ceramics Division Air Force Materials Laboratory Wright-Patterson Air Force Base, Ohio

13. ABSTRACT

The strength properties of S-200E beryllium and 6Al-4V titanium were determined under conditions of combined stress, elevated temperatures and high strain rates. Beryllium specimens were obtained from both extruded rod and hot-pressed block. The range of test conditions included strain rates from 10^{-3} to 1000 sec^{-1}, temperatures from 70 to 1000°F, and both uniaxial and biaxial states of stress. The biaxial stress states were obtained with thin-walled tubular specimens loaded with axial tension or compression, torsion, or internal pressure.

The data presented include the stress-strain curves, yield and failure surfaces in stress space, and the surfaces for total strain to failure. The latter indicates the relative ductility achieved with different applied stress ratios. The effect of temperature and of strain rate on the size and shape of the yield and failure surfaces is determined. In most cases the experimental data correlate well with known yield and failure criteria.

DD FORM 1 JAN 64 1473

Unclassified

Security Classification

Unclassified
Security Classification

14. KEY WORDS	LINK A		LINK B		LINK C	
	ROLE	WT	ROLE	WT	ROLE	WT
Beryllium						
Titanium						
Strain Rate Effects						
Biaxial Strength Properties						

INSTRUCTIONS

1. ORIGINATING ACTIVITY: Enter the name and address of the contractor, subcontractor, grantee, Department of Defense activity or other organization *(corporate author)* issuing the report.

2a. REPORT SECURITY CLASSIFICATION: Enter the overall security classification of the report. Indicate whether "Restricted Data" is included. Marking is to be in accordance with appropriate security regulations.

2b. GROUP: Automatic downgrading is specified in DoD Directive 5200.10 and Armed Forces Industrial Manual. Enter the group number. Also, when applicable, show that optional markings have been used for Group 3 and Group 4 as authorized.

3. REPORT TITLE: Enter the complete report title in all capital letters. Titles in all cases should be unclassified. If a meaningful title cannot be selected without classification, show title classification in all capitals in parenthesis immediately following the title.

4. DESCRIPTIVE NOTES: If appropriate, enter the type of report, e.g., interim, progress, summary, annual, or final. Give the inclusive dates when a specific reporting period is covered.

5. AUTHOR(S): Enter the name(s) of author(s) as shown on or in the report. Enter last name, first name, middle initial. If military, show rank and branch of service. The name of the principal author is an absolute minimum requirement.

6. REPORT DATE: Enter the date of the report as day, month, year; or month, year. If more than one date appears on the report, use date of publication.

7a. TOTAL NUMBER OF PAGES: The total page count should follow normal pagination procedures, i.e., enter the number of pages containing information.

7b. NUMBER OF REFERENCES: Enter the total number of references cited in the report.

8a. CONTRACT OR GRANT NUMBER: If appropriate, enter the applicable number of the contract or grant under which the report was written.

8b, 8c, & 8d. PROJECT NUMBER: Enter the appropriate military department identification, such as project number, subproject number, system numbers, task number, etc.

9a. ORIGINATOR'S REPORT NUMBER(S): Enter the official report number by which the document will be identified and controlled by the originating activity. This number must be unique to this report.

9b. OTHER REPORT NUMBER(S): If the report has been assigned any other report numbers *(either by the originator or by the sponsor)*, also enter this number(s).

10. AVAILABILITY/LIMITATION NOTICES: Enter any limitations on further dissemination of the report, other than those imposed by security classification, using standard statements such as:

(1) "Qualified requesters may obtain copies of this report from DDC."

(2) "Foreign announcement and dissemination of this report by DDC is not authorized."

(3) "U. S. Government agencies may obtain copies of this report directly from DDC. Other qualified DDC users shall request through _____."

(4) "U. S. military agencies may obtain copies of this report directly from DDC. Other qualified users shall request through _____."

(5) "All distribution of this report is controlled. Qualified DDC users shall request through _____."

If the report has been furnished to the Office of Technical Services, Department of Commerce, for sale to the public, indicate this fact and enter the price, if known.

11. SUPPLEMENTARY NOTES: Use for additional explanatory notes.

12. SPONSORING MILITARY ACTIVITY: Enter the name of the departmental project office or laboratory sponsoring *(paying for)* the research and development. Include address.

13. ABSTRACT: Enter an abstract giving a brief and factual summary of the document indicative of the report, even though it may also appear elsewhere in the body of the technical report. If additional space is required, a continuation sheet shall be attached.

It is highly desirable that the abstract of classified reports be unclassified. Each paragraph of the abstract shall end with an indication of the military security classification of the information in the paragraph, represented as *(TS), (S), (C), or (U)*

There is no limitation on the length of the abstract. However, the suggested length is from 150 to 225 words.

14. KEY WORDS: Key words are technically meaningful terms or short phrases that characterize a report and may be used as index entries for cataloging the report. Key words must be selected so that no security classification is required. Identifiers, such as equipment model designation, trade name, military project code name, geographic location, may be used as key words but will be followed by an indication of technical context. The assignment of links, rules, and weights is optional.

Unclassified
Security Classification

EFFECT OF STRAIN RATE, TEMPERATURE AND MULTIAXIAL STRESS ON THE STRENGTH AND DUCTILITY OF S-200E BERYLLIUM AND 6A1-4V TITANIUM

U. S. LINDHOLM
L. M. YEAKLEY

FOREWORD

This report was prepared by the Department of Mechanical Sciences, Southwest Research Institute, San Antonio, Texas under USAF Contract No. F33615-69-C-1248. The contract was initiated under Project No. 7351, "Metallic Materials", Task No. 735106, "Behavior of Metals". The work was monitored by the Metals and Ceramics Division, Air Force Materials Laboratory, Air Force Systems Command, with Dr. T. Nicholas, MAMD, as project scientist.

This report covers work conducted from December 1968 to September 1970. The manuscript of this report was initially submitted by the authors in November 1970 for publication.

This technical report has been reviewed and is approved.

W. J. TRAPP
Chief, Strength and Dynamics Branch
Metals and Ceramics Division
Air Force Materials Laboratory

TABLE OF CONTENTS

LIST OF ILLUSTRATIONS

LIST OF ILLUSTRATIONS (cont'd)

LIST OF ILLUSTRATIONS (cont'd)

LIST OF ILLUSTRATIONS (cont'd)

SECTION I

INTRODUCTION

The strength properties of beryllium and titanium alloys are of extreme interest because of their extensive use in aerospace applications. The present study is concerned with the effect of strain rate and temperature on the strength and ductility of S-200E beryllium and 6Al-4V titanium alloy under both uniaxial and biaxial loading conditions. The yield and failure surfaces for these alloys were determined under conditions of generalized plane stress, produced by combinations of axial tension or compression, torsion and internal pressure on tubular test specimens. The strength tests were performed at several constant rates of deformation and temperatures in order to determine the effect of these parameters on the combined stress yield and failure criteria and on the generalized ductility as defined by the total strain at failure.

In a previous report[1*], the uniaxial tensile and compressive strength properties of 6Al-4V titanium along with several other metals were reported for strain rates from 10^{-3} to 10^{3} sec^{-1} and temperatures from 70 to 750°F. In the present work, tubular specimens of this alloy were tested under conditions of axial tension or compression and internal pressure at 70°F and two different effective strain rates. However, the greater portion of the work reported herein is concerned with S-200E beryllium. Beryllium specimens were obtained from both hot-pressed block and extruded bar, all from the same source and having nominally the same composition. The extruded material was highly textured and evidenced strongly anisotropic strength properties. Uniaxial tensile tests on specimens of both forms of beryllium were conducted at strain rates from 10^{-3} to 10^{3} sec^{-1} and temperatures from 70 to 1000°F. These uniaxial tensile tests complement previous data on beryllium obtained over a similar range in variables and given in two General Motors reports[2,3]. In addition, approximately 90 tube specimens were tested over a wide range in stress ratio controlled by loading in axial tension or compression, internal pressure or pure torsion. All the combined stress tests were performed at constant stress ratio (proportional loading) to failure.

The majority of the tests, including all the biaxial tests, were performed on a high-speed servo-controlled hydraulic testing machine. This machine covered strain rates from 10^{-3} to 10 sec^{-1}. The highest rate uniaxial testing was done with a split Hopkinson bar system producing tensile strain rates of 10^{3} sec^{-1}.

---

* References cited in Section VII.

The authors have previously reported some work on the effect of rate of deformation on the biaxial yielding of mild steel[4] and the plastic flow of aluminum[5]. This, along with the present work, appears to be the first to consider the effect of temperature and strain rate on multiaxial yield and fracture criteria. There is also very little experimental information of this type available for initially anisotropic metals such as the extruded beryllium.

SECTION II

MATERIALS AND SPECIMENS

The materials tested were S-200E beryllium and 6Al-4V titanium. The titanium was obtained as 1-1/4-inch diameter rod and machined into tube specimens for biaxial testing. Uniaxial tension and compression testing of the same alloy was reported previously[1]. The titanium specimens were tested in the as-received and as-machined condition. The chemical analysis of the titanium provided by the supplier is given in Table I.

TABLE I. Chemical Analysis of 6Al-4V Titanium

Carbon	Fe	N_2	Al	V	H_2	O_2
0.024	0.25	0.011	6.29	4.30	0.0066	0.19

The beryllium specimens were provided by the AFML who obtained them under separate contract from the Brush Beryllium Co. The specifications supplied by Brush for the S-200E beryllium are given in Table II. While the specimens were prepared from three material lots, the chemical composition of all specimens is relatively uniform. There was no identification of the specimens received with lot number. Specimens were obtained from both hot pressed block and extruded rod. Uniaxial specimens from the hot-pressed block were cut from both the longitudinal (pressing) and transverse directions. The axis of all the specimens of extruded material and of all the tubular biaxial specimens was aligned in the longitudinal (extrusion or pressing) direction. After machining, all of the beryllium specimens were chemically etched to remove any surface damage. Before delivery for testing, the machined beryllium specimens were radiographed by the AFML to check for internal flaws.

Micrographs of typical hot-pressed block and extruded specimens taken at SwRI are given in Figures 1 and 2. Several transverse and longitudinal sections from both uniaxial (1/4-inch round) and biaxial, tubular specimens were taken. Those shown are typical and are from uniaxial specimens. The sections are unetched and taken with polarized light. The extruded material is highly textured and exhibits a smaller grain diameter in the transverse section than the hot-pressed block. The grain dimensions of the hot-pressed block are relatively symmetric in sections both longitudinal and transverse to the pressing direction.

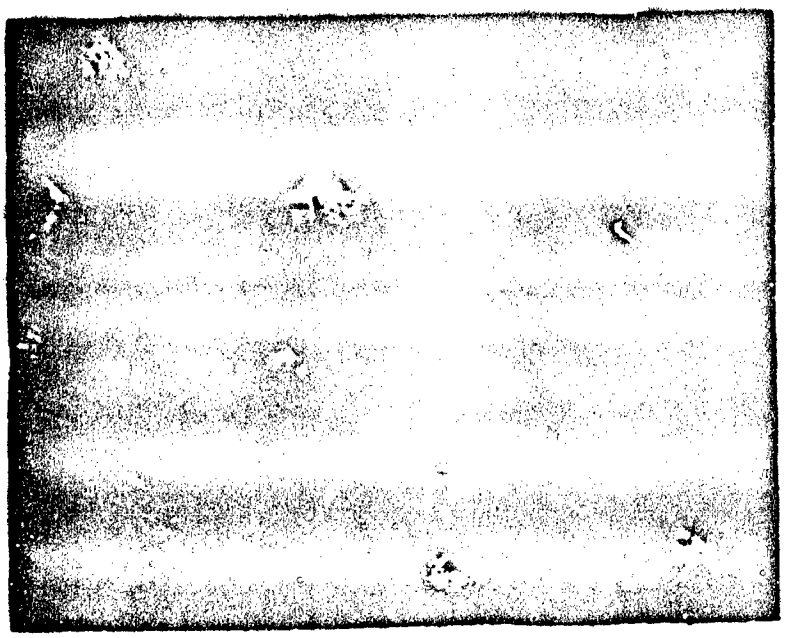

TRANSVERSE SECTION ⊢—50μ—⊣

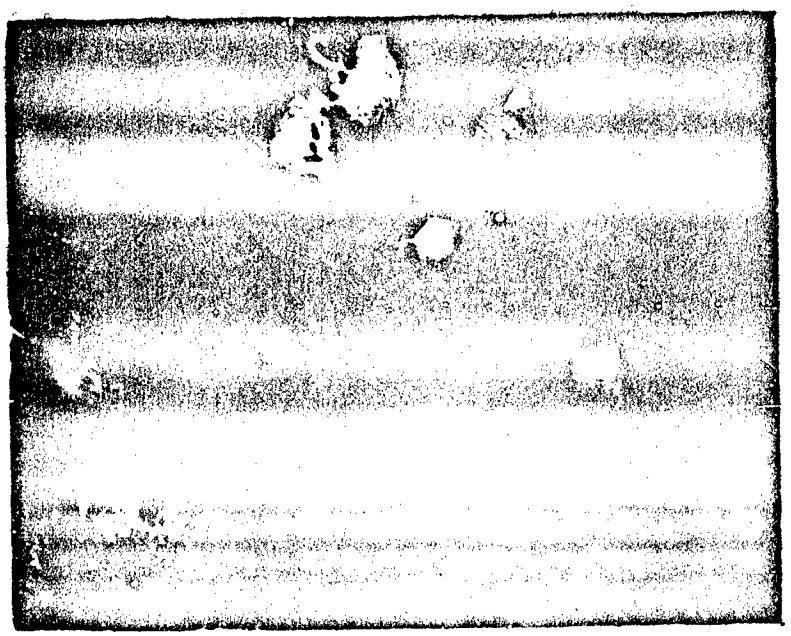

LONGITUDINAL SECTION ⊢—50μ—⊣

FIGURE 1. PHOTO MICROGRAPHS OF S-200E BERYLLIUM HOT-PRESSED BLOCK

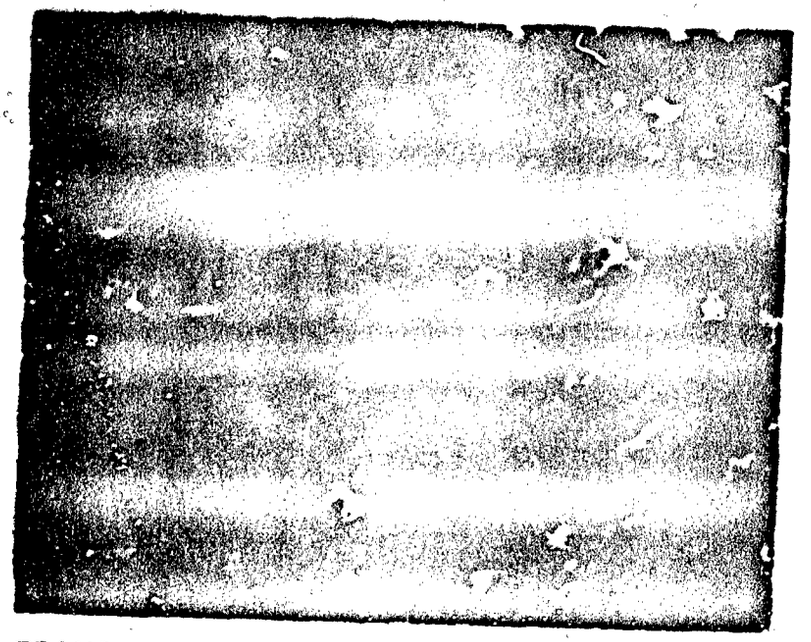

TRANSVERSE SECTION ⊢—50μ—⊣

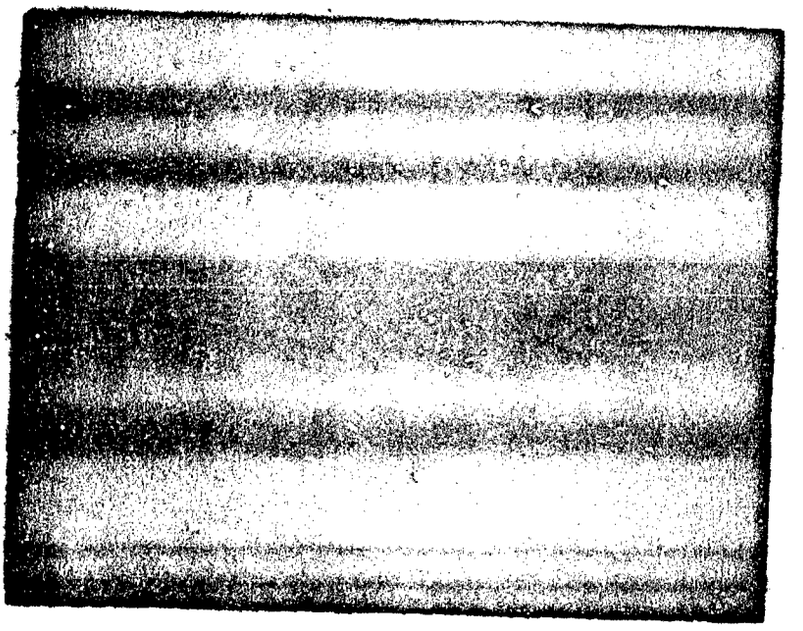

LONGITUDINAL (⁄) SECTION ⊢—50μ—⊣

FIGURE 2. PHOTO MICROGRAPHS OF S-200E BERYLLIUM EXTRUDED ROD

TABLE II. MANUFACTURERS' SPECIFICATIONS FOR S-200E BERYLLIUM

POWDER CHEMISTRY

	Lot 5471	Lot 6542	Lot 6555
Be	99.0	99.02	98.39
BeO	1.2	1.54	1.06
C	.09	.124	.113
Al	.05	.06	.08
Fe	.10	.12	.12
Mg	.04	.04	.07
Mn	.01	.01	.01
Si	.04	.03	.04

All other metallic elements less than .04%.

GRAIN SIZE (HOT PRESSED BLOCK)

Lot 5471	Lot 6542	Lot 6555
23 microns	18 microns	16 microns

BLOCK DENSITY

Lot 5471	Lot 6542	Lot 6555
1.852 gm/cc	1.850 gm/cc	1.853 gm/cc

TENSILE PROPERTIES

		UTS (psi)	YS (.2%) (psi)	Elong (%)
Extruded*	Lot 5471			
	Long	118,700	66,100	5.9
	Long	106,700	51,200	9.1
Hot Pressed Block	Lot 6542			
	Long	52,000	38,700	1.5
	Trans	50,000	33,300	2.5
	Lot 6555			
	Long	53,400	41,600	1.59
	Trans	50,800	32,100	4.5

*Extrusion ratio = 9.5:1.

Three different specimen geometries were used depending upon the type of loading. The nominal dimensions for the three specimens are given in Figure 3. For the uniaxial tension testing of beryllium at low and intermediate rates, the button-head end type specimen shown in Figure 3a was used. The specimen in Figure 3b was used with the split Hopkinson pressure bar for the highest strain rate. Uniaxial hot-pressed block specimens had their axis oriented in both the pressing direction and normal to the pressing direction, while all specimens from the extruded material had their axis aligned in the direction of extrusion. Henceforth, the directional designation "longitudinal" will be used to indicate either the pressing or the extrusion axis of the material and "transverse" will define any direction normal to this axis. The assumption of transverse isotropy will be employed, i.e., the strength properties are assumed symmetric in the transverse plane.

The tubular biaxial specimens used for both beryllium and titanium are shown in Figure 3c. The nominal inside diameter and wall thickness are 0.750 and 0.025 inch, respectively. This yields a thickness to diameter ratio of 1/30. The length of uniform gage section was either 2.250 inch as shown or 2.00 inch. The longer gage length was used with internal pressure loading. Stresses were computed from actual dimensions measured on each specimen prior to testing.

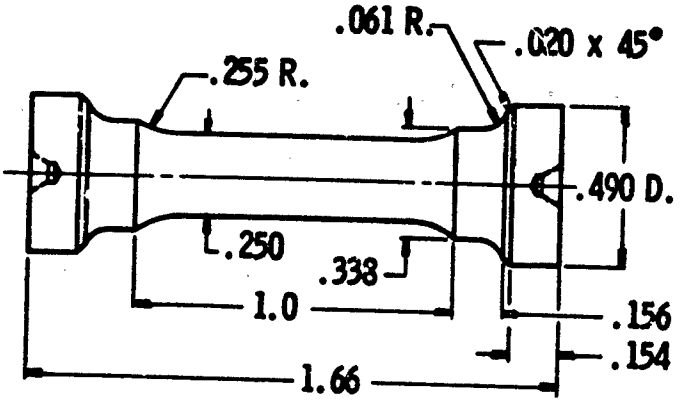

(a) Button Head End Tensile Specimen

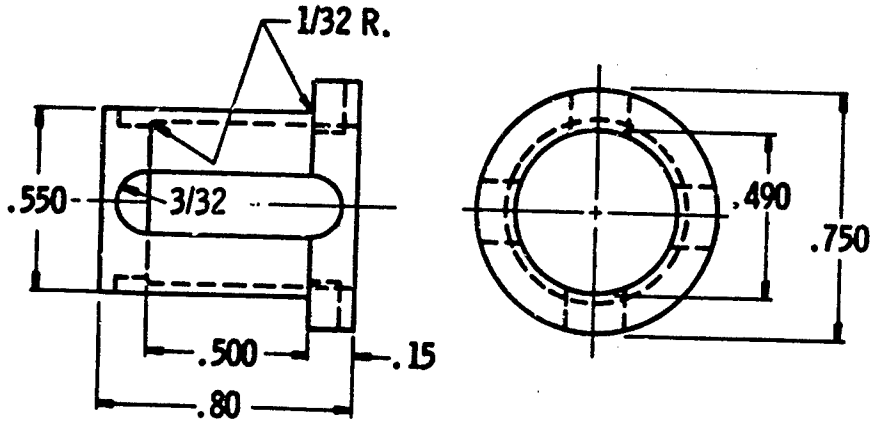

(b) Hopkinson Bar Tensile Specimen

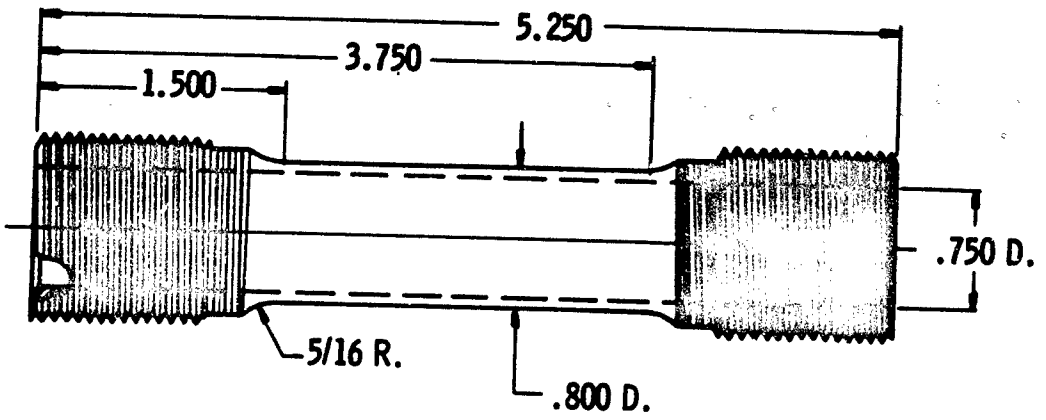

2981

(c) Biaxial Tube Specimen

FIGURE 3. NOMINAL SPECIMEN DIMENSIONS

SECTION III.

TEST METHODS

The testing program presented several unique challenges, particularly with beryllium which is nominally a relatively brittle material. The combination of multiaxial loading, elevated temperatures, high testing speeds and low ductility compound the usual problems involved with strength testing. This section will describe the equipment and procedures used to obtain the data presented.

A few beryllium tests were made with the split Hopkinson pressure bar system. Tensile testing with this sytem was developed earlier on this program and is described in detail in Ref. 1. The technique assumes a dynamic stress equilibrium within the specimen, a condition which may be violated for small times or small strain amplitudes. For this reason there is considerable uncertainty about the interpretation of the test results for a material as brittle as beryllium where tensile fracture occurs at very low total strain. Fracture of the Hopkinson bar specimens occurred irregularly and not always within the uniform region of the gage section. For these reasons Hopkinson bar data is presented for ultimate strength and total elongation only, and even these values must be viewed with some uncertainty. Similar problems with Hopkinson bar tests on beryllium were noted by Schierloh and Babcock[3].

All of the remaining tests were performed on an SwRI developed dynamic biaxial materials testing facility. This facility, along with some of the specialized instrumentation developed, will be described in the following pages.

A. Biaxial Testing Machine

An overall view of the testing facility is shown in Figure 4. The loading is generated by either of three independent hydraulic piston or vane type actuators. A linear actuator controlling the axial tension or compression mode is rigidly mounted below the bottom platten of the load frame. A torsional, vane type actuator is mounted directly above the platten, in series with the linear actuator and the bottom grip of the specimen. The torsional actuator housing is free to move vertically, guided by three ball bushing supports which take up the torsional reaction. The specimen is mounted between the torsional actuator and a biaxial load cell which is connected to the upper movable crosshead of the three column load frame. A piston-type hydraulic pressure intensifier mounted on one column of the load frame can be seen in Figure 5. This intensifier supplies internal pressure to the tubular specimens.

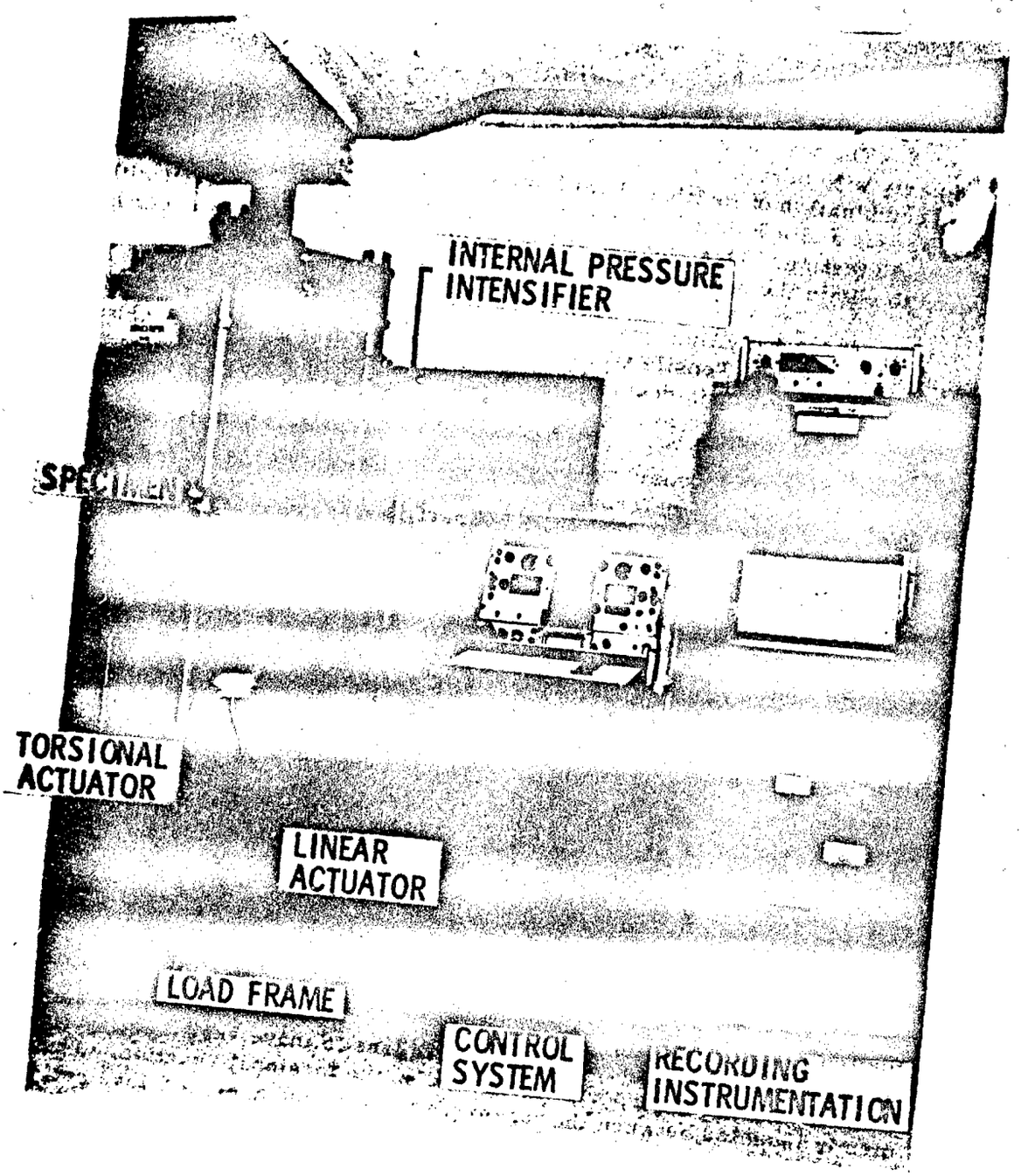

FIGURE 4. OVERALL VIEW OF THE SwRI MULTIAXIAL TESTING FACILITY

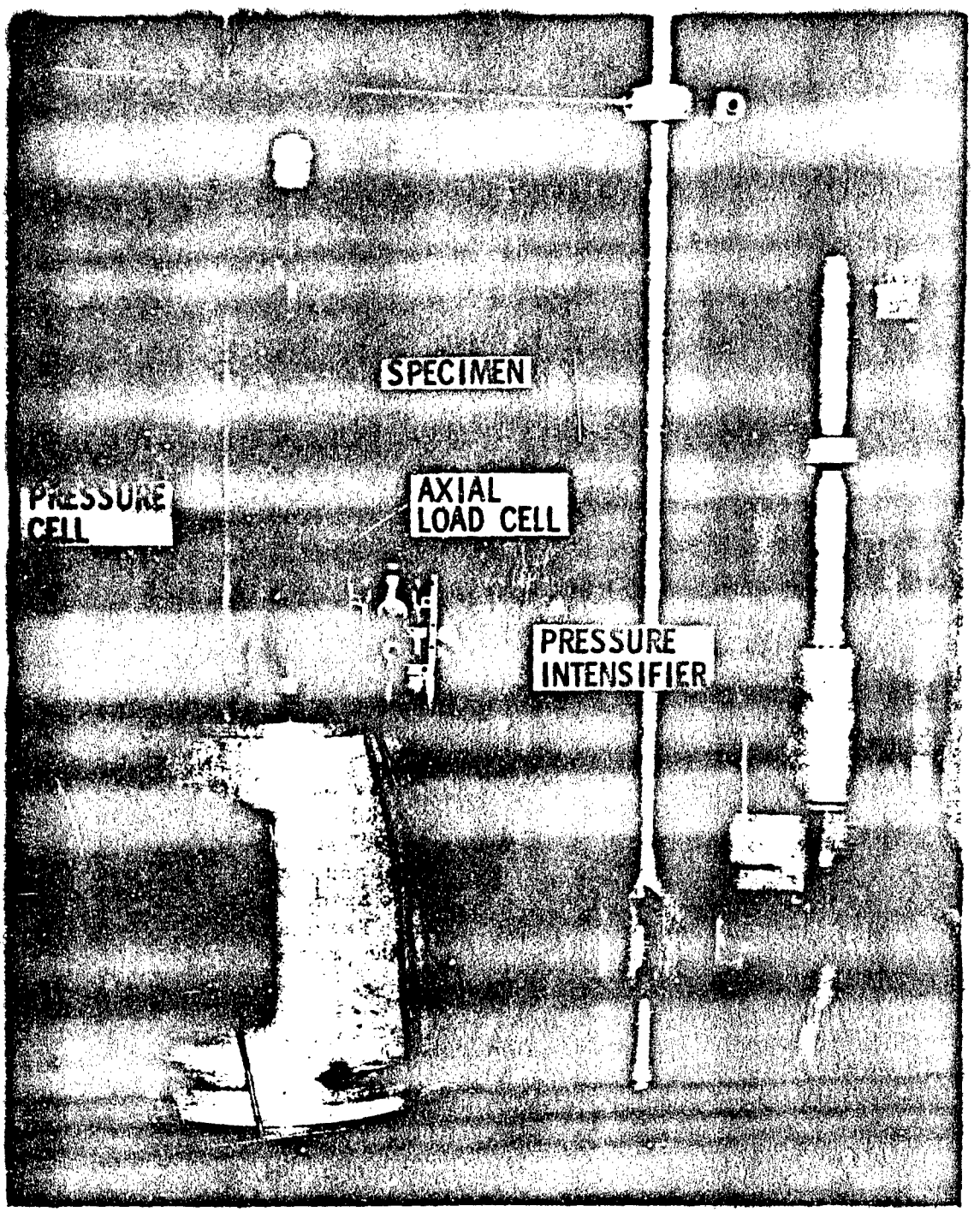

FIGURE 5. CLOSEUP SHOWING SPECIMEN SETUP FOR INTERNAL PRESSURE AND AXIAL LOADING (TORSIONAL ACTUATOR NOT ACTIVE)

While all three loading modes can be operated simultaneously, usually, as in this report, either of two alternate modes of biaxial loading is used. These are axial tension/compression and torsion or axial tension/compression and internal pressure. Since each load component is independently programable, a continuous variation in load ratio may be obtained, including uniaxial testing.

For programming, each load actuator has its own servo-valve and independent feedback control system. The hydraulic power is controlled electronically by means of the servo-valve which accepts electrical command signals and accordingly adjusts the flow of hydraulic fluid into the actuator. The electrical signal to the servo-valve is derived by comparing a response signal from the system (specimen) with a command signal so as to minimize the difference (error). The response signal may be either load, strain or head displacement measured at the specimen. The command signals can be derived from any programable voltage source (0 - 20 Hz) or from a built-in ramp generator for constant rate tests.

The hydraulic power supply for the system is 50 HP capacity and delivers a maximum flow rate of 23 gal/minute at 3000 psi. The load capacity of the machine in the configuration used for these experiments is $\pm$ 10,000 lb. axial tension/compression, $\pm$ 6,800 in-lb. torque, and 20,000 psi internal pressure. The axial displacement range is $\pm$ 1.5 in. and the torsional range is $\pm$ 50 deg. rotation. The maximum crosshead velocities are $\pm$ 14 in/sec axial and $\pm$ 750 deg/sec rotational.

The specimen is attached in series with a machined, cylindrical section which is strain-gaged to serve as a biaxial load cell. This load cell section is instrumented with four, 0°-45°-90° strain gage rosettes arranged in bridge circuits to measure the axial and torsional components of the load and to monitor the bending about two axes. The bending signal is used as a check on alignment of the system. The internal pressure is measured by a pressure cell mounted between the pressure intensifier and the specimen, see Figure 5.

The grips for the uniaxial beryllium specimens (Figure 3a) transferred the load through split, tapered rings matched to the conical surface of the button-head end. These tapered rings were ground in place in the grips to assure alignment. Axiality of the loading depended upon both the bearing surface within the grip and the external alignment of the machine components. Final alignment of the uniaxial specimens was checked with a strain gaged specimen having two gages 180° apart. For any orientation of this specimen within the grips, the difference in strain across the specimen diameter was within 5% at any load. Maintaining this alignment criteria required considerable effort in the machine alignment and in close tolerances in the grips.

Two types of grips were used with the tubular specimens (Fig. 3c). The titanium specimens were held with threaded, collet-type grips. The beryllium tube specimens were gripped with modified Jacob's chucks. The jaws of the chuck were ground to conform to the threaded ends of the specimen. Both types of grip were capable of transmitting both the axial and torsional maximum loads. The Jacob's chuck has the advantage of not transferring torsional load to the specimen as the grip is being tightened.

B. Strain Extensometers

Several different electro-mechanical strain extensometers were developed to measure the various modes of deformation. The direct application of resistance strain gages on each specimen was avoided because of the expense of gaging the large number multiaxial specimens tested, the desire to measure large plastic strains, and the high temperatures (to 1000°F) involved in some of the tests. The following paragraphs will describe the three types of extensometer used.

1. Uniaxial Capacitance Extensometer

For use with 1/4-inch diameter round tensile specimens, a parallel plate capacitance extensometer was developed. Mechanically the extensometer consists of two plate elements mounted independently on the gage section of the specimen as shown in Figure 6a. Each half of the extensometer attaches to the specimen with three set screws*. A 0.010-inch thick mylar spacer is used to set the initial spacing between the plates and thus the gage length (distance between set screws). For the extensometer shown in Figure 6, the gage length is 3/8-inch.

The extensometer is constructed with a stainless steel housing and brass capacitance plates bonded and insulated with epoxy. One half contains the driver capacitance plate and the other a sensing plate. The driver plate (left side of Figure 6b) is larger in area and overlaps the sensing plate by 0.050-inch. The faces of these capacitance plates can be seen in Figure 6b. Stainless steel tubing used to conduct cooling water is bonded to the back of each element with copper filled epoxy. Both the electrical and the cooling leads can be seen in Figure 6. With water cooling, this extensometer has been used on specimens heated resistively up to 2000°F.

A mechanical advantage of this extensometer is its high resonant frequency. The two halves of the gage are essentially rigid bodies. Thus, the mechanical resonances associated with flexural, compliance type, clip gages are eliminated. Therefore, the extensometer is useful at high speeds (or accelerations) as well as at high temperatures.

* With beryllium, care was required to avoid failure initiation at the attachment points.

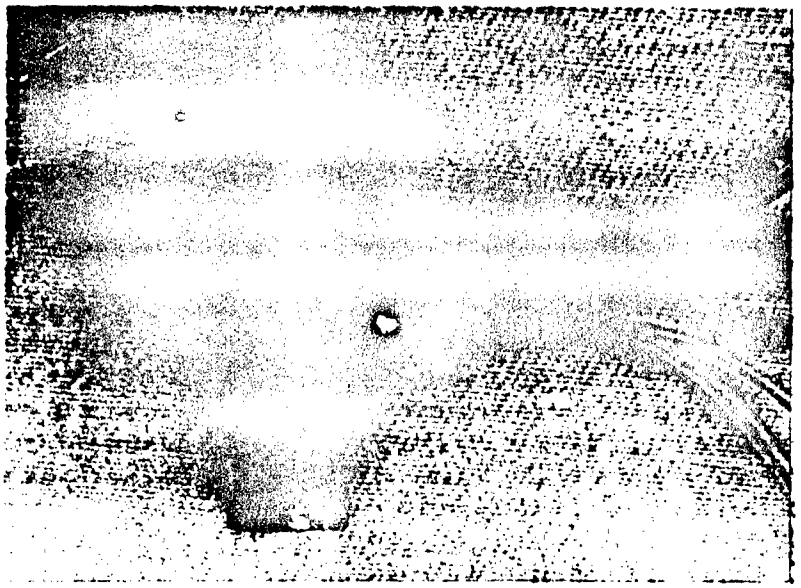

(a)

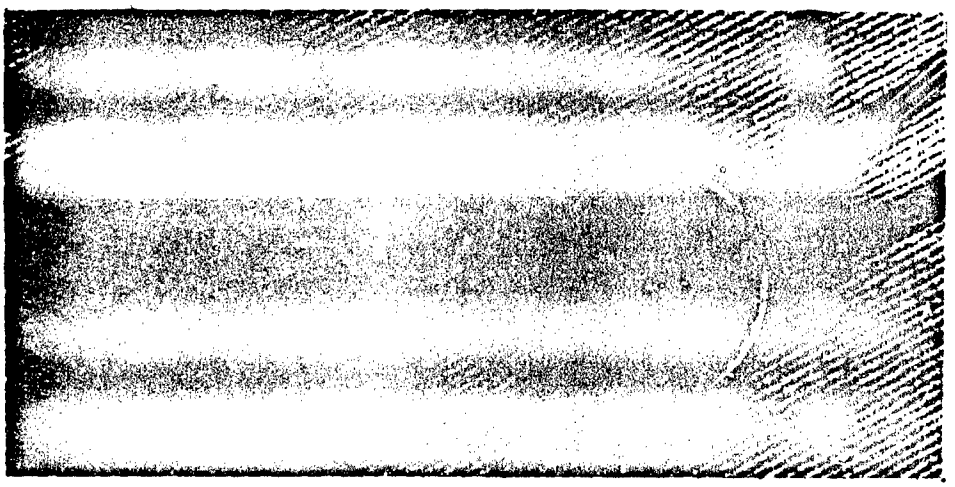

(b)

FIGURE 6. UNIAXIAL CAPACITANCE EXTENSOMETER MOUNTED ON SPECIMEN (a) AND SHOWING PLATE ARRANGEMENT (b)

The extensometer is sensitive to the change in spacing between two capacitance plates. Since the capacitance betwen two parallel plates is inversely proportional to the spacing between them, such plates normally form a nonlinear sensing element. However, the output of the extensometer can be linearized by using it as the feedback capacitor in a charge amplifier, since the gain of a charge amplifier is inversely proportional to its feedback capacitor. With the extensometer as the feedback element in the charge amplifier and with a fixed capacitor, C_i , as the input element for a carrier signal, the amplifier output becomes a carrier signal proportional in amplitude to the spacing of the extensometer plates. An electrical schematic of the system is given in Figure 7. The gain is adjusted by varying the carrier signal to the input. The output of the charge amplifier is summed with a fixed carrier signal to balance out the zero displacement plate separation. A phase sensitive demodulator is then used to produce an analog signal proportional to the separation of the two capacitor plates.

By proper adjustment of the gain and making a compensating adjustment for fringing, the extensometer can be used up to approximately 0.25 inch separation of the plates. For the beryllium specimens, a calibration constant of 0.0026 in/in/volt was determined over a strain range of approximately 30%.

2. Biaxial Linear-Torsional Extensometer

For tests in the tension-torsion plane, a biaxial strain extensometer was developed which also uses variable capacitance elements. This extensometer is shown in Figure 8. The extensometer mounts inside the tubular specimen and grips. It is water cooled for elevated temperature operation also. In this extensometer, displacement is sensed by varying the area between opposite sets of capacitance plates rather than the variable gap used in the uniaxial transducer.

The extensometer consists of an armature (or rotor) containing one set of capacitance plates and a concentric housing (or stator) containing a second set of plates. The extensometer is supported on axes inside the hollow tubular specimen by six spring loaded reference arms. The arms have knife-edge tips at the end where they contact the inner wall of the specimen. Three arms support the armature shaft and are normally referenced 1/4-inch above the center of the specimen. The other three arms support the outer housing and are referenced 1/4-inch below the center of the specimen. Thus, the gage length is normally 1/2-inch. However, the armature is held in place on the central shaft by friction and its position may be changed to give a variable gage length of 0.35-inch to 2.5-inches. The friction mounting also gives protection for the extensometer by providing a slip-clutch in the loading train.

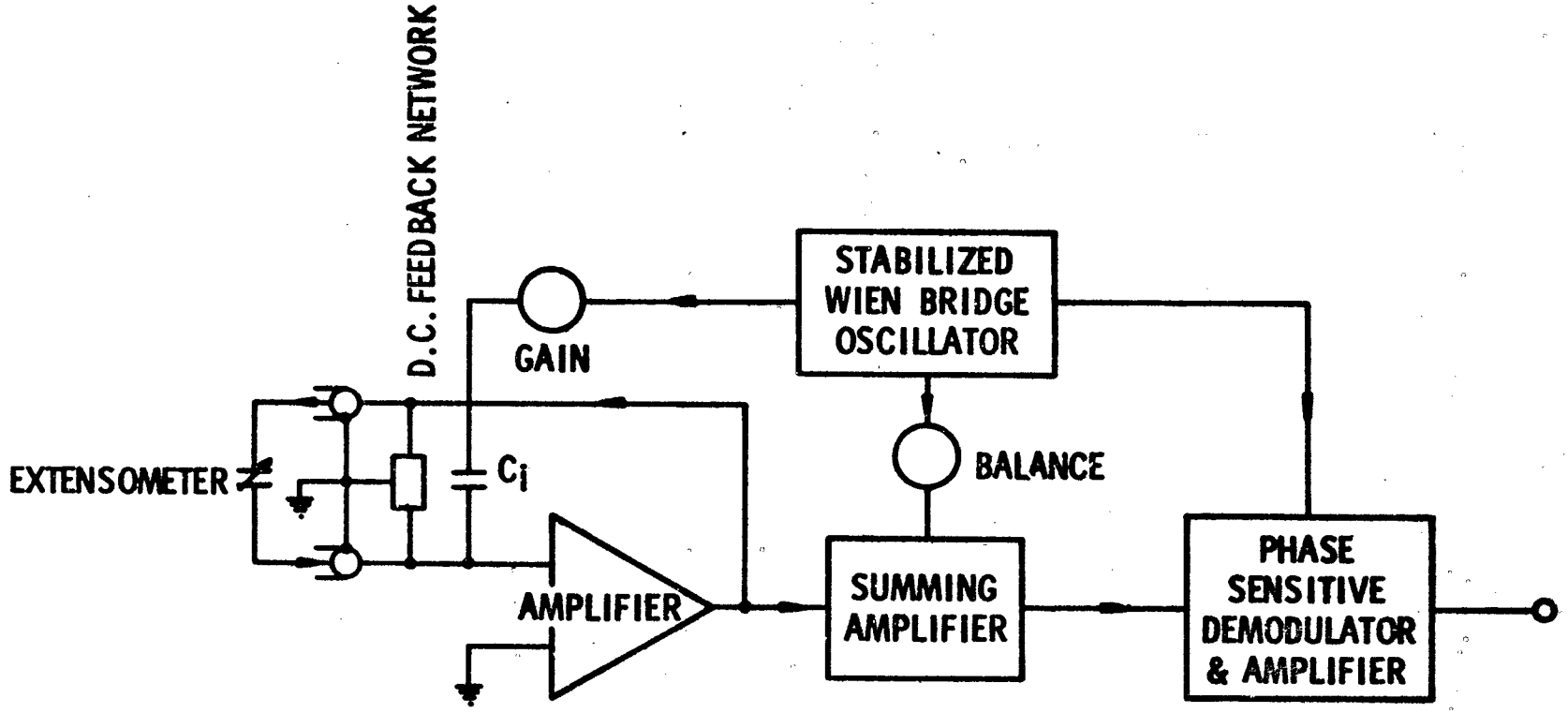

FIGURE 7. ELECTRICAL SCHEMATIC FOR UNIAXIAL CAPACITANCE EXTENSOMETER

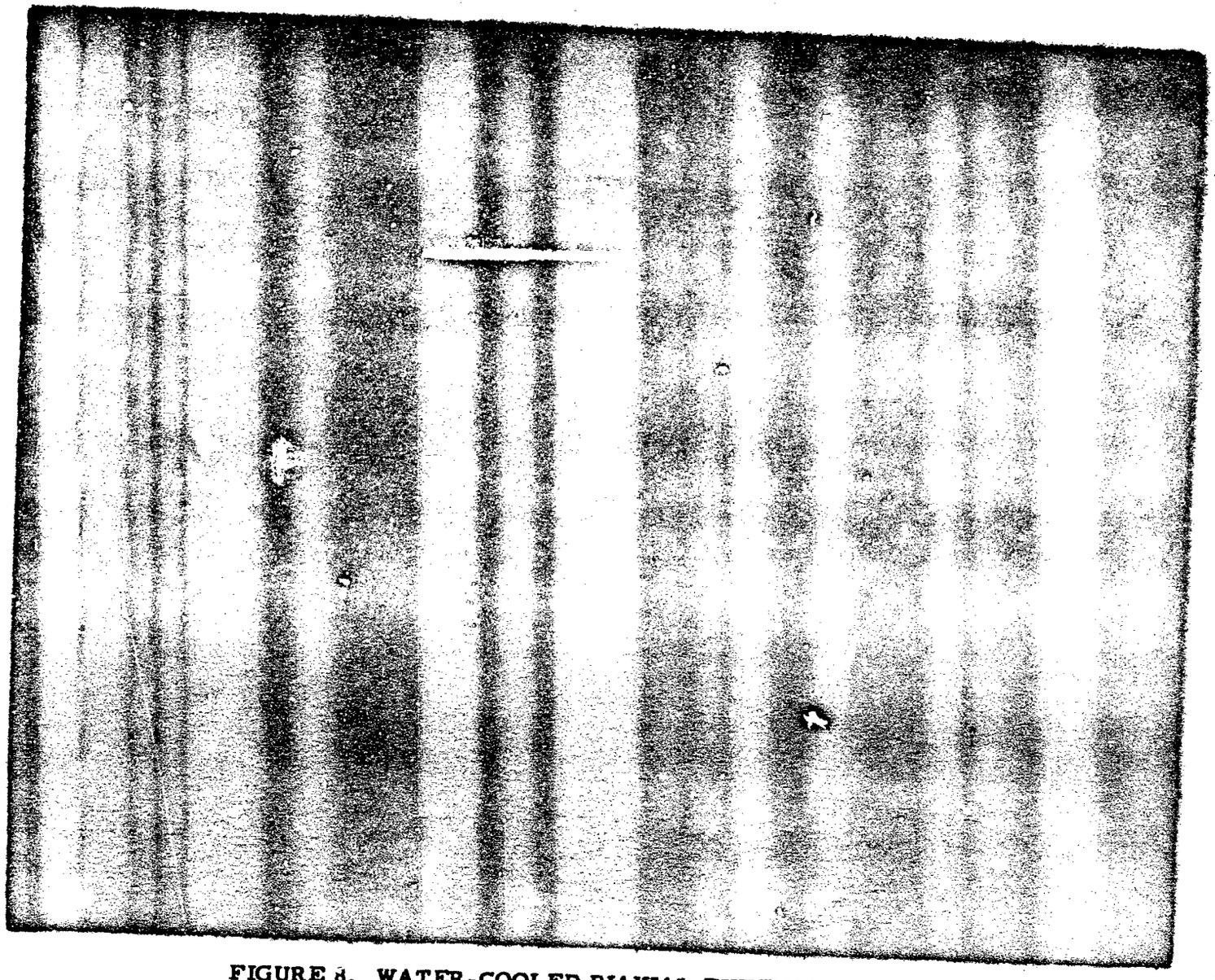

FIGURE 8. WATER-COOLED BIAXIAL EXTENSOMETER
FOR MEASURING AXIAL AND TORSIONAL STRAINS

The central shaft of the armature and the reference attachment arms each consist of two concentric stainless steel tubes. Cooling water is passed through this tubing when testing specimens at elevated temperatures. The cooling water for the armature reference arms is carried through the central shaft into the arms, and back out again through the central shaft. A stainless steel tube is also contained in either side of the outer housing. These tubes supply the cooling water for the housing and its reference arms.

Motion between the armature and the body of the extensometer is constrained to the axial and rotational directions by teflon bushings located in either end of the housing and acting on the armature shaft. A third bushing, acting on the armature shaft is mounted in the lower grip and maintains the extensometer alignment in the specimen, preventing the housing from making contact with the specimen.

A cross-sectional view of the extensometer is shown in Figure 9a. The armature (rotor) contains a set of four active capacitance plates. Each of these is 0.60-inch long and covers a 45° arc. The remainder of the armature is grounded. This ground isolates the plates and cuts down on fringing effects. The overall dimensions of the armature are 1.00 inch long by 0.314 inch in diameter. All of the active plates are tied together and are connected to the center conductor of a small shielded cable which enters the extensometer through a slot in the lower end of the housing. The shield of this cable provides the ground connection for the armature. The armature plates are driven with a constant amplitude carrier signal and act as the driven elements for both axial motion and rotational motion.

The housing of the extensometer contains ten separate capacitance plates. Eight cylindrical segments, each 0.20-inch long and covering an arc of almost 45°, are located in the center between two 0.40-inch long continuous rings. All of these plates have an inside diameter of 0.334-inch. The two outer rings (2 and 3 in Figure 9b) along with the armature form two arms of a capacitance half-bridge sensitive to axial strain only. The center segments (4 and 5) are alternately connected to form the two output capacitance elements for rotational measurement. Along with the armature plates(1),these form two arms of a torsional strain half-bridge. The outer housing of the extensometer is ground providing a guard element for all of the output capacitance plates.

The arrangement of the capacitance plates as they would be if laid out on a flat surface is shown in Figure 9b. The plates labeled "1" are on the armature and are separated from the housing plates by a 0.010-inch air gap. As the armature moves upward relative to the housing capacitance C_{12} increases and C_{13} decreases, while C_{14} and C_{15} remain constant. On the other hand, as the armature rotates clockwise relative to the housing,

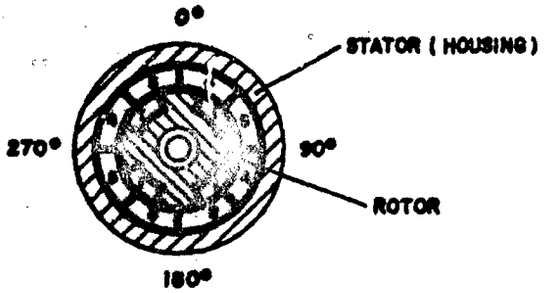

a. Cross Section Showing Capacitor Plate Layout.

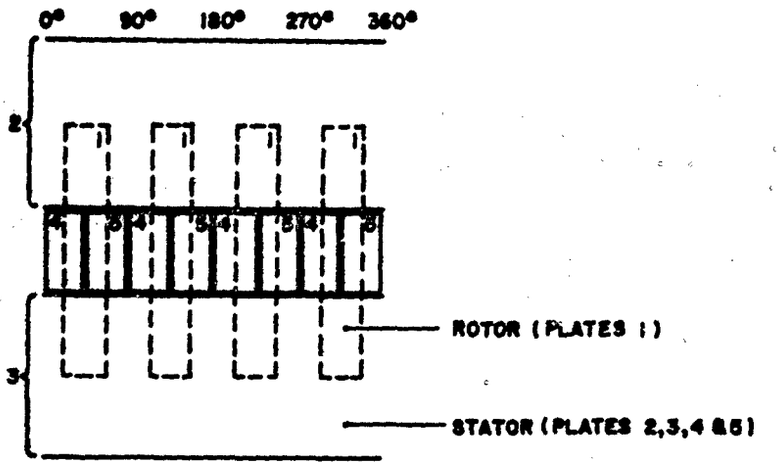

b. Plan-view of Capacitor Plates.

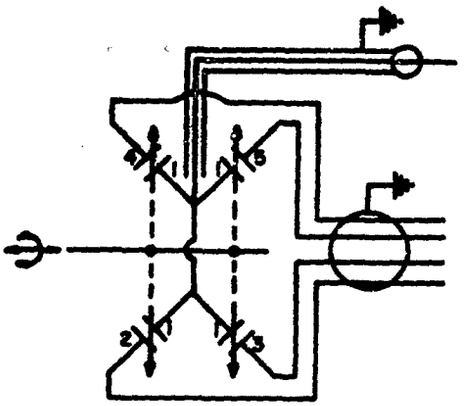

c. Electrical Schematic.

FIGURE 9. MECHANICAL AND ELECTRICAL LAYOUT OF BIAXIAL CAPACITANCE EXTENSOMETER

C_{14} decreases and C_{15} increases while C_{12} and C_{13} remain constant. Figure 9c shows the capacitance bridge arrangement.

The use of this extensometer design is made possible by the electronic instrumentation which has been developed. The total capacitance change in the extensometer is low (approximately 10 pico farad in the axial and 5 pico farad in the torsional directions). It is desirable to be able to resolve one part in 10^5 of full scale. In addition, there are two half-bridges in a single extensometer which means crosstalk must be kept at a minimum. The effect of cable capacitance must be minimized also. A schematic of the signal conditioning circuit is shown in Figure 10.

The preamplifiers used with this extensometer eliminate the problems of crosstalk and cable noise. The preamplifiers are essentially differential charge amplifiers. Thus, each input is the summing junction in an operational amplifier circuit and is, therefore, a "virtual" ground. This means that the output capacitance plates and the output leads of the extensometer are held at ground potential (except for the residual null voltage which is negligibly low), and therefore, the capacitance between elements and the shunt capacitance to ground has virtually no effect on the output of the amplifier. Because of the independence of shunt capacitance, relatively long shielded cables can be used and the four output leads can be contained in a single shield.

The charge amplifier produces a signal proportional to the amount of charge supplied in keeping the output of the transducer at ground potential. For the capacitance transducer, the charge supplied is equal to the capacitance times the carrier voltage. Additional capacitive balance and shunt calibration circuits are provided at the input to the amplifier. The output of the differential charge amplifier is a carrier signal proportional in amplitude to the difference in capacitance between the two elements of the extensometer plus the balance and calibration capacitances.

In order to obtain the large dynamic range needed for a feedback extensometer, the demodulator must have a large dynamic range. This means that it must be stable and remain linear through the null region. Nonlinearity near null can be caused by nonlinear switching elements or sensitivity to out-of-phase components in the carrier signal. Because of this, a phase sensitive demodulator circuit is used.

The demodulator consists of a variable gain differential amplifier with a field-effect switch on each input. The carrier signal

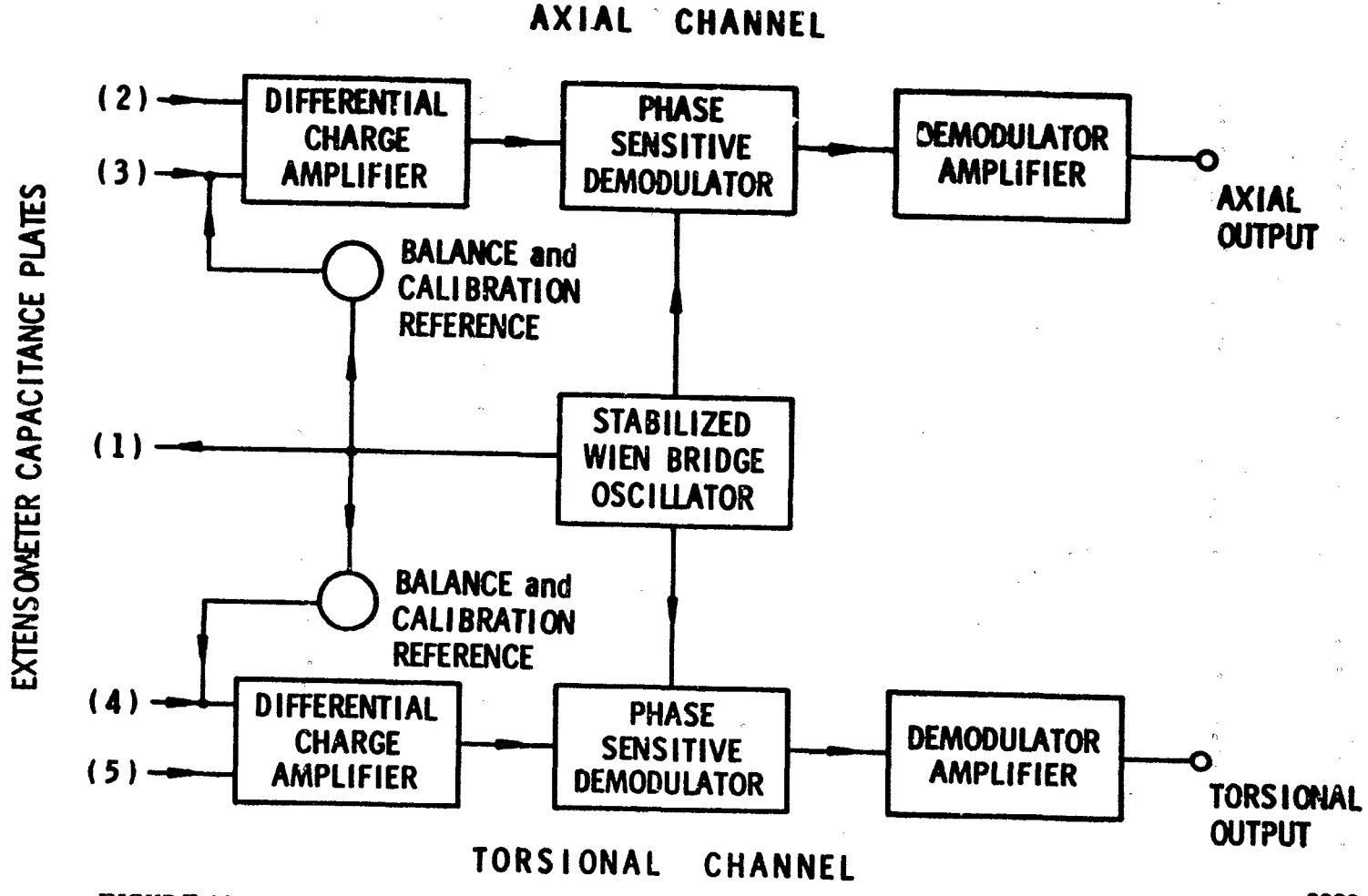

FIGURE 10. BLOCK DIAMGRAM OF CIRCUITS FOR BIAXIAL CAPACITANCE EXTENSOMETER 2980

from the preamplifier is connected to both inputs. Reference signals from the carrier oscillator switch the field-effect gates in the inputs so that full wave, phase-sensitive demodulation is obtained. The frequency response of the demodulator is rolled off at the upper end with the 3 db point approximately one-tenth the frequency of the carrier. A unity-gain amplifier is used following the demodulator to buffer and further filter the carrier. This demodulator is stable and linear through the null region. It has a dynamic range of at least 10^5.

Since the charge output of the capacitance transducer is proportional to the excitation voltage, it is necessary that the carrier oscillator output have a stable amplitude. Variations in amplitude cause variations in sensitivity of the transducer. Small variations in indicated strain from the extensometer when used as the feedback element for control of the load actuators, can cause large variations in load. Therefore, it is necessary that the oscillator stability (including hum and noise) be in the order of 0.01%. The oscillator used for this application is a Wien bridge oscillator, using an instrumentation lamp for amplitude stabilization.

Typical calibration plots for the extensometer are shown in Figure 11. By holding machining tolerances in the transducer, the linear and torsional axes are completely orthogonal and there is no observable crosstalk. The calibration was found to be independent of the relative position of the armature within the housing. A remarkable feature of this type of capacitance extensometer is its linear dynamic range. This instrument is able to resolve relative displacements from approximately 10μin. to 0.30 inch.

3. Biaxial Extensometer for Axial Load and Internal Pressure

Strain gaged flexural elements were used for measurement of axial strain and change in specimen diameter during tests with internal pressure. Figure 5 shows a titanium specimen held in the collet grips and enclosed in half of a split shell which contains the extensometer. The outer shell housing is also used to contain hydraulic fluid which is lost when the specimen ruptures.

The two clip-type elements attached to the specimen by soft springs record the axial strain. The strain gage sensing element is attached to the thin cross member which is placed in flexure by relative axial motion between the two attachment points. The radial displacement of the tube is measured by four cantilever arms contacting the tube at 90° intervals and attached at their root to the outer cylindrical housing. Two cantilever arms are contained in each half of the housing.

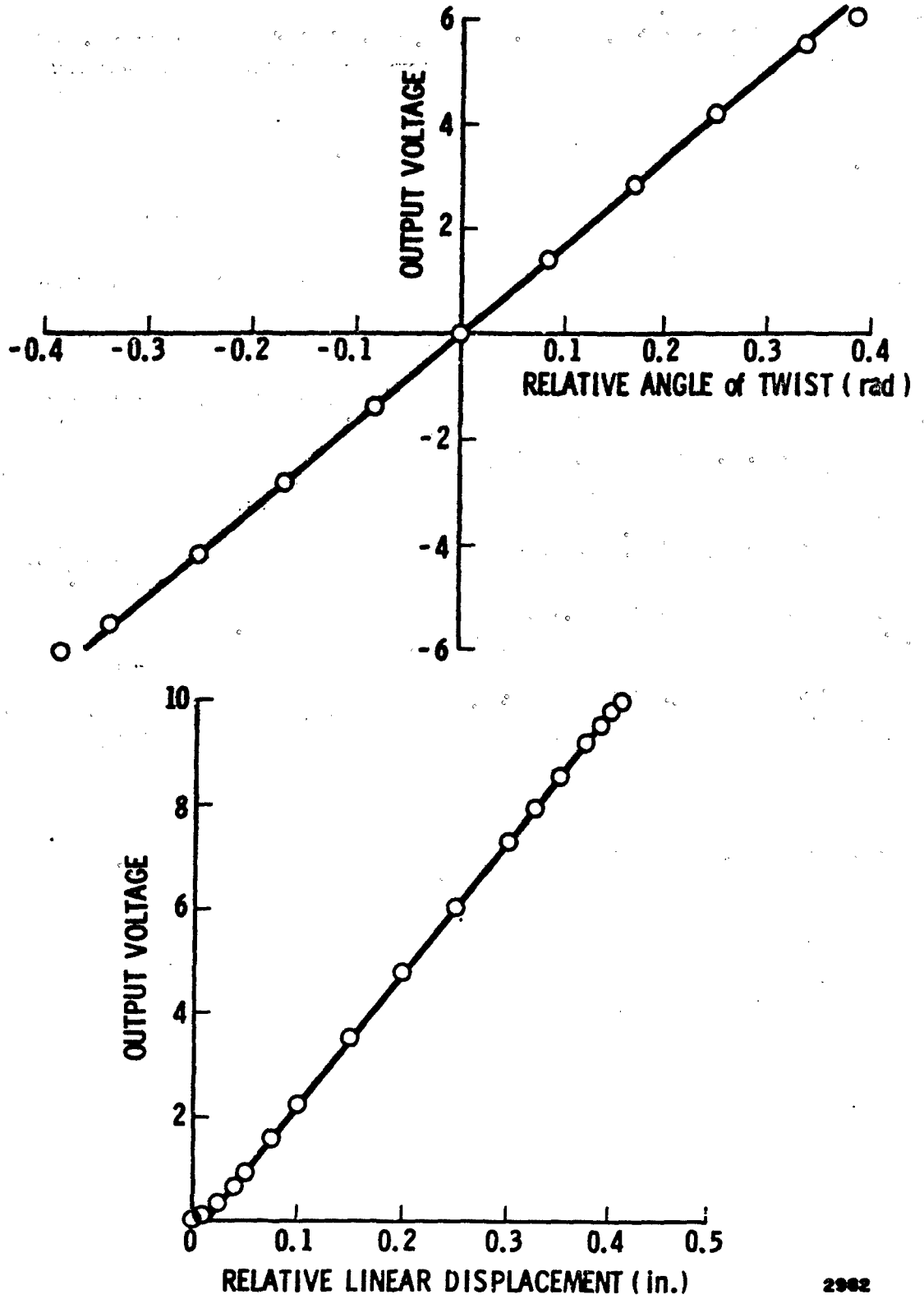

FIGURE 11. CALIBRATION CURVES FOR BIAXIAL CAPACITANCE EXTENSOMETER

At higher testing speeds the flexural elements are subject to vibrational excitation. Coating the flexures with silicone grease helps to damp such oscillations. Most of the internal pressure tests were run at slow speeds and at room temperature. The temperature in this mode is limited by the internal working fluid.

C. Temperature Control

For the elevated temperature tests at 300°, 600° and 1000°F the specimens were heated by a coaxial, three-zone quartz lamp oven. The temperature was measured in the gage section of the specimen by a chromel-alumel thermocouple. The most reproducible thermocouple readings were obtained by looping each thermocouple wire so that it was in contact with the specimen over 180° of the specimen circumference. The contact was maintained by a light spring force holding the thermocouple wire. Each wire, chromel and alumel, was looped separately so that the specimen formed an intermediate metal in the thermocouple junction. Good contact with the specimen was maintained throughout the deformation as will be seen later when a record showing the adiabatic temperature rise during high speed deformation is presented. The thermocouple also served as a feedback element in an automatic temperature controller holding the set temperature during the test.

The problem of axial temperature gradients in the specimen caused by the large heat sinks existing in the grips is minimized by measuring strain only over the center 1/2-inch of the gage section. Within this central region the temperature gradient is symmetric and small.

SECTION IV

EXPERIMENTAL RESULTS

A. Uniaxial Tests on S-200E Beryllium

The uniaxial tensile tests were conducted at constant temperatures and at nominally constant strain rates. At the highest strain rates on the hydraulic machine (10 sec^{-1}) and on the Hopkinson bar, constant strain rate could not be held exactly because of lack of feedback control. An example of data obtained at 10 sec^{-1} is given in Figure 12 for a hot-pressed block specimen tested at 70°F. The upper oscilloscope record gives the crosshead displacement, x, strain at two amplifications, $\epsilon_2 = 10\epsilon_1$, and stress, σ, recorded vs. time. It can be seen that the strain accelerates through the elastic portion of the deformation and reaches a near constant rate only after yielding, indicated by the sharp break in the stress-time curve. At lower speeds (≤ 1 sec^{-1}) the control system is capable of maintaining constant rate throughout the test. For the higher speeds, the rate cited is an average plastic strain rate. Stress-strain curves were also recorded directly with two different strain amplifications as seen in the lower record in Figure 12. For the hot-pressed block the "elastic" region below yield was characteristically nonlinear as shown in Figure 12. While the elastic moduli were checked to be within the nominal range for beryllium, the overall accuracy of the analog recording system was not sufficient to compare moduli between test conditions. Only the plastic strength and ductility data will be reported.

The complete stress-strain curves for all the uniaxial beryllium specimens are given in Appendix A for reference. In general, the extruded material exhibited a very sharp yield drop under all conditions except the slow tests at 1000°F. The hot-pressed block shows a smaller and less abrupt yield drop, the drop being more pronounced in the transverse than in the longitudinal direction.

The yield strength, ultimate strength and elongation at failure for the uniaxial specimens are plotted in Figures 13-15 as functions of temperature and strain rate. The yield strength has been defined as the upper yield stress for the extruded material and as an 0.2% offset stress for the hot-pressed block. The extruded material shows more temperature and rate sensitivity than the hot-pressed block, both for yield and ultimate strength. For the hot-pressed block, the uniaxial specimens show a slight difference in offset yield strength between the longitudinal and transverse directions, particularly at the lower temperatures. This would suggest some anisotropy of this material. However, the effect appears to be primarily associated with the elevated yield point phenomena which is somewhat more pronounced

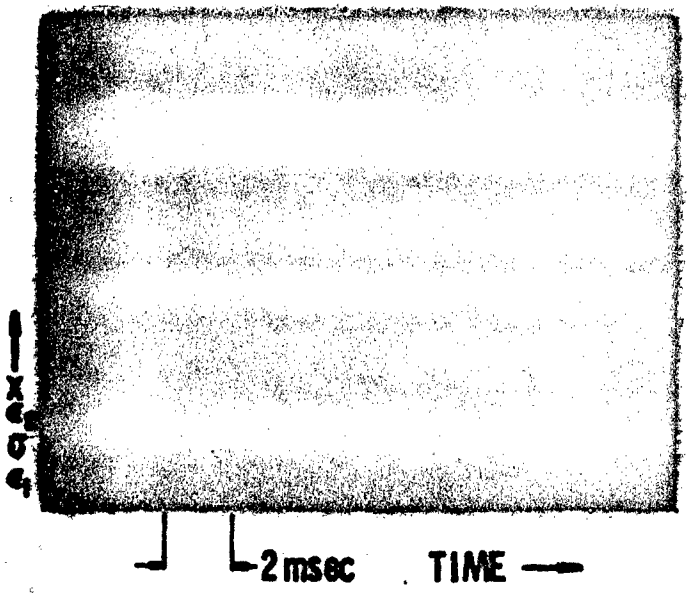

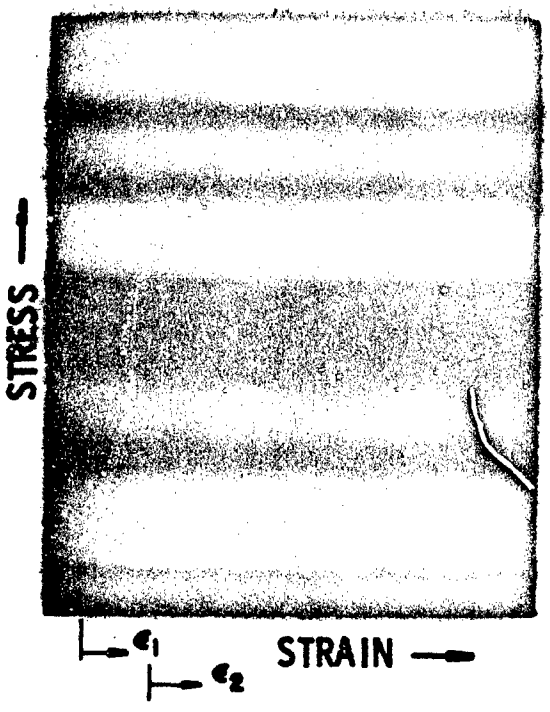

FIGURE 12. OSCILLOSCOPE RECORDS FROM UNIAXIAL TENSILE TEST OF BERYLLIUM PRESSED BLOCK SPECIMEN AT 70°F and 10 sec^{-1}

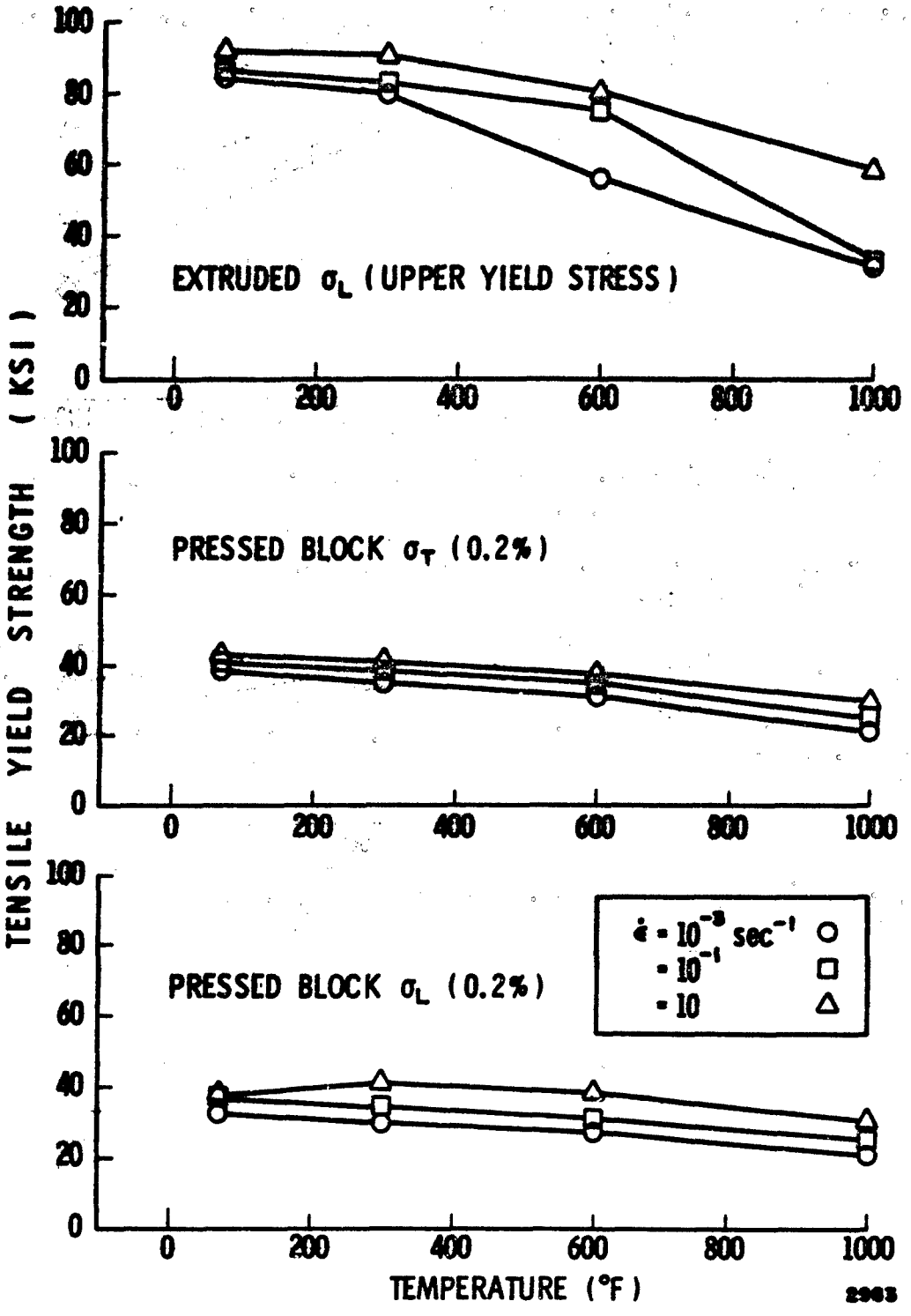

FIGURE 13. EFFECT OF TEMPERATURE AND STRAIN RATE ON THE TENSILE YIELD STRENGTH OF S-200E BERYLLIUM

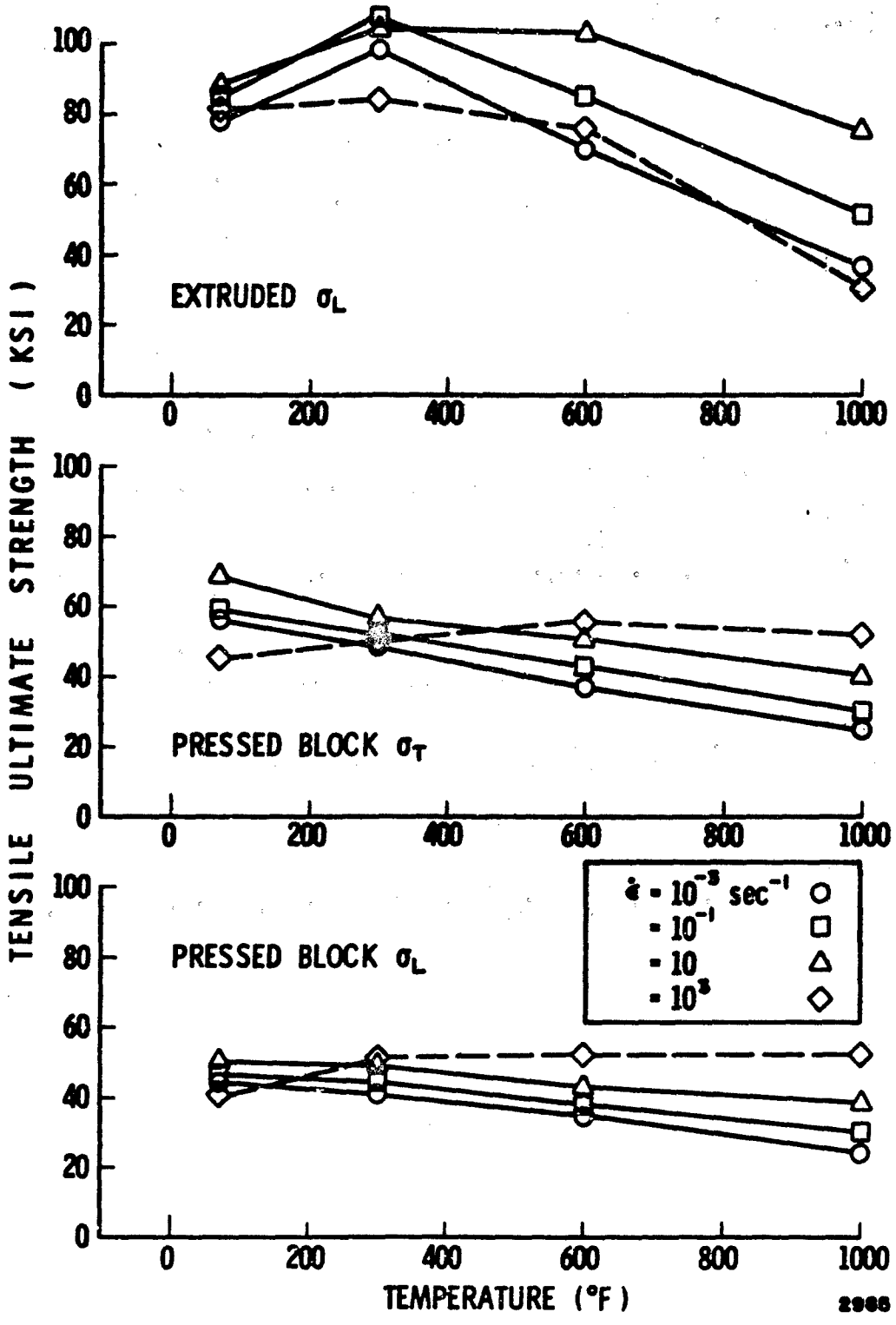

FIGURE 14. EFFECT OF TEMPERATURE AND STRAIN RATE ON THE ULTIMATE TENSILE STRENGTH OF S-200E BERYLLIUM

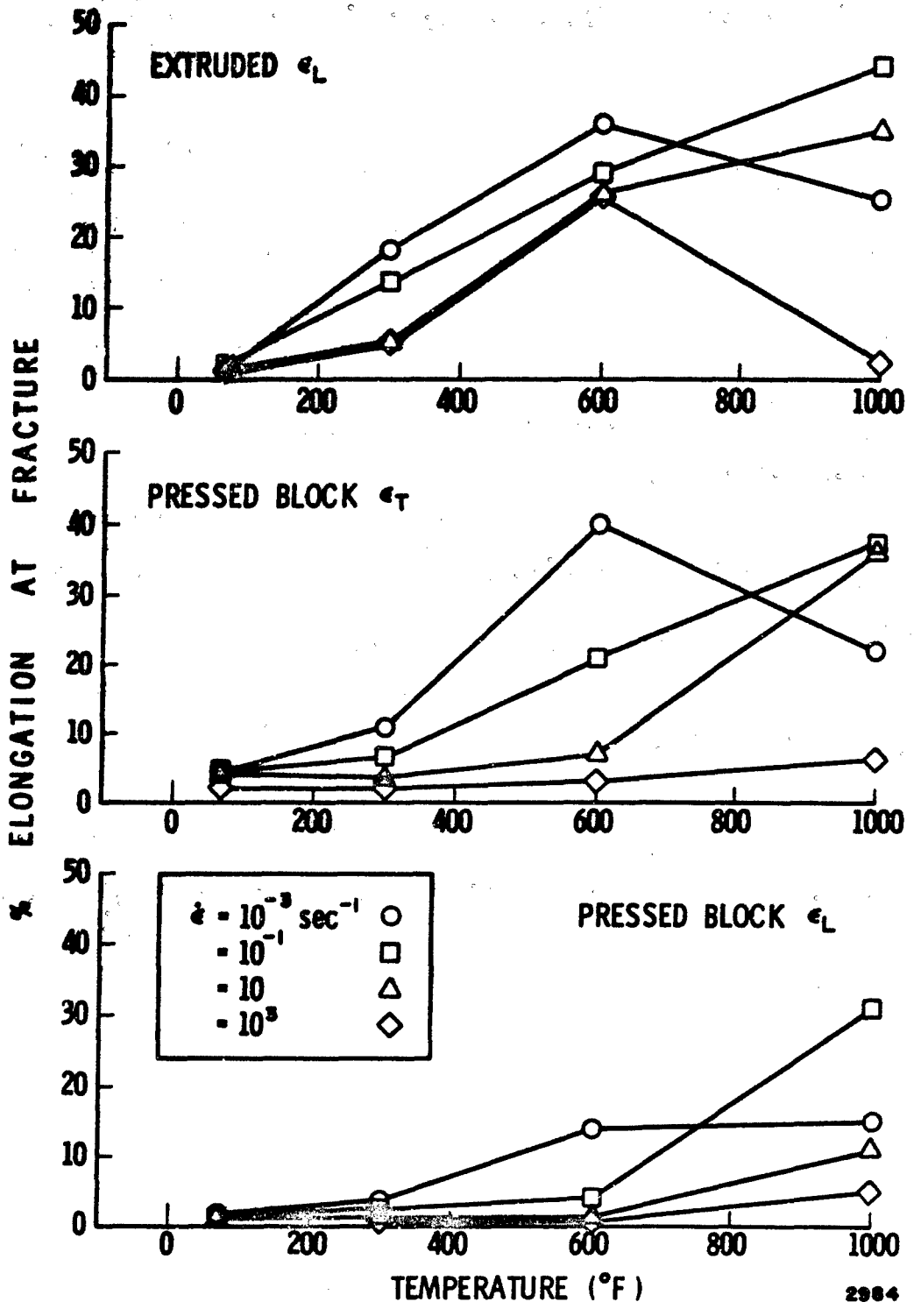

FIGURE 15. EFFECT OF TEMPERATURE AND STRAIN RATE ON THE DUCTILITY OF S-200E BERYLLIUM

in the transverse direction than in the longitudinal when the distinct upper yield point develops. At higher temperatures, where yielding is smooth for both directions, the yield stresses are equal. The tube specimens did not develop a distinct upper yield point, and the yield locus for the pressed block material will be shown to be isotropic from the biaxial tests.

The ultimate (maximum stress achieved after yielding) strength in a tensile test may be either the stress reached at the onset of plastic instability (necking) or the stress at fracture, whichever occurs first. For beryllium the ductility varies greatly, so that fracture may occur during the work-hardening portion of the stress-strain curve or well after necking begins. The low ultimate strength (relative to yield) of the extruded beryllium at 70°F results from its very low ductility at this temperature, and fracture occurs before any appreciable work-hardening can take place. The increased ductility at 300°F results in an increase in ultimate strength. At temperatures greater than 300°F the ultimate strength decreases again because of both a decreased yield strength and work-hardening rate.

In Figure 14 the ultimate strengths obtained at 10^3 sec^{-1} with the Hopkinson bar are shown by a dashed line to indicate the uncertainty in these values because of the difficulties mentioned earlier. The strength values at higher temperature become more consistent because of the increased ductility. Yield stresses at this rate could not be determined.

The ductility maximum at around 600 - 800°F for S-200E beryllium deformed at slow rates has been previously noted by King[6]. King's data also shows the increased ductility of the S-200 hot-pressed block in the transverse direction over the pressing (longitudinal) direction which is apparent in the present results. The general effect of increasing strain rate is to shift the brittle to ductile transition to higher temperatures. Even at the moderate rate of 0.1 sec^{-1}, the ductility maximum observed at 10^{-3} sec^{-1} (if it still occurs) is shifted to temperatures above 1000°F. The increase in ductility with increasing temperature is generally attributed to the decreased stress required to produce slip on prism planes and the increase in stress required to produce fracture on basal planes. At 70°F, slip occurs mainly on basal planes which have little ductility. There is a transition from cleavage to a more ductile fibrous fracture with increasing temperature[3].

The appearance of the fractured specimens is shown in Figures 16-18. The hot-pressed block specimens broke in a single plane, roughly normal to the tensile axis. Appreciable necking occurs at the higher temperatures. The fractures of the extruded specimens, Figure 16, were interesting in that, for all specimens tested below 1000°F, fracture apparently initiated at one point, presumably a local flaw, and propagated on two planes simultaneously. This resulted in two conical fracture surfaces oriented

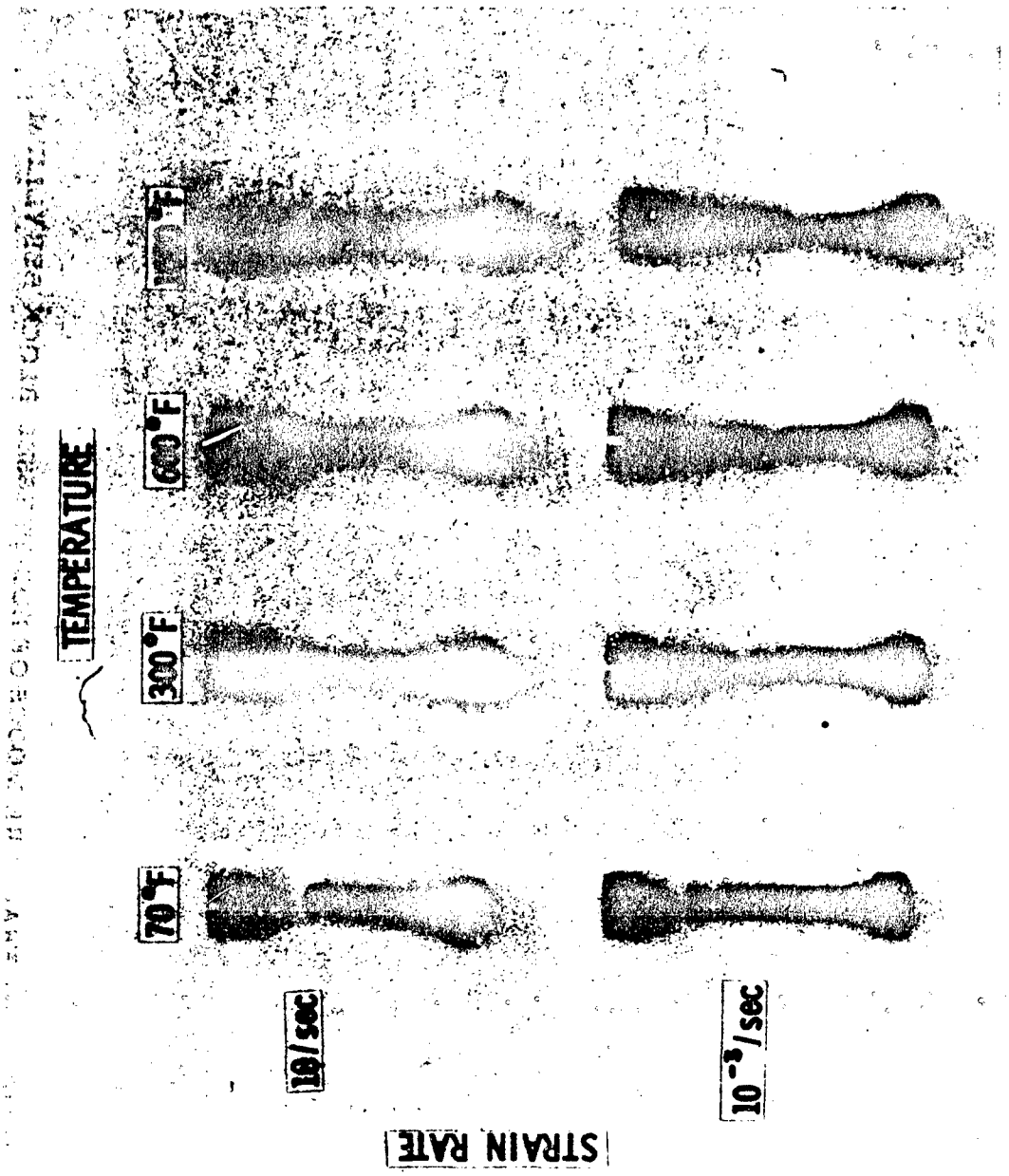

FIGURE 16. FRACTURE MODES OF EXTRUDED BERYLLIUM

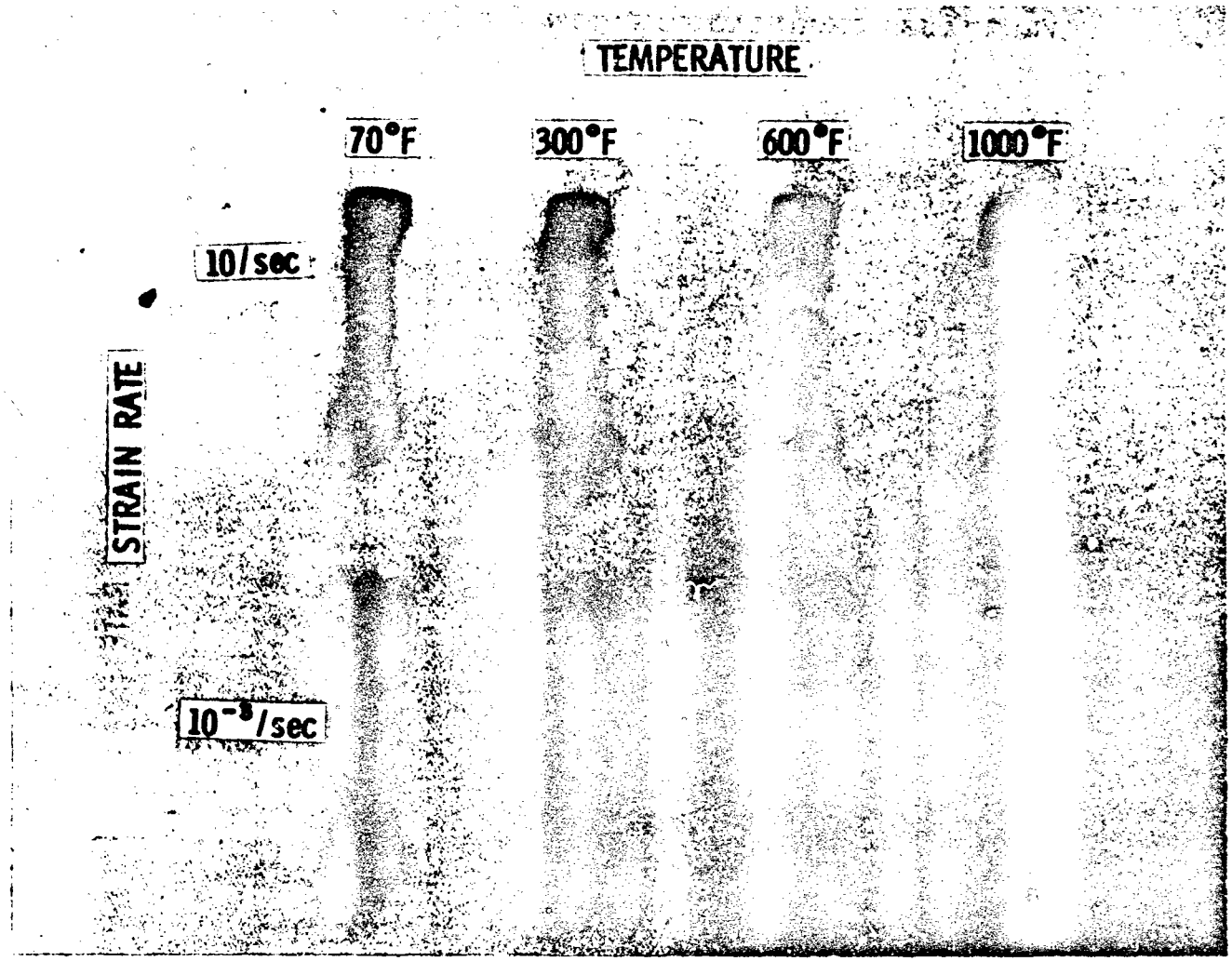

FIGURE 17. FRACTURE MODES OF HOT-PRESSED BLOCK BERYLLIUM TRANSVERSE ORIENTATION

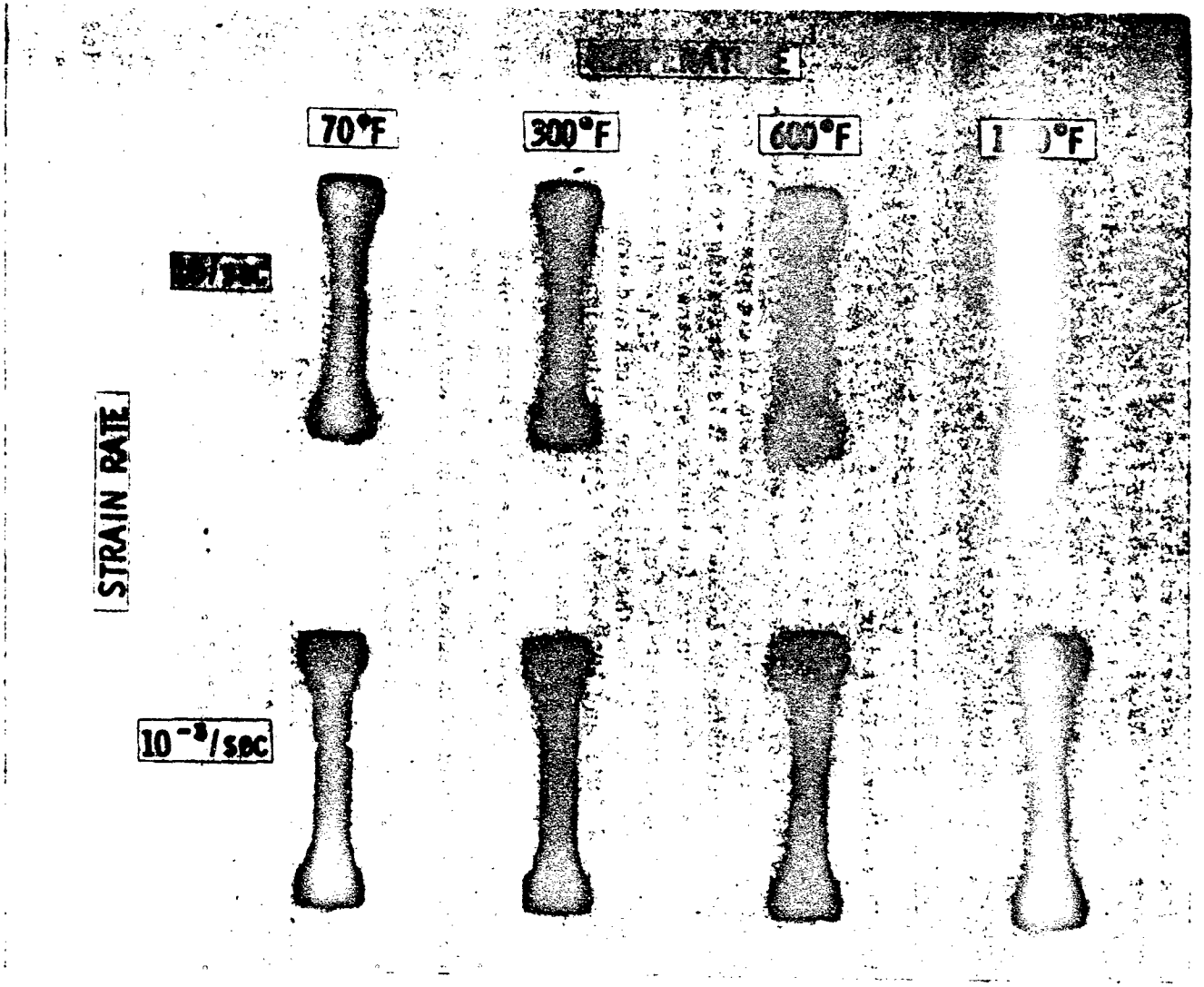

FIGURE 18. FRACTURE MODES OF HOT-PRESSED BLOCK BERYLLIUM, LONGITUDINAL ORIENTATION

approximately 62° to the tensile or extrusion axis. The initial bifurcation of the crack will also be seen later in the tube specimens with the same fracture angle of 62°. Tauer and Kaufmann[7] also show pictures of typical fracture markings developed in brittle, highly oriented, beryllium rods and tubes, which indicate the same angle of the fracture plane to the extrusion axis. They claim the cracks are essentially parallel to the position of the $\{11\bar{2}0\}$ plane positions in a rod having a $\langle 10\bar{1}0\rangle$ texture with basal planes parallel to the surface.

B. Biaxial Tests on Beryllium

1. Stress-Strain Behavior

Proportional loading tests to failure were performed on the tubular specimens in the $\pm\ \sigma_L$, σ_T half-plane and in the $+\ \sigma_L$, σ_{LT} quadrant. The positive and negative signs refer to tension and compression, respectively. Before describing the biaxial tests, it is interesting to note the shape of the stress-strain curves for tubular specimens tested along each of the four uniaxial stress axes, $+\sigma_L$, $-\sigma_L$, $+\sigma_T$, σ_{LT}. These curves are given in Figures 19 and 20 for the hot-pressed block and extruded material, respectively, at 70°F and 10^{-3}sec^{-1}. Additional tension, σ_L, and shear, σ_{LT}, curves are given in Appendix B for elevated temperature tests.

It should be pointed out that the test matrix generally allowed only one specimen per test condition, so that comparison of individual curves as in Figures 19 and 20 is subject to the uncertainty of an unknown specimen to specimen variation. (King[6] has presented data showing the variation to be expected in S-200 hot-pressed block.) However, several points can be noted from the stress-strain curves presented. First, is the considerable variation in ductility with mode of deformation. Later in this report, the failure strains from all the biaxial tests will be presented emphasizing the strong effect of stress ratio on ductility. As mentioned previously, the tube specimens do not exhibit the strong yield instability evidenced in the round tensile specimens. Only the stress-strain curve for longitudinal tensile loading of the tube of extruded material shows some evidence of yield point elevation. This elevation produces a difference in tensile and compression yield strengths, although the subsequent work-hardening slope is very similar in tension and compression for the extruded specimens. For the hot-pressed block, the work-hardening rate appears dependent upon the direction of the normal stress, although the initial yield strength agrees with an isotropic Mises yield criteria.

A typical record for a biaxial test of extruded beryllium is given in Figure 21. The records include two channels of stress and two of strain. For elevated temperature tests, a fifth channel records the output from the thermocouple attached to the specimen.

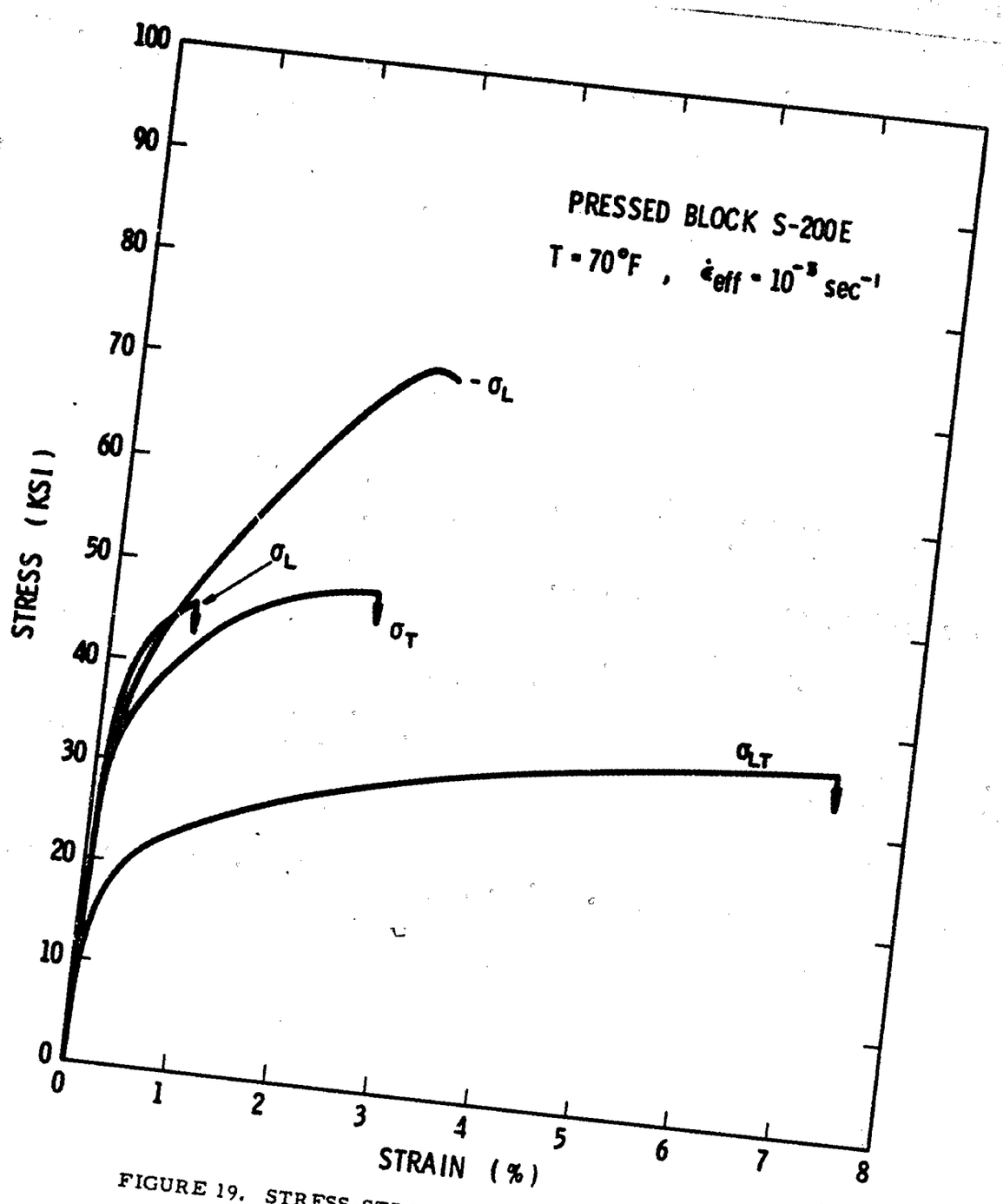

FIGURE 19. STRESS-STRAIN CURVES FOR HOT-PRESSED BLOCK TUBE SPECIMENS

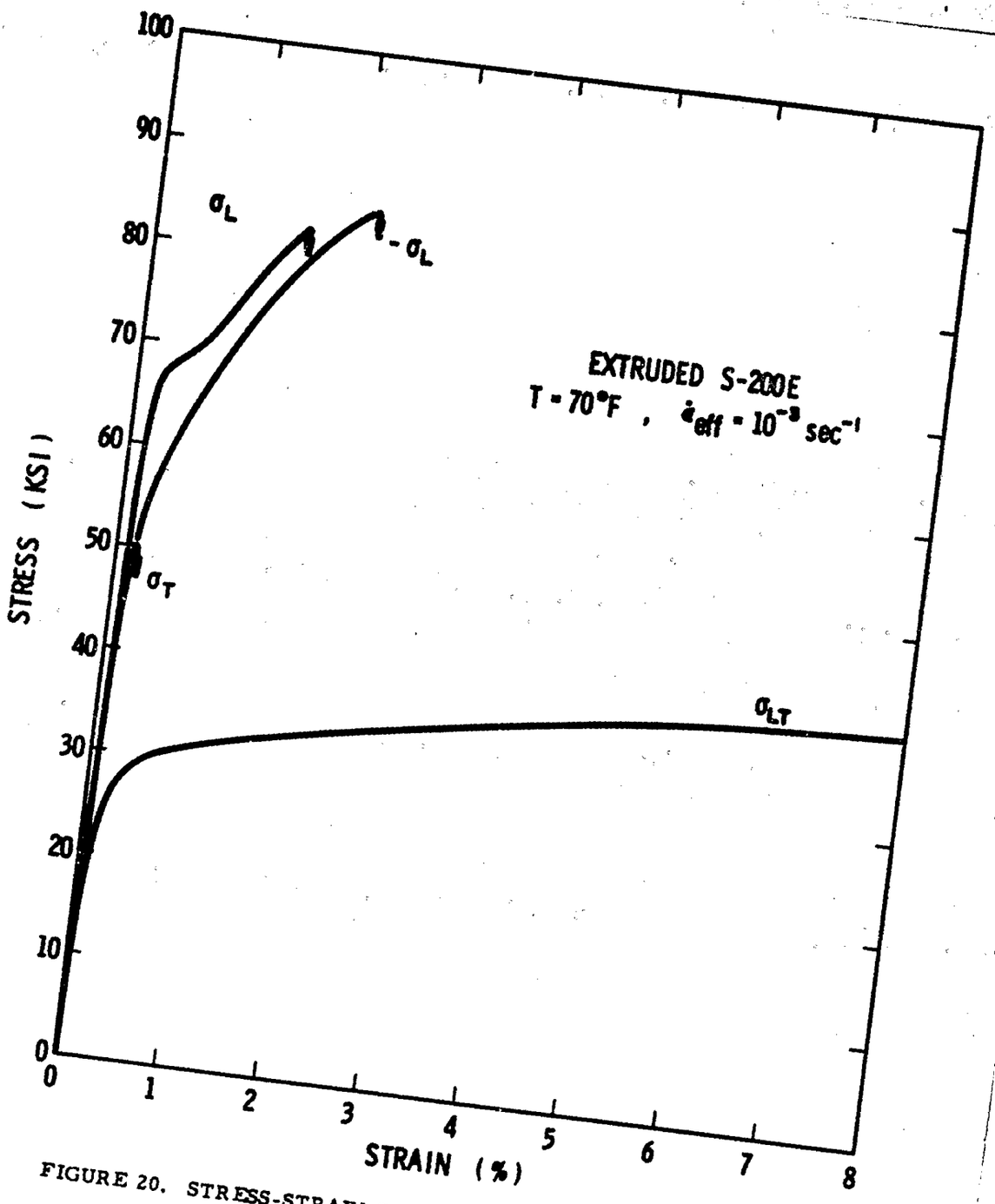

FIGURE 20. STRESS-STRAIN CURVES FOR EXTRUDED TUBE SPECIMENS

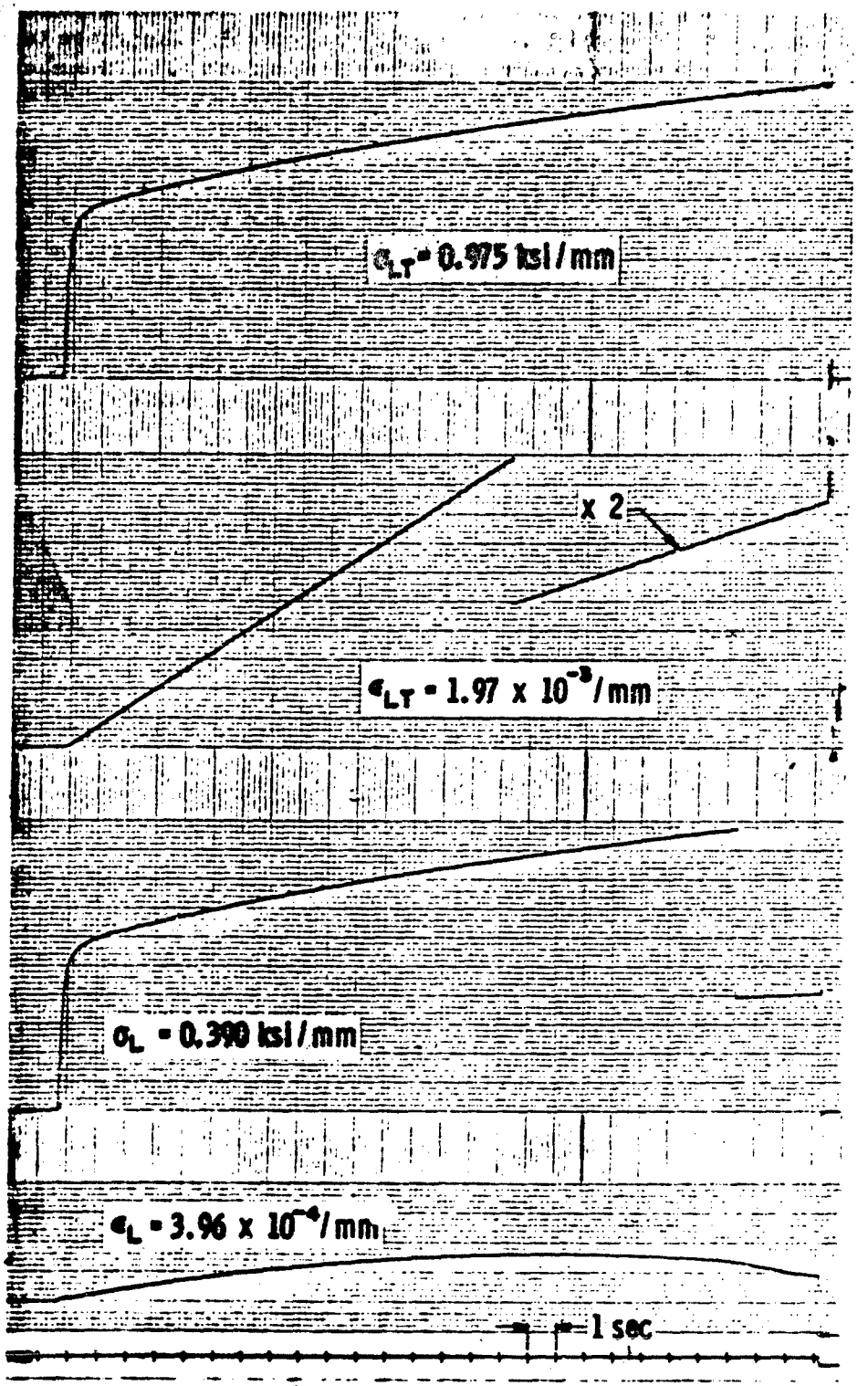

FIGURE 21. A TYPICAL BIAXIAL RECORD OBTAINED AT 70° F AND 10^{-3} sec^{-1} IN COMBINED TENSION AND TORSION. THE SPECIMEN IS S-200 BERYLLIUM, EXTRUDED P.OD.

For the biaxial tests, there are two independent control elements, and there is a choice as to which two variables to control. For these tests, the strain rate was always controlled to be constant on one axis (the shear axes in Figure 21). The second axis (load actuator) was controlled so as to provide a constant stress ratio, i.e., maintain proportional loading in stress. For example, in Figure 21, σ_{LT}/σ_L = constant and $\dot{\epsilon}_{LT}$ = constant. For control purposes, it is necessary to define an effective strain rate, $\dot{\epsilon}_{eff}$, during biaxial loading which is some function of the two independent strain rates. The input rate for the single strain channel controlled must be varied depending upon the stress ratio in order to hold $\dot{\epsilon}_{eff}$ = constant between tests.

While the choice of $\dot{\epsilon}_{eff}$ is somewhat arbitrary, it seems appropriate to use the second invariant of the deviatoric strain rate tensor. Thus, we define

$$\dot{\epsilon}_{eff}^2 = \frac{1}{2}\,\dot{\epsilon}'_{ij}\,\dot{\epsilon}'_{ij} = \frac{1}{6}\left[(\dot{\epsilon}_1-\dot{\epsilon}_2)^2 + (\dot{\epsilon}_2-\dot{\epsilon}_3)^2 + (\dot{\epsilon}_3-\dot{\epsilon}_1)^2\right] \qquad (1)$$

where ϵ_1, ϵ_2, ϵ_3 are the principal strains. Since we have control over only one of the strain components, some further assumptions are necessary. First, we assume the isotropic flow rule

$$\frac{\dot{\epsilon}_1}{\sigma_1'} = \frac{\dot{\epsilon}_2}{\sigma_2'} = \frac{\dot{\epsilon}_3}{\sigma_3'} \qquad (2)$$

where the primes denote deviatoric stress components. Since

$$\sigma_1' + \sigma_2' + \sigma_3' = 0$$

we have, for $\sigma_3 = 0$,

$$\frac{\dot{\epsilon}_1}{2\sigma_1-\sigma_2} = \frac{\dot{\epsilon}_2}{2\sigma_2-\sigma_1} = \frac{\dot{\epsilon}_3}{-(\sigma_1+\sigma_2)} \qquad (3)$$

If we define the stress ratio, $\beta \equiv \sigma_2/\sigma_1$, then

$$\frac{\dot{\epsilon}_2}{\dot{\epsilon}_1} = \frac{2\beta-1}{2-\beta} \equiv \alpha \qquad (4)$$

From (4) and the assumption of incompressible flow ($\dot{\epsilon}_1 + \dot{\epsilon}_2 + \dot{\epsilon}_3 = 0$), we obtain

$$\dot{\epsilon}_2 = \alpha \dot{\epsilon}_1$$

and

$$\dot{\epsilon}_3 = -(1+\alpha)\,\dot{\epsilon}_1$$

Then, substituting in (1) and performing the necessary algebra yields

$$\dot{\epsilon}_1 = \dot{\epsilon}_{eff}(\alpha^2+\alpha+1)^{-1/2} \qquad (5)$$

Thus, for a selected stress ratio $\beta = \sigma_2/\sigma_1$ ($=\sigma_L/\sigma_T$, for instance) and a prescribed $\dot{\epsilon}_{eff}$, the appropriate $\dot{\epsilon}_1 = \dot{\epsilon}_L$ can be programmed. The programmed rate, $\dot{\epsilon}_L$, will then vary according to the stress ratio. For the σ_L, σ_{LT} quadrant a similar procedure leads to

$$\dot{\epsilon}_L = 2\,\dot{\epsilon}_{eff}\,(3\gamma^2+4)^{-1/2}$$

where $\gamma = \sigma_{LT}/\sigma_L$

An alternate procedure is to control both strain components directly and, thus, assure a constant value of the strain rate invariant (or equivalently the octahedral shear strain rate). In this case, the stress ratio would not be controlled.

For the extruded beryllium, it was found that in pure torsion with no axial load a negative axial strain or shortening of the tube occurred as the angle of twist increased. This coupling depends upon both the initial anisotropy of the material and upon the further plastic anisotropy induced by the deformation as is discussed by Hill[8]. Twist can produce either shortening or extension of the tube depending upon the coefficients of the anisotropic plastic flow rule. Extension is the more common result for metals according to the references cited by Hill. In Figure 21, it is rather interesting to observe that at large deformation, the uncontrolled axial strain component, ϵ_L, reaches a maximum value and then decreases, although the axial stress continues to increase. At large angles of twist the anisotropic shortening effect apparently overcomes the extension produced by the axial tensile loading.

2. Yield and Ultimate or Fracture Strength

The biaxial strengths were determined for monotonic proportional stress loading to failure at several temperatures and rates. This

data will be presented as yield and failure loci in the three-dimensional stress space (σ_L, σ_T, σ_{LT}) corresponding to the generalized plane stress test conditions. Only the intercept of the complete yield and failure surfaces with the σ_L, σ_T plane and the σ_L, σ_{LT} plane have been determined. No tests were performed under triaxial loading.

Figure 22 presents the results for the hot-pressed block specimens tested at a temperature of 70°F and an effective strain rate of 10^{-3}sec^{-1}. For a correct three-dimensional representation the bottom half-plane should be folded up so that the σ_{LT} axis is normal to the σ_L, σ_T plane. The half-shaded data points along the σ_L and σ_T axes correspond to results from the uniaxial tensile specimens. All other data points are from tube specimens.

The solid curves in Figure 22 are fits to the data points according to the second order equations in stress appearing on the figure. The yield locus is seen to fit reasonably accurately the isotropic Mises yield criteria

$$\sigma_L^2 - \sigma_L \sigma_T + \sigma_T^2 + 3\sigma_{LT}^2 = k^2 \qquad (6)$$

where k = 40 ksi is the yield strength in the normal stress directions. The physical basis for this criteria can be given either as a surface of constant strain energy of distortion or of constant value of shear stress on the octahedral planes. Equation (6) also corresponds to a constant value of the second invariant of the deviatoric stress tensor. This is the criteria most often found to describe the yield of isotropic, ductile metals. Although the uniaxial data obtained at 70°F indicated some differences in yield strength (Fig. 13), the combined data in Figure 22 indicates the hot-pressed block material is essentially isotropic in yield strength.

The outer locus in Figure 22 corresponds to the fracture strength, since at this temperature the behavior is essentially brittle and fracture occurs before the onset plastic instability or necking. The failure point in pure compression may have been influenced by a localized structural buckling of the tube just prior to fracture. Otherwise, structural buckling was not observed under these test conditions. The failure surface is given by the equation

$$\sigma_L^2 - \sigma_L\sigma_T + 1.44\,\sigma_T^2 + 30\,\sigma_L - 10.1\,\sigma_T + 2.6\,\sigma_{LT}^2 = 58.2^2 \qquad (7)$$

This surface is again an ellipsoidal surface, as in Equation (6); however, the ellipse is no longer symmetric with respect to the principal axes.

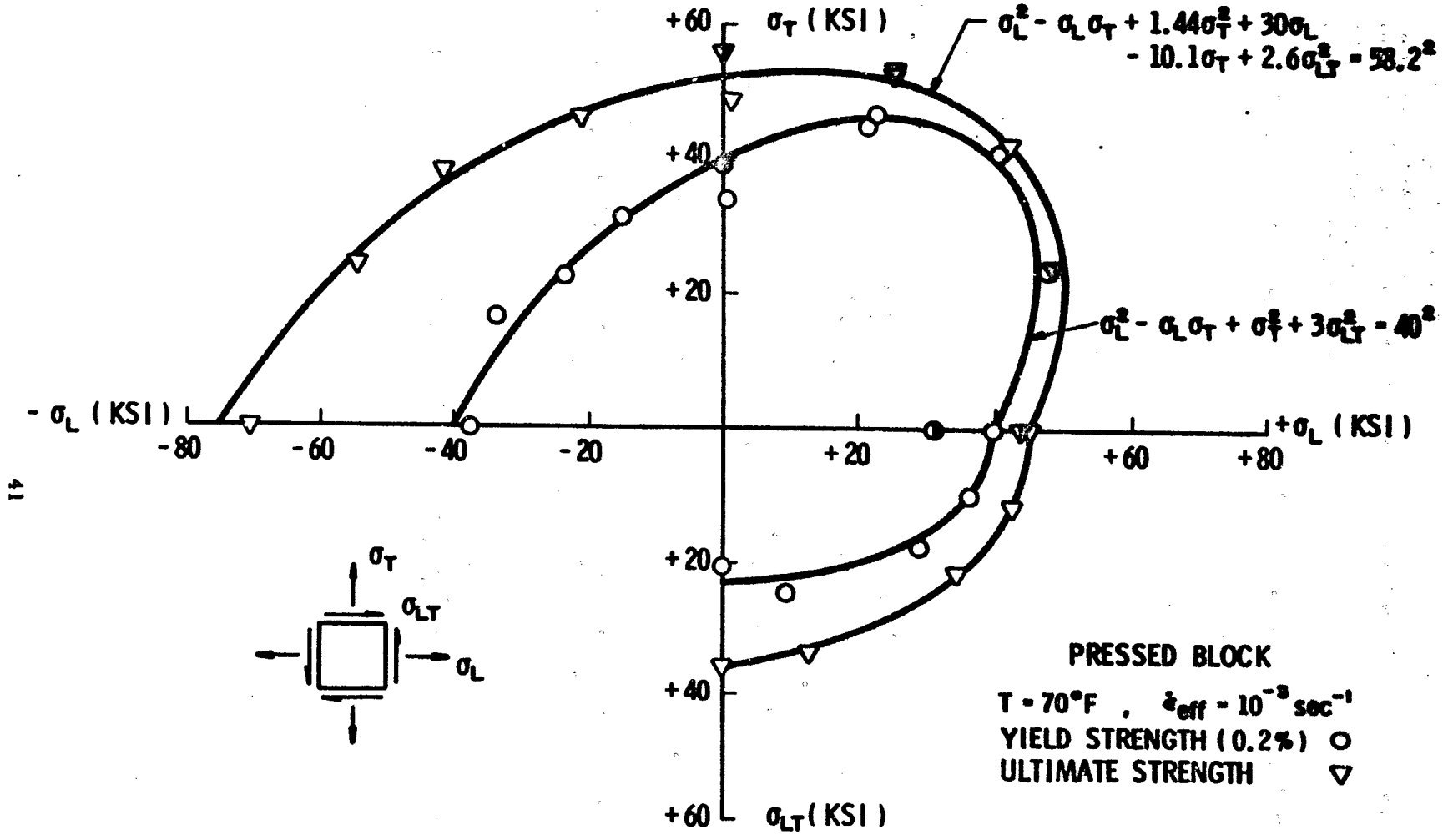

FIGURE 22. YIELD AND ULTIMATE (FRACTURE) STRENGTH FOR HOT-PRESSED BLOCK (UNIAXIAL SPECIMENS ●, ▼, TUBE SPECIMENS ○, ▽)

Equation (7) is a special case of the empirical fracture criteria proposed by Hoffman[9] for orthotropic materials. Hoffman extended Hill's anisotropic plasticity theory to include linear terms in the normal stresses so as to account for differences between tensile and compressive strengths. The symmetry in shear stress is retained. For plane stress, the Hoffman criteria can be expressed by the equation:

$$\frac{\sigma_L^2 - \sigma_L\sigma_T}{F_{L_c} F_{L_t}} + \frac{\sigma_T^2}{F_{T_c} F_{T_t}} + \frac{F_{L_c} - F_{L_t}}{F_{L_c} F_{L_t}} \sigma_L + \frac{F_{T_c} - F_{T_t}}{F_{T_c} F_{T_t}} \sigma_T + \frac{\sigma_{LT}^2}{F_{LT}} = 1 \qquad (8)$$

where F_L, F_T and F_{LT} are the uniaxial fracture strengths in the normal and shear directions and the subscripts c and t denote compression and tension, respectively. The fit obtained for the hot-pressed block and expressed in Equation (6), corresponds to the following uniaxial strengths:

$$F_{L_t} = 45 \text{ ksi}$$

$$F_{L_c} = 175 \text{ ksi}$$

$$F_{T_t} = 52 \text{ ksi}$$

$$F_{T_c} = 45 \text{ ksi}$$

$$F_{LT} = 36 \text{ ksi}$$

The increased fracture strength in the longitudinal compressive direction appears due to both an increased work-hardening rate and an increased ductility as compared with the tensile direction. The derived transverse compressive strength, however, is lower than the corresponding tensile strength. No compressive tests were made for the transverse direction, this strength being derived from the fit to the data points in the other quadrants.

The effect of elevated temperature on the surfaces for yield and ultimate strength is illustrated in Figures 23 and 24. This data was obtained only in the σ_L - σ_{LT} quadrant. The data at 600 and 1000°F indicate only a change in size but not in shape of the Mises ellipse obtained at 70°F. Thus, the reduction in yield strength with temperature does not appear to be directionally dependent. The size of the yield locus is characterized by the tensile strengths of 40, 26 and 21.6 ksi at 70°, 600° and 1000°F, respectively.

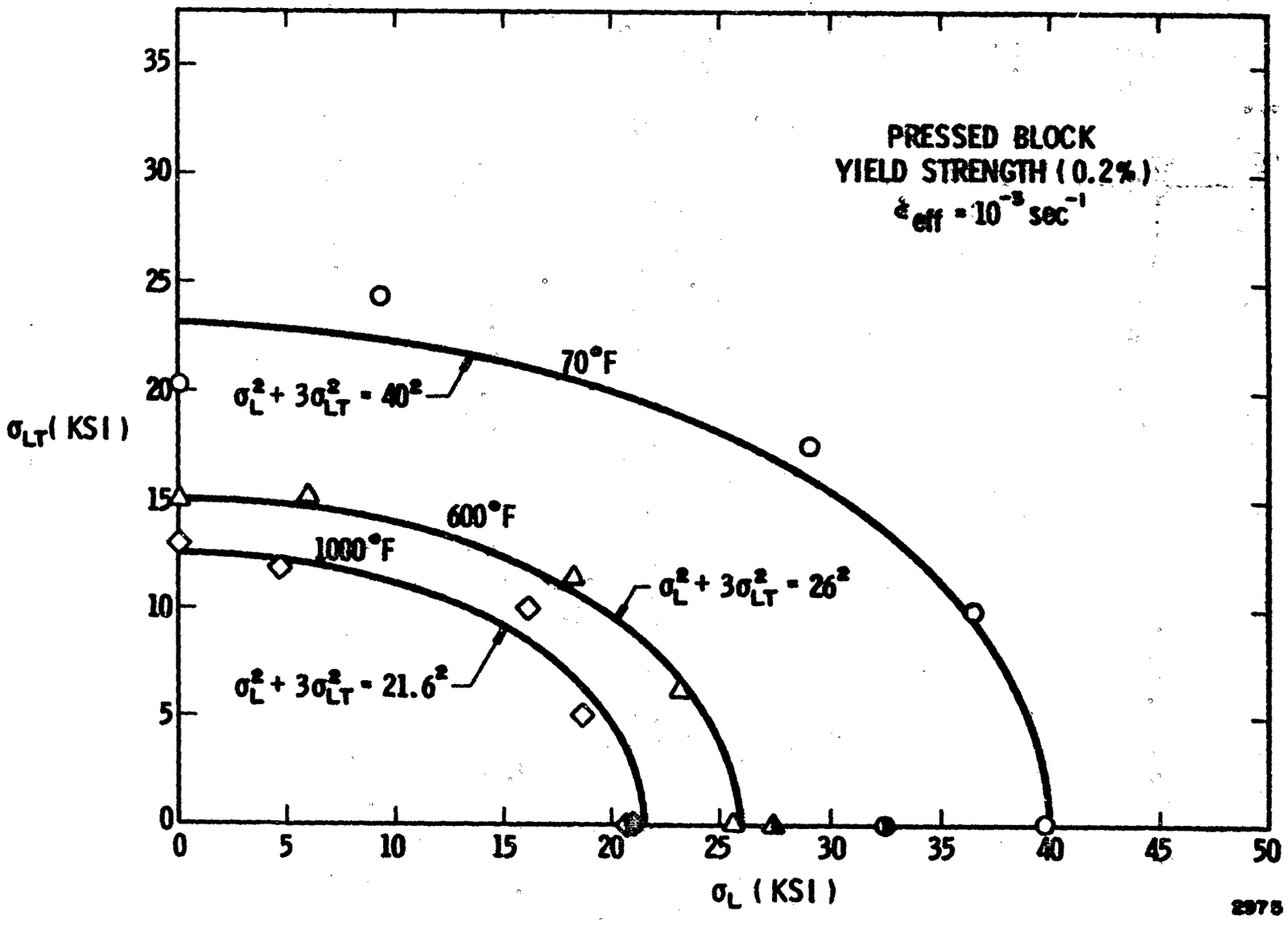

FIGURE 23. EFFECT OF TEMPERATURE ON THE YIELD SURFACE OF HOT-PRESSED BLOCK

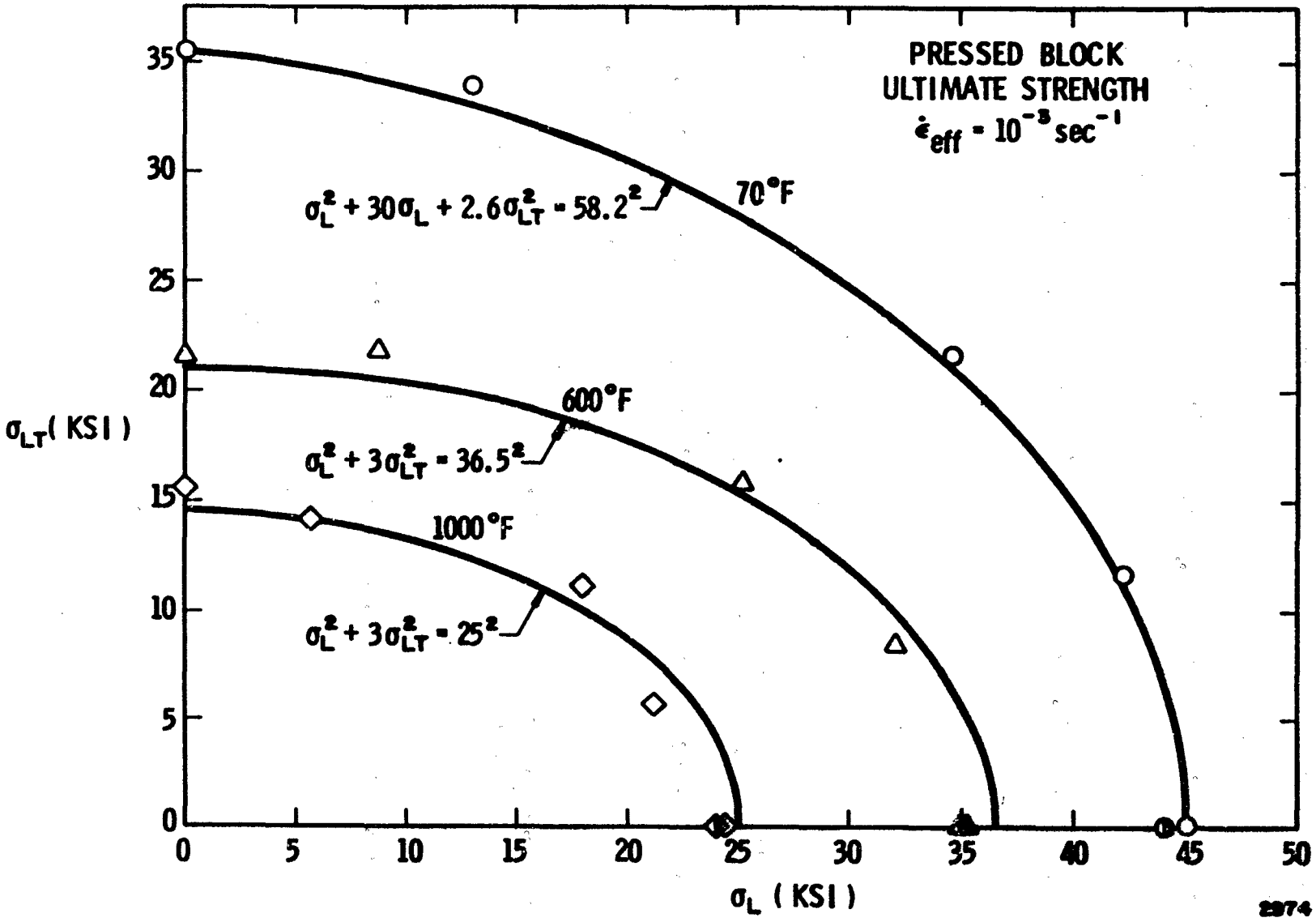

FIGURE 24. EFFECT OF TEMPERATURE ON THE ULTIMATE STRENGTH OF HOT-PRESSED BLOCK

The loci for ultimate strength, Figure 24, shows a change in shape between 70°F and 600°F. However, at 70°F the locus is defined by the fracture stress. At 600 and 1000°F the beryllium becomes ductile and the loci are defined by a maximum in the engineering stress-strain curve. At these temperatures, rupture occurred only after a maximum in the applied load had occurred indicating a plastic instability and appreciable necking. The curves for ultimate strength at 600° and 1000°F are concentric with the yield curves, having only a somewhat larger diameter. Since at elevated temperature, there is little work-hardening between the offset yield strength and the maximum strength, the two loci have nearly the same shape.

The extruded material exhibited very low ductility in the transverse direction. In the σ_T, σ_L plane, fracture usually occurred before an 0.2% offset strain was reached. This is indicated in Figure 25 where, for a large number of stress ratios, the failure surface falls within the offset strain criteria. In torsion the ductility is greatly increased, as can be seen from the stress-strain curves of Figure 20.

In the σ_L, σ_T plane the fracture surface for extruded beryllium is defined by the St. Venant maximum strain criteria. This is one of the classical criteria for brittle materials. It states that failure will occur when the maximum normal strain reaches a critical value. In stress space the surface becomes an oblique parallelepiped because of the Poisson coupling between the principal axes. The limiting stress surface is determined from the strains by using the elastic stress-strain relations. Thus, a negligible amount of plastic yielding is assumed. The linear regions of the fracture surfaces are defined by the relations

$$\sigma_T = F_T + \nu_{LT} \left(\frac{E_L}{E_T}\right) \sigma_L \qquad (9)$$

and

$$\sigma_L = F_L + \nu_{LT}\, \sigma_T$$

where F_L and F_T are the uniaxial fracture strengths, ν_{LT} is Poisson's ratio, and E_L and E_T are the elastic moduli. For the elastic properties a value of 0.085 for Poisson's ratio was used and the modulus ratio was assumed to be essentially unity. These values were not measured directly but are in general agreement with measured values for similar beryllium alloys obtained by Fenn, et al.[10]. The uniaxial strengths are $F_L = 82.5$ ksi and $F_T = 51.5$ ksi.

In the torsion plane the ductility increases markedly. The yield locus is given by

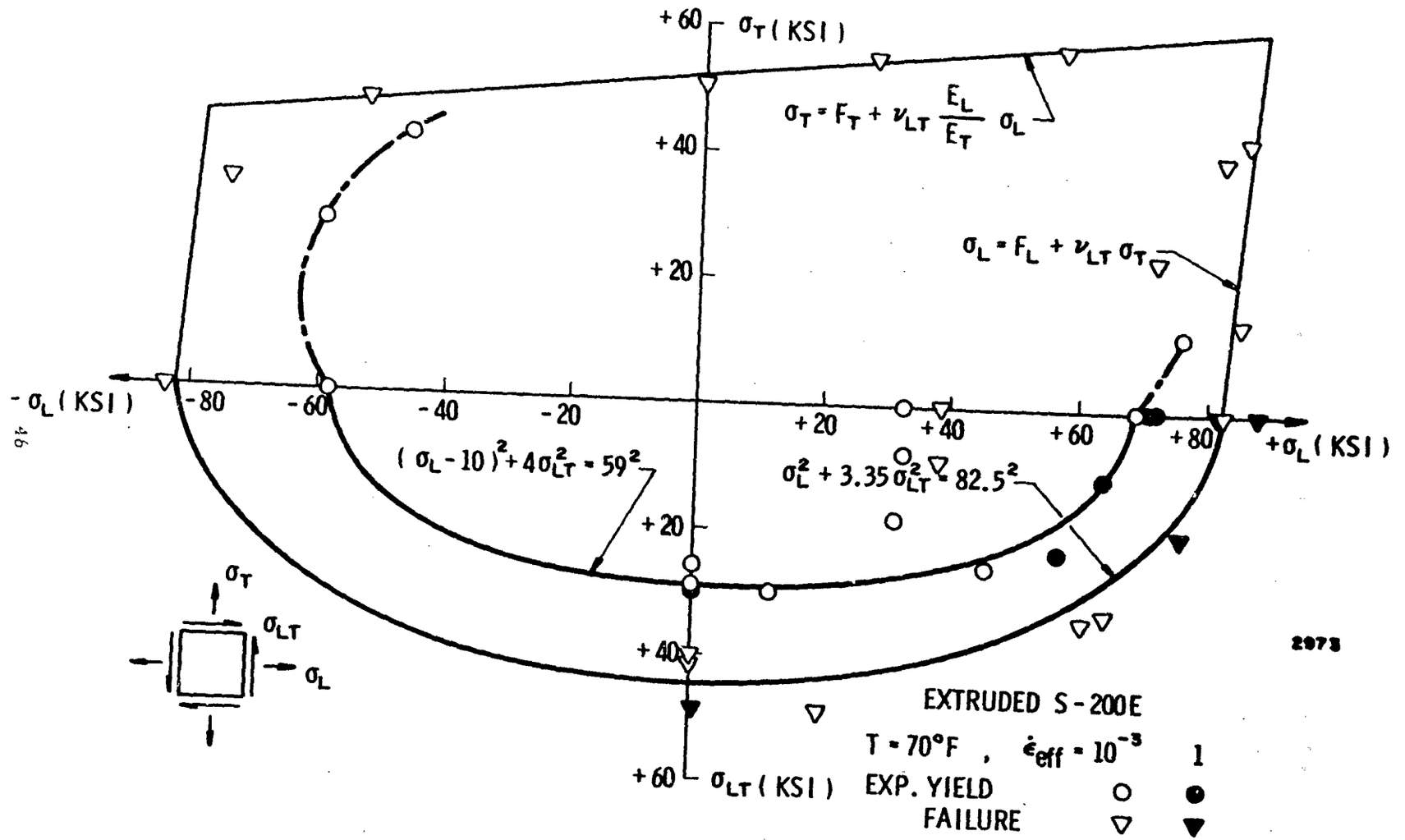

FIGURE 25. YIELD AND FRACTURE STRENGTH FOR EXTRUDED BERYLLIUM AT 70°F

$$(\sigma_L - 10)^2 + 4\sigma_{LT} = 59^2 \qquad (10)$$

and the failure locus by

$$\sigma_L^2 + 3.35\,\sigma_{LT}^2 = 82.5^2 \qquad (11)$$

A number of the extruded specimens tested exhibited excessively low tensile strength (σ_L <40 ksi). These specimens are included in Figure 25, but their strengths do not correlate with the remaining population of uniaxial and tubular specimens. The reason for these anomalously low strengths is uncertain. The yield and failure loci given by Equations (10) and (11) therefore rely on only a limited number of tests at 70°F. Test points are included for two different effective strain rates, 10^{-3} and 1 sec^{-1}. The higher speed tests yield slightly higher strengths with no apparent change in shape of the loci. The yield ellipse, defined by Equation (10), has the shape of the Tresca (maximum shear stress) criteria but is translated in the direction of the tensile axis. This translation is analogous to kinematic hardening. In comparison with the hot-pressed block, the severe work-hardening produced during extrusion increases the strength properties in all directions tested, most markedly the longitudinal tensile strength which is approximately doubled. However, this strength increase is accompanied by a significant decrease in the transverse ductility of the extruded material.

The effect of strain rate and temperature on the yield strength in the tension-torsion mode for extruded beryllium is compared in Figure 26. The yield loci are fit with quadratic surfaces although at the higher temperatures there is a pronounced bulging or point effect along the tensile (or extrusion) axis as indicated by the dashed lines. This is the type of behavior that would be predicted by a slip-line theory for strain hardening along this axis. The yield loci, indicated by the solid curves, are given by the relations listed below for the indicated test conditions.

$$\begin{aligned}
70°F \begin{cases} 10^{-3}\ sec^{-1} \\ 1\ sec^{-1} \end{cases} & \quad (\sigma_L - 10)^2 + 4\,\sigma_{LT}^2 = 59^2 \\
& \quad (\sigma_L - 10)^2 + 4\,\sigma_{LT}^2 = 61^2 \\
600°F \begin{cases} 10^{-3}\ sec^{-1} \\ 1\ sec^{-1} \end{cases} & \quad (\sigma_L - 5)^2 + 3\,\sigma_{LT}^2 = 30.3^2 \\
& \quad (\sigma_L - 5)^2 + 3\,\sigma_{LT}^2 = 40.7^2 \\
1000°F \begin{cases} 10^{-3}\ sec^{-1} \\ 1\ sec^{-1} \end{cases} & \quad (\sigma_L - 5)^2 + 3\,\sigma_{LT}^2 = 28.2^2 \\
& \quad (\sigma_L - 5)^2 + 3\,\sigma_{LT}^2 = 34.6^2
\end{aligned} \qquad (12)$$

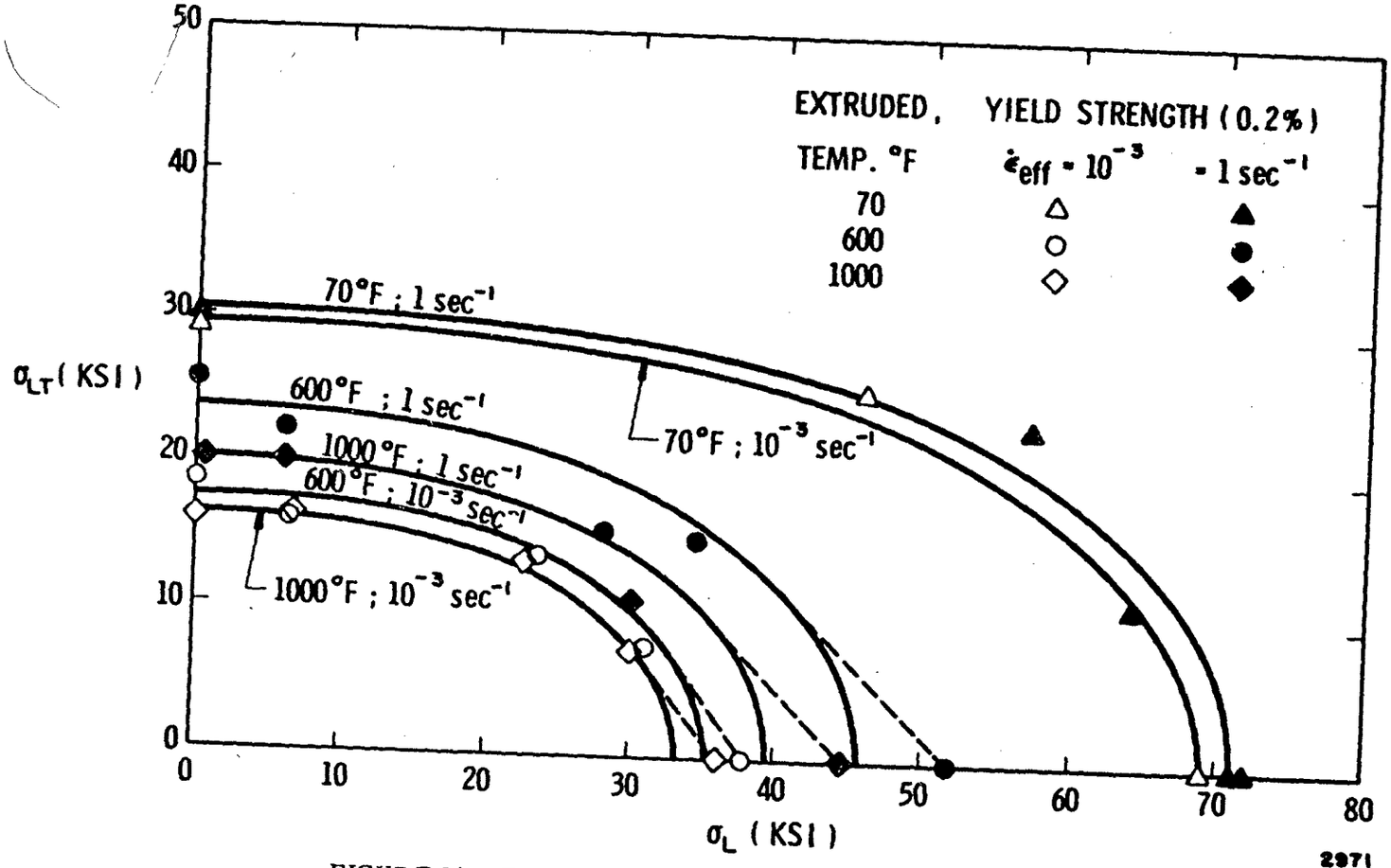

FIGURE 26. EFFECT OF TEMPERATURE AND STRAIN RATE ON THE YIELD STRENGTH OF EXTRUDED BERYLLIUM

Qualitatively, these results indicate that there may be some relaxation of the degree of anisotropy of the yield surface with temperature. Both the kinematic (translation) and the anisotropic (eccentricity) coefficients are reduced in magnitude between 70°F and 600°F. This might indicate some mild annealing is occurring tending to equalize the differential work-hardening produced during extrusion although these temperatures are still well below the recrystallization temperature (> 1290°F). The effect of strain rate at each temperature is an isotropic expansion of the yield locus. The expansion is greater at the higher temperatures in agreement with the uniaxial tests.

3. Ductility* Under Combined Stress

As has been noted several times, the ductility of the beryllium specimens as measured by the total strain to failure varies greatly with the state of stress. Figure 27 shows the magnitude of strain at fracture for the hot-pressed block. Note that the vertical strain axis is split between the transverse normal strain and the shear strain, similar to the stress plots. The values plotted are actually the measured strains projected on the indicated two-dimensional planes (only two strain components were measured for any stress condition). The actual strain state is three-dimensional.

The most prominent observation is the relatively high ductility in shear and the low ductility in the tension-tension quadrant. The shear ductility is evidenced in the tests for pure torsion and for tests with the stress ratio $\sigma_T/\sigma_L = -1$, which also yields maximum shear on 45° planes. The data shows that even a small torsional stress increases the amount of elongation that can be accommodated in the longitudinal direction. Conversely, biaxial tension produces failure strains considerably less than the maximum uniaxial tensile strain.

The modes of failure of the biaxial tubes corresponding to Figures 22 and 27 for hot-pressed block tested at 70°F and 10^{-3} sec^{-1} are indicated in Figure 28. The applied stress condition is indicated by the element shown below each tube. The fractures generally occur in a direction perpendicular to the maximum normal tensile stress. For example, in the tension-torsion plane the angle of the helical type fractures with respect to the specimen axis rotated from 45° to 90° in accordance with the direction of the maximum principal stress. In the tension-tension and tension-compression quadrants the fractures were

---

* In this report the term ductility is used in the general sense as the ability to deform in the plastic range without breaking, rather than designating only the elongation at failure in a tension test.

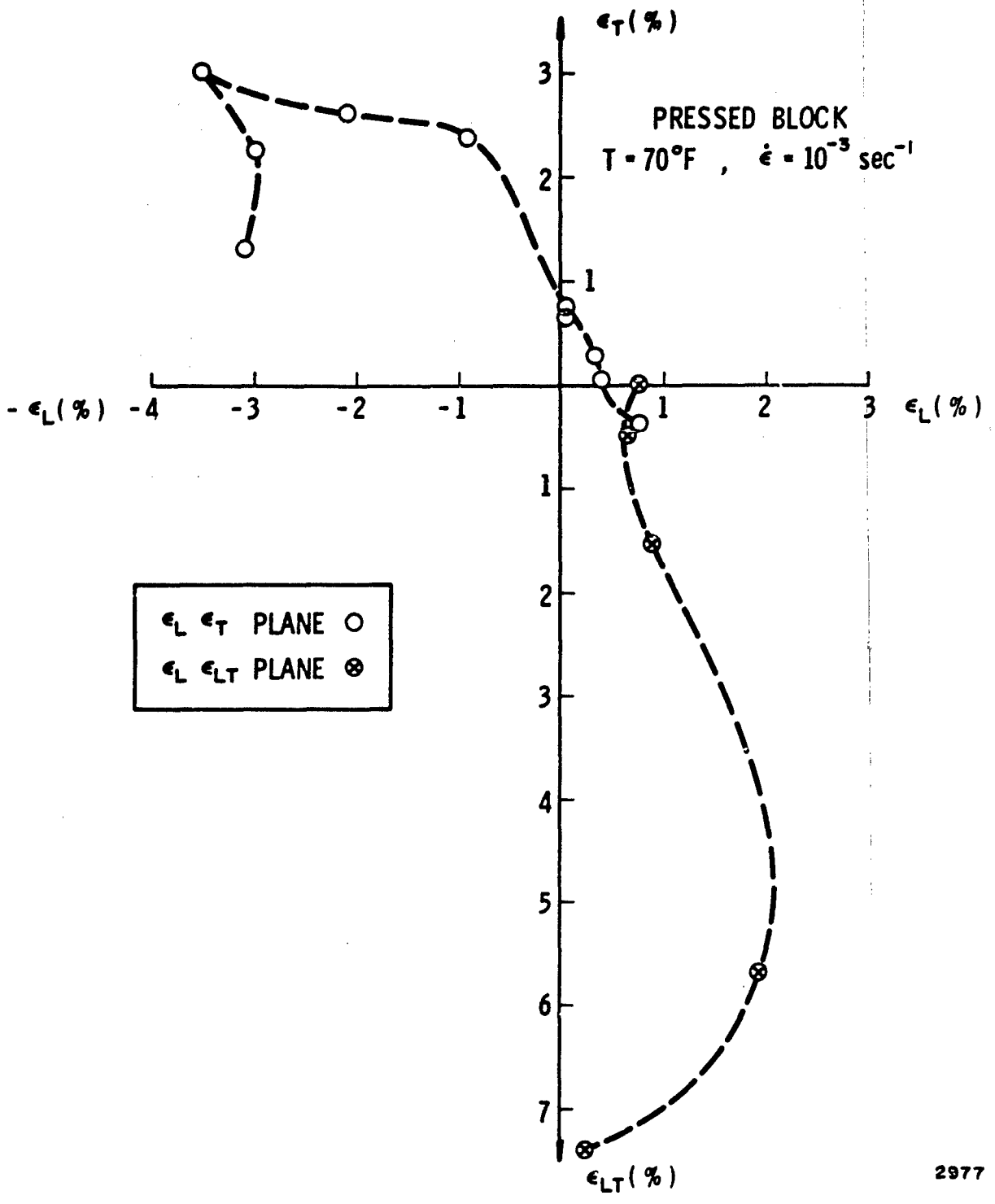

FIGURE 27. FRACTURE STRAINS FOR HOT-PRESSED BLOCK

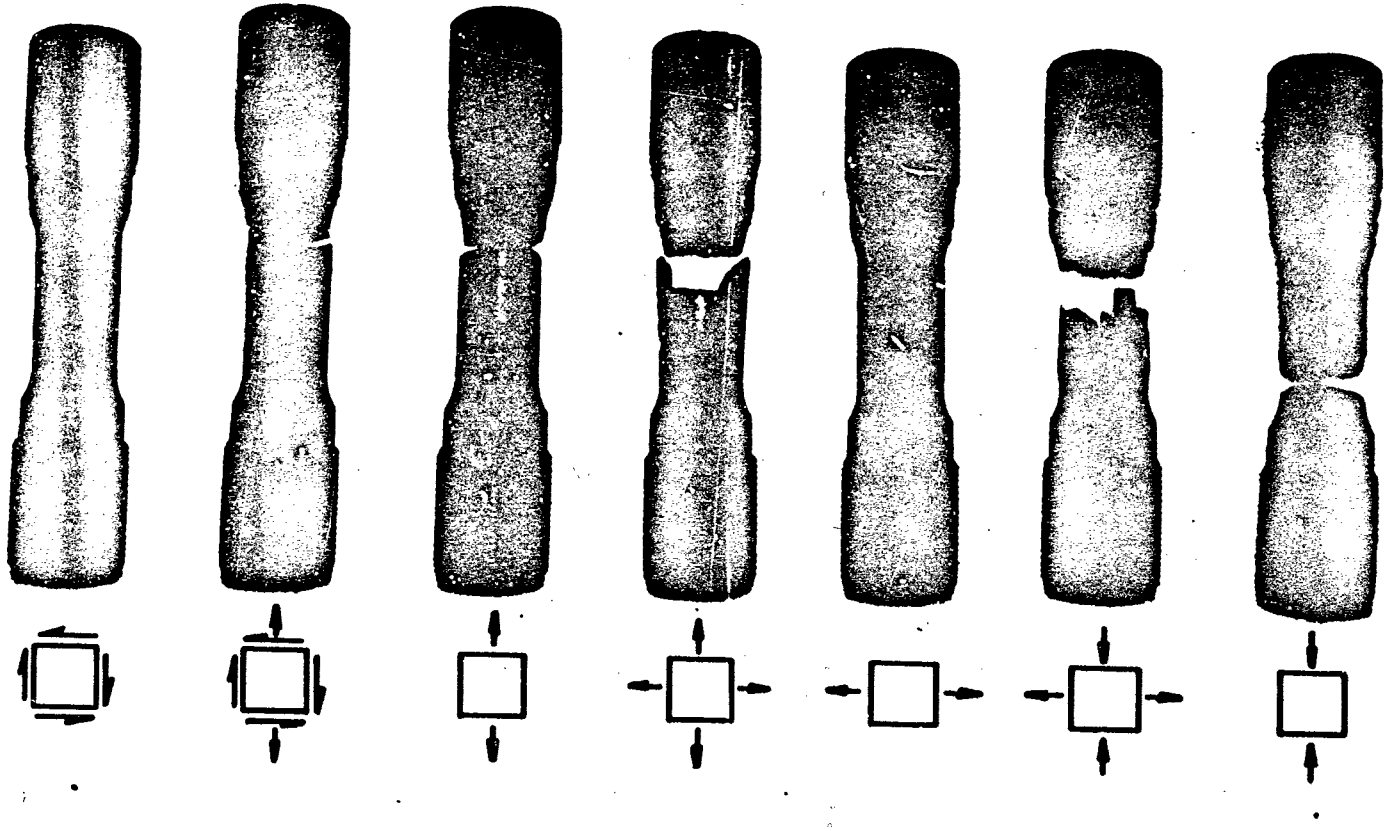

FIGURE 28. FRACTURE MODES FOR HOT-PRESSED BLOCK BERYLLIUM SPECIMENS TESTED AT 70°F

generally irregular of mixed 0° and 90° surfaces. In pure compression, the fracture may have been preceded by a localized buckling.

Figure 29 shows the fracture strain plot for extruded beryllium at 70°F and 10^{-3} sec^{-1}. Data was available to define the ϵ_L, ϵ_T plane only. In pure torsion, however, the maximum shear strain was in excess of 8%, again indicating a high shear. The minimum on the ϵ_T axis corresponds to a stress ratio $\sigma_T/\sigma_L = 0$, being an elastic fracture with very small Poisson's ratio ($\nu_{LT} = 0.085$). The minimum on the ϵ_L axis occurs at a stress ratio $\sigma_T/\sigma_L = 1/6$. There appears to be a relative maximum in the tension-tension quadrant. A similar effect will be seen later for titanium. As in the pressed block, the ductility is very low in the tension-tension quadrant, with almost no transverse ductility.

The fracture modes are shown in Figure 30. For the extruded beryllium specimens there are two dominant fracture orientations; one parallel to the axis of the tube and to the grain structure and a second at an angle of 62° to the extrusion axis. The fractures at 62° were characteristic of specimens having a stress component in the longitudinal direction and this fracture angle was previously observed in the uniaxial extruded specimens. For extruded specimens under transverse stress (or strain), longitudinal fractures generally developed. Only in pure torsion, where a helical fracture at an angle of 52° occurred, was another significant fracture orientation observed. The pure compression specimen (right-hand side of Figure 30) has multiple longitudinal fractures and a circumferential fracture which is actually made up of many small facets oriented at $\pm 62°$.

The failure due to pure tension in the longitudinal direction is interesting because it obviously initiated at one point and propagated in two planes at $\pm$ 62° simultaneously. This is the analog of the twin conical fracture surfaces developed in the uniaxial specimens, Figure 16. As in the uniaxial specimen this phenomenon persisted at 600°F but was not observed at 1000°F where the fracture was more a ductile tearing rather than cleavage. The effect of temperature is shown in Figure 31. Figure 32 shows the dominance of the 62° fracture angle for all three types of specimen tested in tension.

4. Adiabatic Effects During High Speed Tests

During the high speed tests on the tubular specimens it was possible to observe the temperature rise of the specimen during the deformation. At a strain rate of 1 sec^{-1}, the test is adiabatic and the thermocouple has sufficient response to follow the temperature rise. The automatic controller for the applied radiant heating cannot compensate at this deformation rate for the adiabatic temperature rise. Figure 33 shows a typical

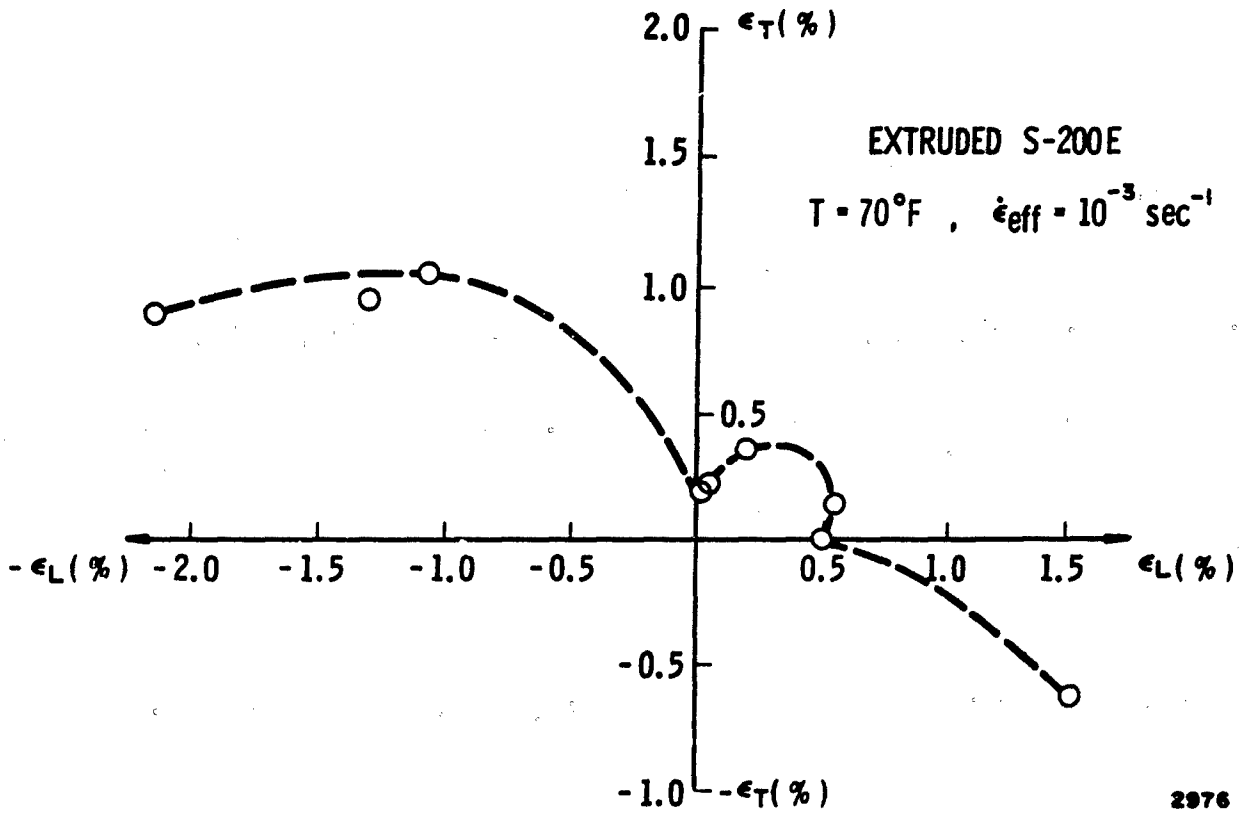

FIGURE 29. FRACTURE STRAINS FOR EXTRUDED BERYLLIUM

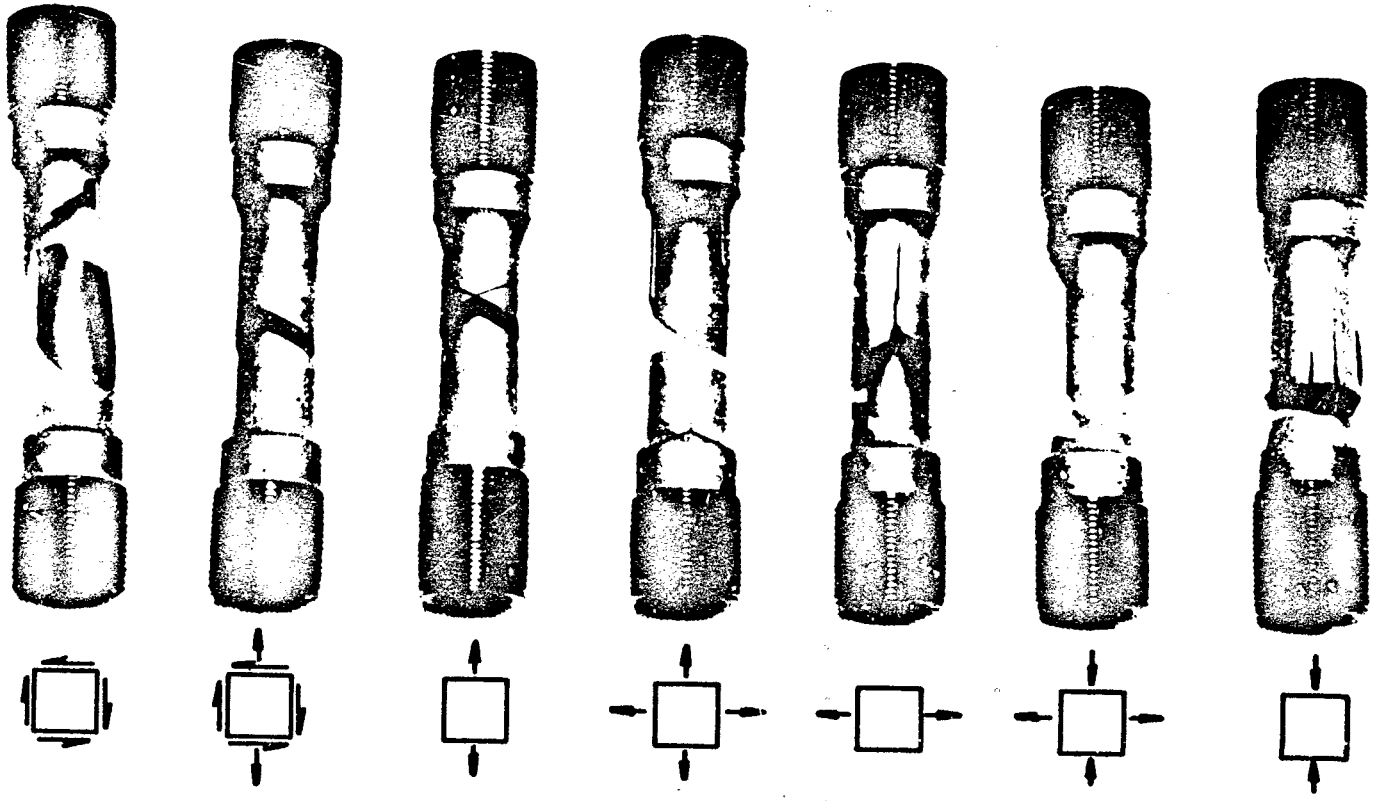

FIGURE 30. FRACTURE MODES FOR EXTRUDED BERYLLIUM SPECIMENS TESTED AT 70°F

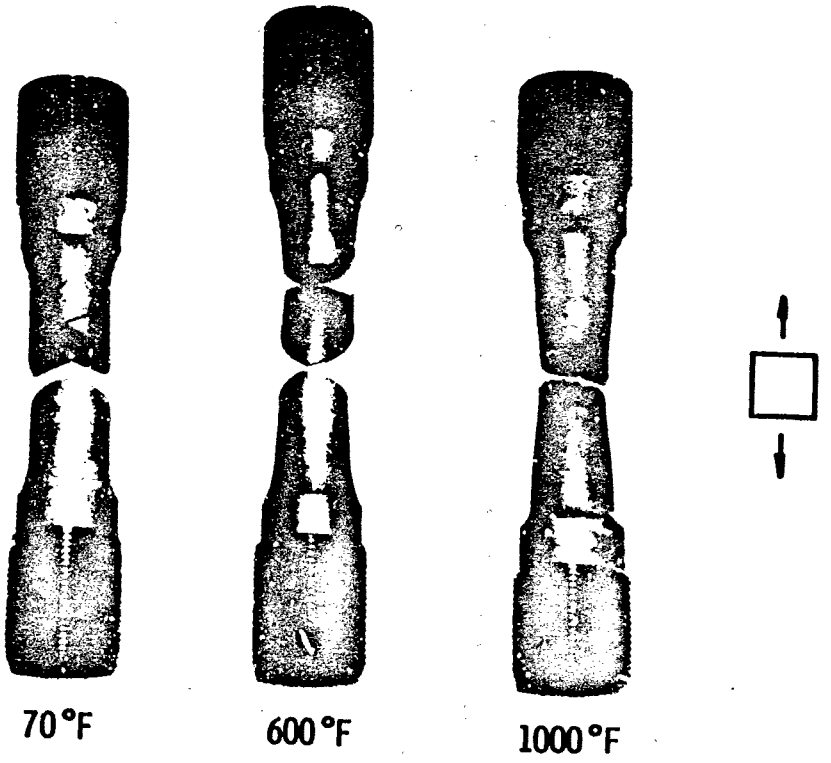

FIGURE 31. FRACTURE MODES FOR EXTRUDED BERYLLIUM AT THREE TEMPERATURES

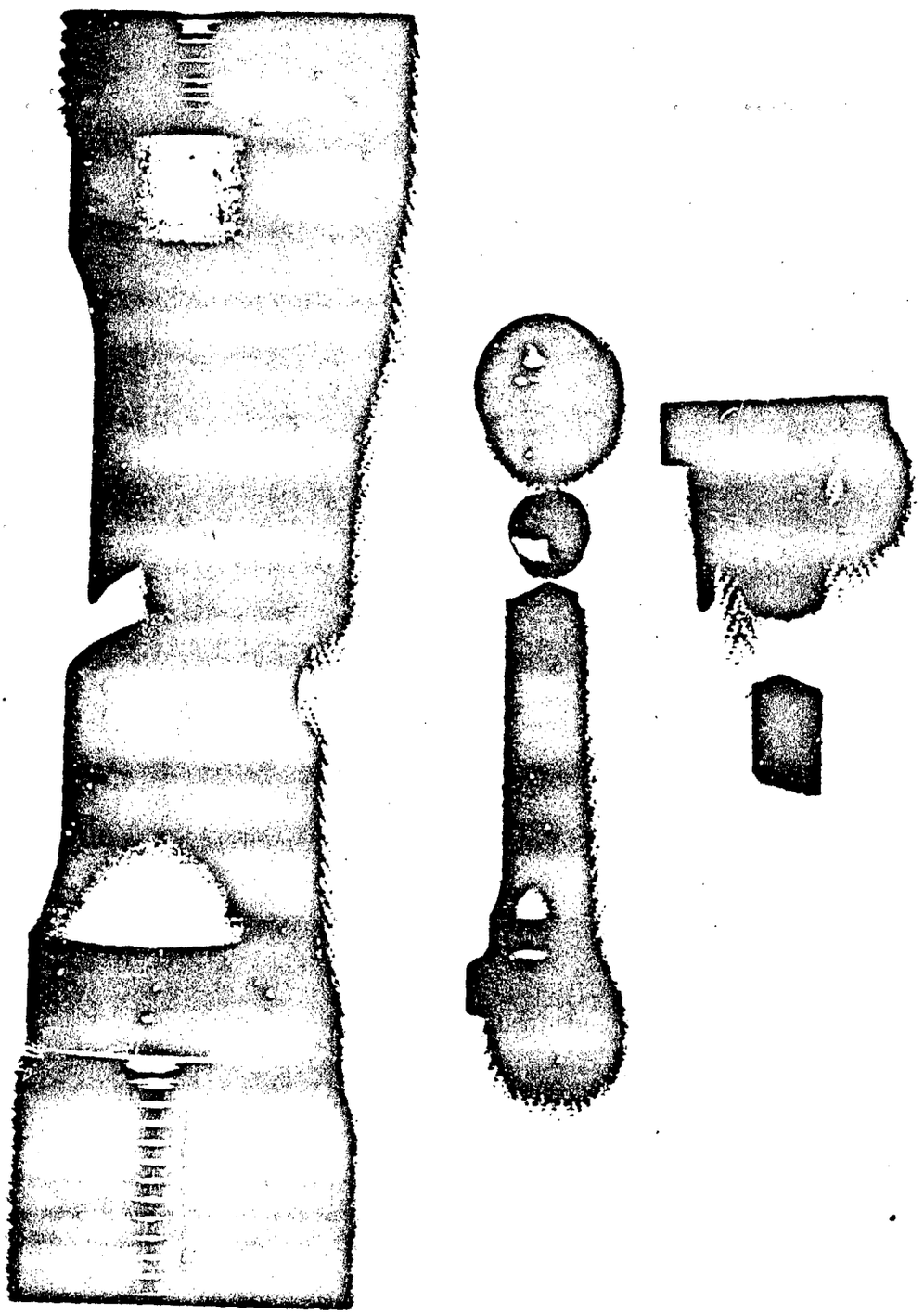

FIGURE 32. TENSILE FRACTURES FOR THREE DIFFERENT EXTRUDED BERYLLIUM SPECIMENS

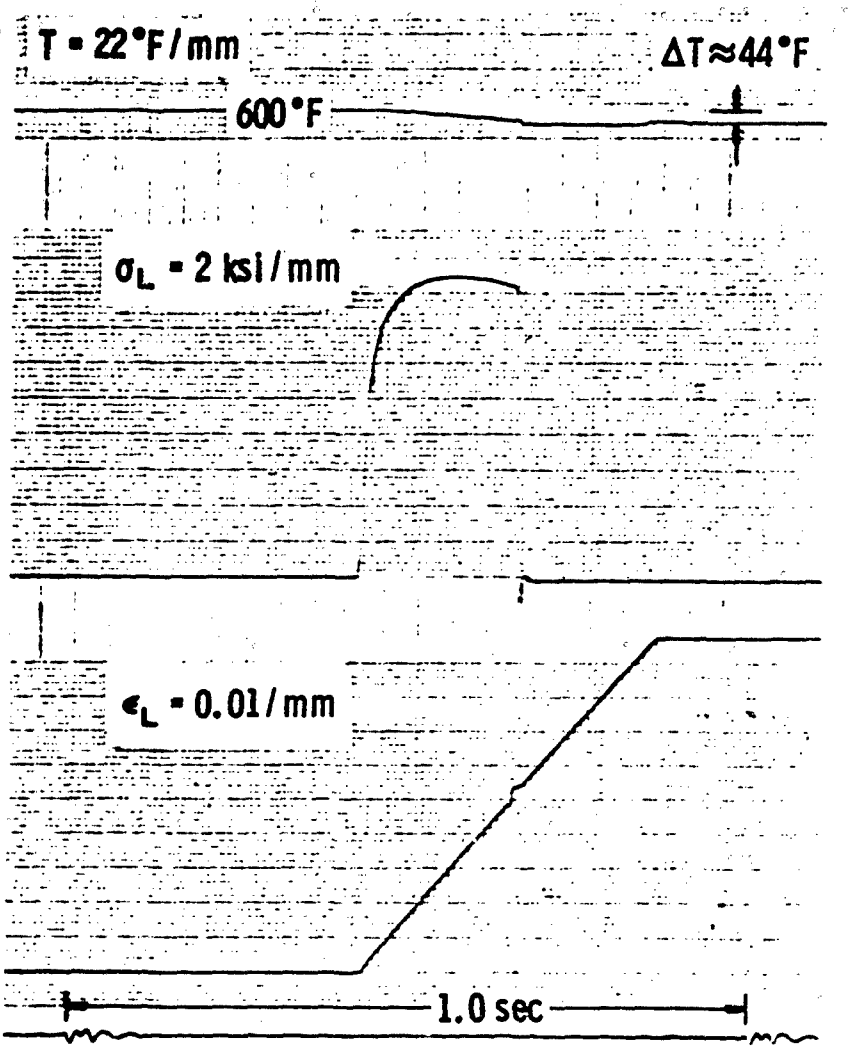

FIGURE 33. ADIABATIC TEMPERATURE RISE DURING A TENSILE TEST OF EXTRUDED BERYLLIUM AT 600°F and 1 sec^{-1}

record for a test at 600°F (temperature was not recorded on the 70°F tests). This is an extruded beryllium specimen tested in longitudinal tension. The maximum strain is 25% obtained in about 1/4 second.

The adiabatic temperature rise, ΔT, is proportional to the plastic work according to the relation

$$\Delta T = \frac{k_1}{\gamma c} \int_0^{\epsilon^P_{max}} \sigma \, d\epsilon^P \qquad (13)$$

where γ is the density and c is the specific heat of beryllium. The proportionality constant k_1 is generally of the order of 0.85 - 0.90, indicating that a portion of the energy is stored in the lattice and not dissipating as heat. Using the values $\gamma = 1.85$ gm/cc (Table 2), $c = 0.6$ cal/gm/°C (Ref. 11) and evaluating the integral in Equation (13) from the data of Figure 33, the estimated ΔT is 53°F for $k_1 = 1$, i.e., all the plastic work is dissipated as heat. The measured temperature rise is approximately 44°F. Exact agreement would be obtained with $k_1 = 0.83$. The accuracy of the temperature measurement and the uncertainty in the value for specific heat of beryllium make this value of k_1 only approximate. However, the correlation does show the general agreement and the magnitude of the adiabatic effect.

C. Biaxial Tests on 6A l -4V Titanium

A limited number of biaxial tests with titanium specimens were performed under axial loading and internal pressure. Uniaxial test data on 6A l -4V titanium had been obtained earlier[1] for a wide range in strain rate and temperature. The present biaxial tests are for 70°F and two effective strain rates, 10^{-3} sec^{-1} and 0.5 sec^{-1}.

Figure 34 shows the values for yield (0.2%) and ultimate strength. Under these test conditions the ultimate strength is a fracture strength. The control during these tests was such that the yield strength could be determined accurately only at the slower rate. The yield data appears to fall between the straight dashed lines corresponding to a maximum shear stress (Tresca) yield criteria and a Mises ellipse (dashed). The outer solid lines are also isotropic Mises ellipses for comparison with the fracture data points. The quantity and accuracy of this titanium data did not seem to warrant further fitting with alternate criteria. In the compression quadrant the data behaves somewhat like the extruded beryllium; however, the titanium is considerably more ductile and would not be expected to follow a brittle failure criteria.

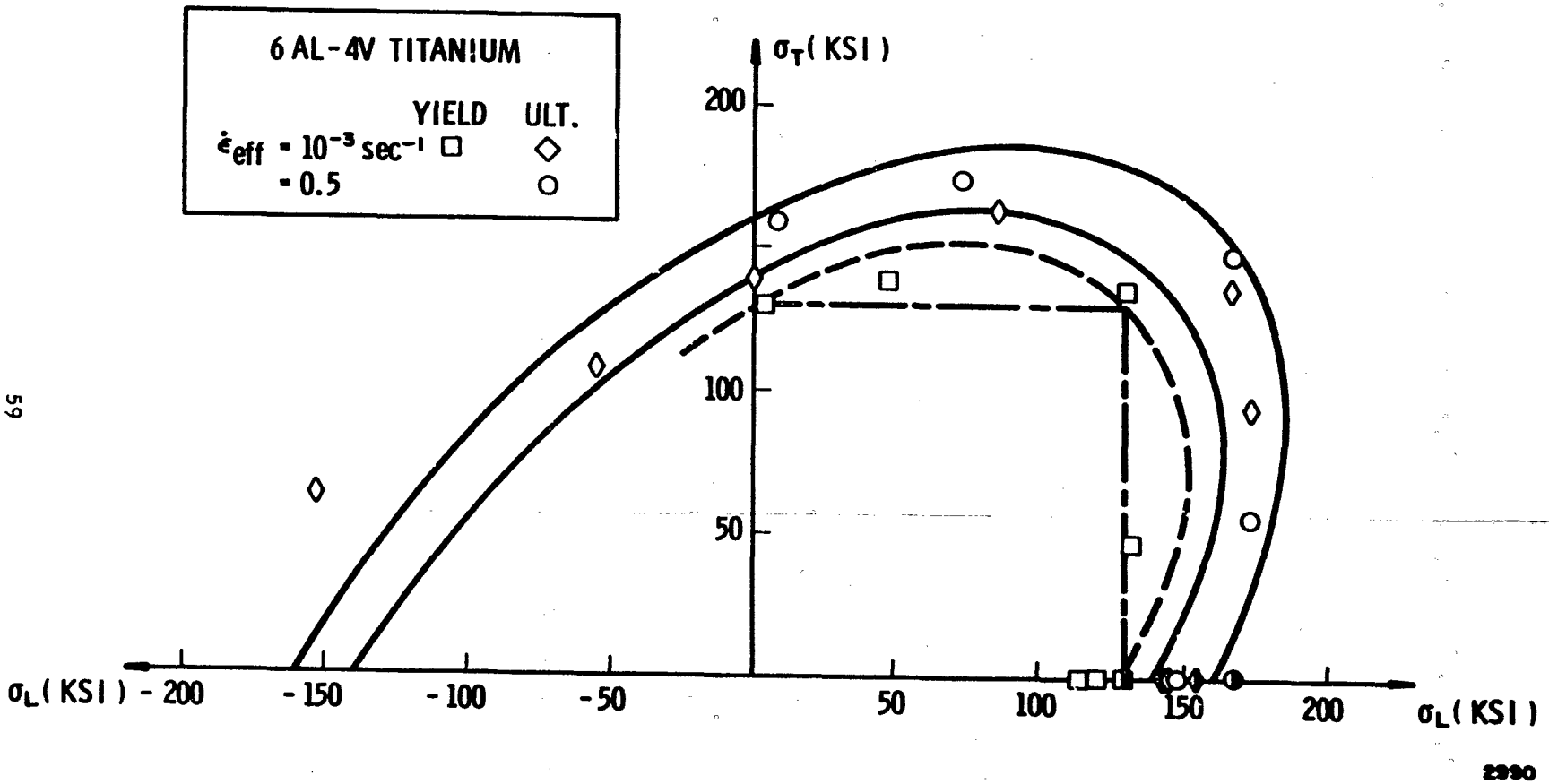

FIGURE 34. YIELD AND ULTIMATE STRENGTHS OF 6A1-4V TITANIUM

The fracture strains for the two different strain rates are shown in Figure 35. These loci are very similar in shape to the extruded beryllium, Figure 29. The minimums in elongation along the longitudinal and transverse strain axes correspond to stress ratios of $\sigma_T/\sigma_L = 1/3$ and 3, respectively. The elongations corresponding the uniaxial stress are approximately 8% in both longitudinal and transverse direction. The titanium is more isotropic than the extruded beryllium in both strength and ductility. While an increase in rate of deformation isotropically expanded the fracture surface for titanium, the strain at fracture is nearly isotropically decreased.

The fracture modes of the titanium tubes are shown in Figure 36. The fracture of the tube under uniaxial tensile stress seemed to follow localized concentrated slip bands oriented at $\pm 54°$ to the tube axis. This produced the serrated fracture contour observed.

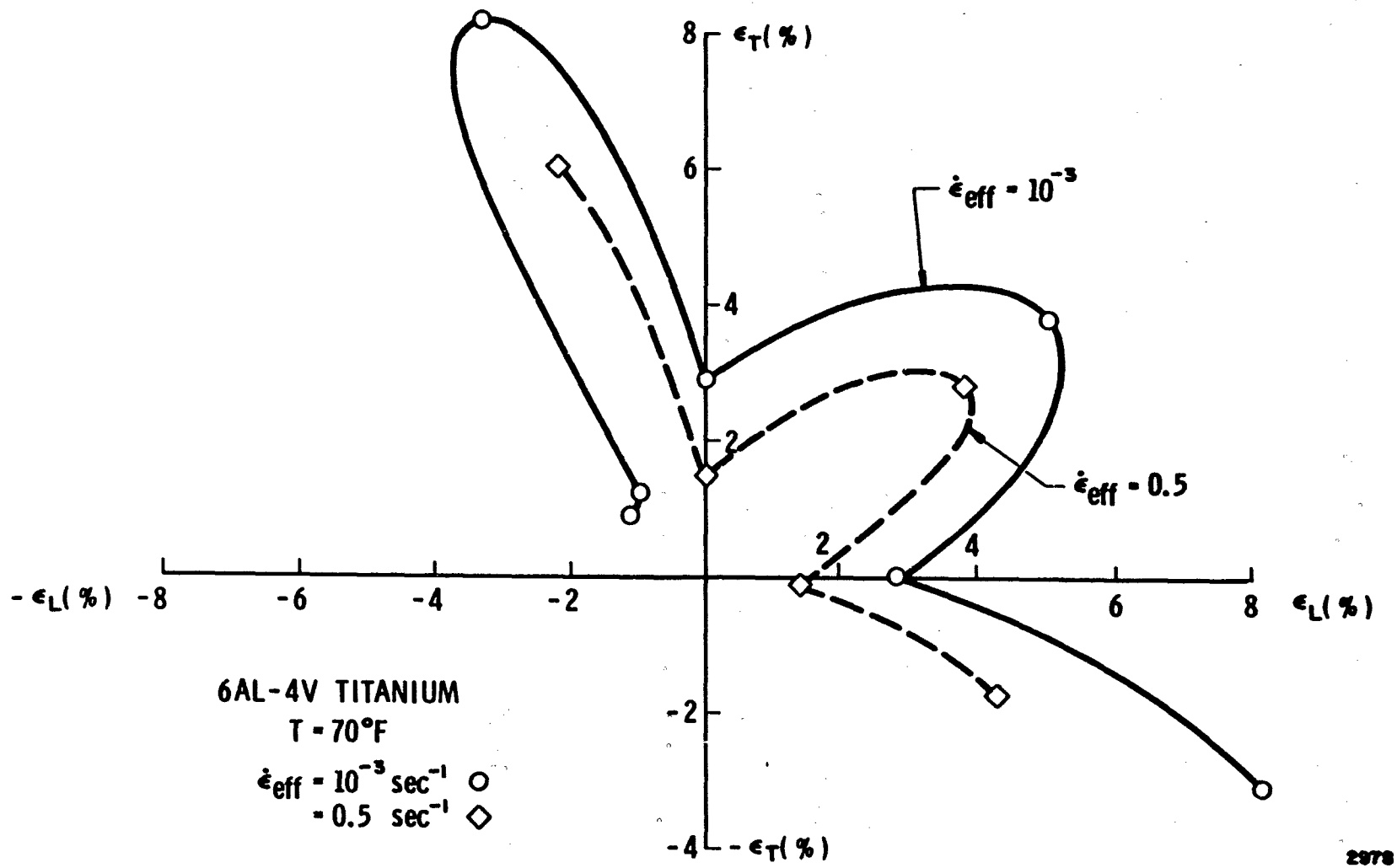

FIGURE 35. FRACTURE STRAINS FOR 6A1-4V TITANIUM TESTED AT TWO RATES

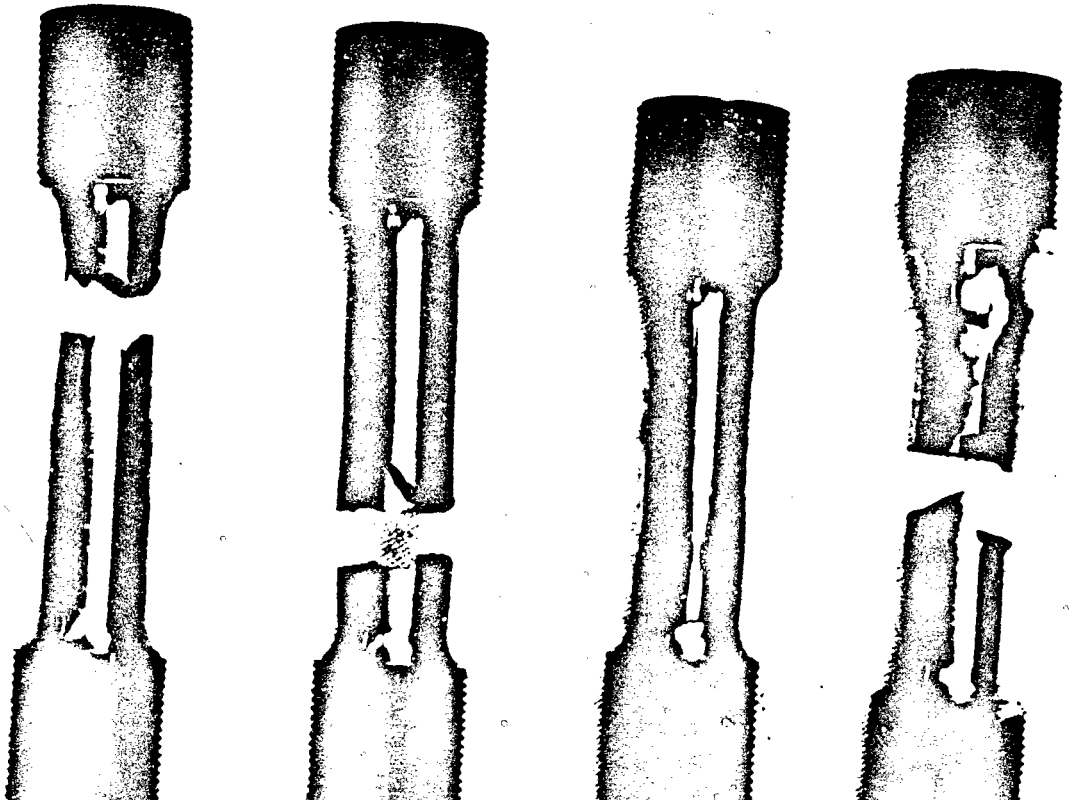

FIGURE 36. FRACTURE MODES FOR 6Al-4V TITANIUM SPECIMENS

SECTION V.

DISCUSSION

During the course of this effort considerable headway was made in the development of both the equipment and the test techniques for programmed multiaxial strength testing of materials over a wide range in temperature and in rate of deformation. The recent development of closed-loop hydraulic equipment opens up a wide range of new capability in materials testing that is yet to be fully exploited. The present tests were complicated by the multiple requirements of combined loading, high strain rates and high temperature. Additional complications are introduced when testing a brittle material such as beryllium. A few comments on the state of development of these techniques may prove useful to others working in the same area.

The development of biaxial strain transducers is a critical problem. Besides requiring the resolution of strain in two orthogonal directions, the transducer should be capable of measuring over a wide range in strain, temperature and frequency (or rate). Directly bonded resistance strain gages are limited in strain and temperature range. Clip type compliance gages are restricted in temperature and frequency response. Optical type displacement tracking devices offer promise but, as yet, have been used primarily for one-dimensional strain measurement. The cost of multiple channel optical tracking equipment may be excessive for the multiaxial application. The biaxial capacitance transducer described in Section III has proved very successful. Because of its wide dynamic range, it is able to resolve strain from the elastic region out to 50% or more plastic deformation. Wide dynamic range is a requirement for its use as the feedback element in the servo-control system. It has been used at temperatures to 1700°F with water cooling. Because the transducer mounts inside the tubular specimen and the grip, it does not interfere with external radiant heating. Another important feature is the measurement over a short gage length (0.5 inch) in the center of the tubular specimens. This minimizes the error due to nonuniformity in strain caused by end restraint effects, and to nonuniform axial temperature gradients at elevated temperatures. Such temperature gradients are unavoidable because of the massive grips required for biaxial specimens. These grips are generally water cooled.

The frequency response of the capacitance transducer is restricted only by the compliance of the attachment arms. These arms are spring loaded against the inside diameter of the specimen and must have sufficient flexibility to accommodate changes in diameter of the specimen during deformation. They also carry cooling water to protect the body of the

transducer from excessive heating. Thus, the attachment compliance cannot be eliminated. The lowest resonant frequency of the transducer is its torsional frequency which occurs at 250 Hz. However, we have observed no resonance problems with the transducer over the range in accelerations produced in the biaxial tests conducted to date.

We have applied the internal pressure mode only at room temperature. High temperature application is restricted by the properties of the internal working fluid. Because of the limited temperature range, compliance type extensometers were used for the tests involving internal pressure and axial loading. Development of better extensometers and also high temperature capability is needed for this mode of loading. The tension-tension quadrant is particularly important in many practical applications.

For accurate control of high rate tests a very tight servo-control loop is required. Our control capability at high rates is continuously improving. With feedback from an extensometer on the specimen, the control system has to make up for the compliance in the rest of the system as well as maintain the prescribed strain-time history in the gage section. While the biaxial mode has two independent control systems, they are coupled together by the plastic response of the specimen. Present capabilities provide good control, even in biaxial modes, at strain rates up to approximately 1 sec^{-1}. While the equipment can reach rates in excess of 10 sec^{-1} in plastic deformation there are limitations on the magnitude of the initial strain acceleration before constant rate is achieved. This was observed in Figure 12. The main limitation at present is in the hydraulic servo valve and its opening time and frequency response. In biaxial testing it is necessary to use a tight grip system with no self-aligning mechanisms. Thus, it is not possible to have any crosshead travel time before the load is applied. Future improvements will be made in the closed-loop frequency response of the entire system. It is felt that hydraulic machines of this type will be capable of testing at rates over at least six orders of magnitude, e.g., from 10^{-5} to 10 sec^{-1}.

Classical experiments in plasticity under combined stress have been concerned primarily with determination of the static yield surface and its change in shape caused by various degrees of work hardening. Detailed analysis of the yield surface depends very much on the criteria for yielding used in the definition of the surface. Paul[12] has recently given an excellent review of both the analytical and the experimental basis of macroscopic yield and fracture criteria. He notes the almost complete lack of information concerning the effects of temperature and rate of deformation on yield or

failure criteria under multiaxial stress. Blass and Findley[13] report some recent experimental work concerning biaxial creep surfaces including temperature effects. Another interesting time effect on the yield surface was noted in recent tests on aluminum by Smith and Almroth[14] who found that strain hardening corners developed in the yield surface tended to relax or recover toward the initial yield surface after a period of rest under zero stress.

From the present tests on beryllium and titanium and from some limited previous work[4,5], the effect of temperature or strain rate on the yield surface is isotropic, i.e., the yield surface expands or contracts in size but does not change its shape. An exception is the case where the metal has been worked so that it has been preferentially strain hardened in some direction. In this case, if the temperature is increased to the point where recovery or annealing can take place, the accompanying change in strength properties will also probably be preferential, the surface contracting toward its annealed or initial state. An example is the extruded beryllium rod which is initially severely worked in the longitudinal direction. At elevated temperatures the yield surface contracted more in the longitudinal or extrusion direction than in shear. Smith and Almroth's[14] aluminum data showed preferential recovery of the prestrained yield surface with time, even at room temperature.

When plotting or correlating the effects of strain rate and temperature on the strength or ductility of metals, it is useful to keep in mind the character of the engineering tensile stress-strain curve. A typical family of such curves is illustrated schematically in Figure 37. In this figure, the effective stress and strain may be defined as some appropriate functions of the scalar invariants. The individual stress-strain curves represent tests conducted under a combination of constant temperature and strain rate, designated by the parameter T^*. For instance, T^* could be defined by the usual thermal activation equations as $T^* = T \log (A/\dot{\epsilon}_{eff})$, similar to the Zener-Holloman parameter. The accessible region of this stress-strain plane is bounded on the left by some limiting curve, obtained at absolute zero temperature or very high strain rate ($T^* \rightarrow 0$). On the right, it is bounded by failure of the specimen. This is denoted as fracture if the inelastic strain is small or rupture if large amounts of plastic deformation precede complete failure (separation of the specimen).

The intermediate region is divided into three zones; elastic, stable plastic and unstable plastic. The boundary between the elastic and stable plastic region when plotted in stress space is the yield surface. The

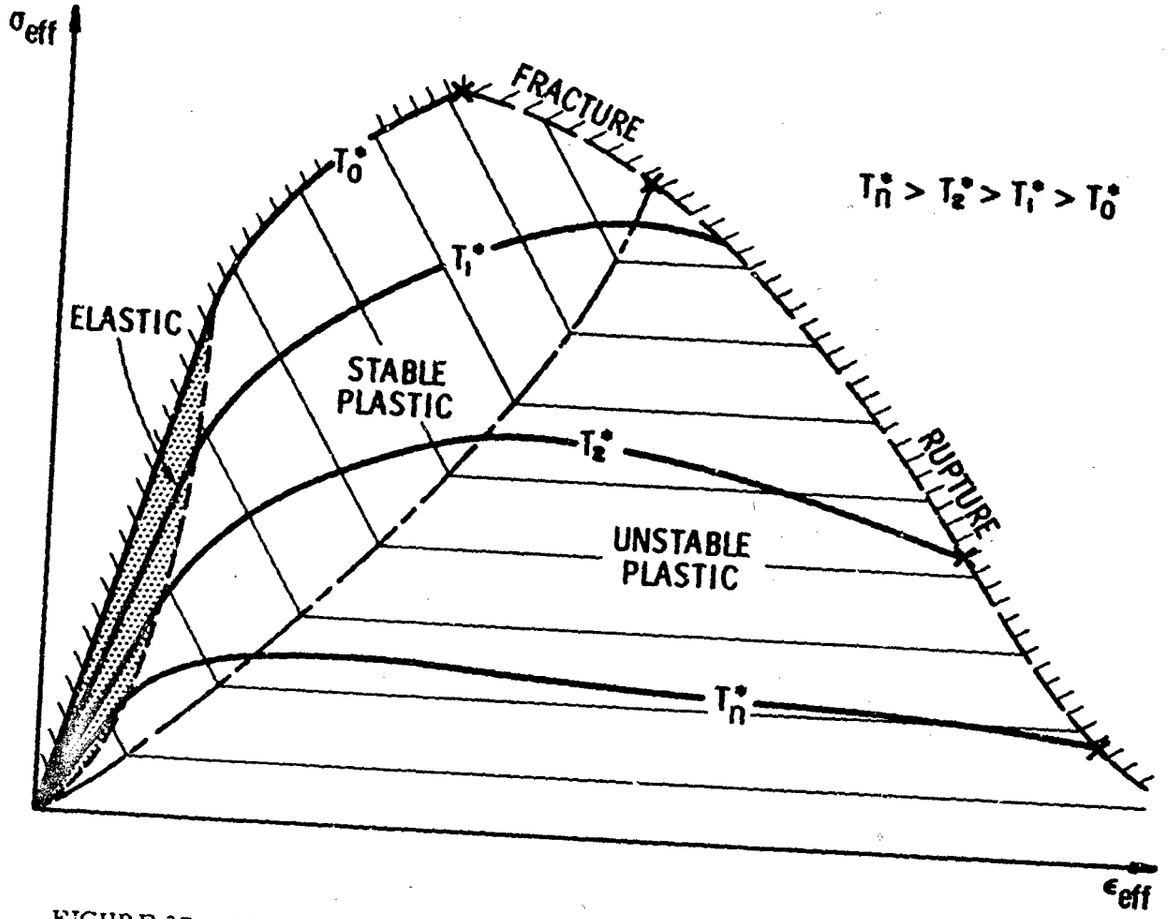

FIGURE 37. SCHEMATIC REPRESENTATION OF ELASTIC, STABLE PLASTIC AND UNSTABLE PLASTIC REGIONS IN STRESS-STRAIN SPACE

3035

boundary between stable plastic flow and unstable plastic flow is defined by a relative maximum in the engineering stress-strain curve. This point is the limit of uniform deformation of the specimen and is characterized by the development of localized plastic flow and necking. The boundary between stable and unstable plastic flow will intersect the fracture boundary for some value of T^*. Therefore, depending upon the value of T^*, the ultimate strength may correspond to either the stress at fracture or to a maximum in the stress-strain curve. For beryllium at 70°F, fracture generally occurred before instability. At higher temperatures, depending upon the strain rate, failure generally occurred after a maximum stress had been reached.

In a uniaxial tensile test the boundary for stable plastic flow is determined from the strain-hardening curves in the stable region. Thus, if the true flow stress, $\bar{\sigma}$, in tension is a unique function of the true strain, $\bar{\epsilon}$, strain rate, $\dot{\bar{\epsilon}}$, and temperature, T, the stability boundary is given[15] by

$$\frac{\partial \bar{\sigma}}{\partial \bar{\epsilon}} + \frac{\partial \bar{\sigma}}{\partial \dot{\bar{\epsilon}}} \frac{d\dot{\bar{\epsilon}}}{d\bar{\epsilon}} + \frac{\partial \bar{\sigma}}{\partial T} \frac{dT}{d\bar{\epsilon}} = \bar{\sigma}(\bar{\epsilon}, \dot{\bar{\epsilon}}, T)$$

For constant strain rate and temperature, the well-known relation

$$\frac{d\bar{\sigma}}{d\bar{\epsilon}} = \bar{\sigma}(\bar{\epsilon})\Big|_{\dot{\bar{\epsilon}}, T}$$

is obtained. The boundary may not always have the positive slope as shown in Figure 37. Campbell[16], in fact, finds the boundary slopes in the opposite direction for mild steel over a certain range in strain rate. Appropriate stability criteria for multiaxial stress tests can be constructed based upon an assumption of an appropriate flow rule.

For both beryllium and titanium, there was a marked effect of the applied stress ratio on the total strain to failure. Therefore, for tests under combined stress, a single failure boundary as drawn in Figure 37 may not be applicable. The mechanisms controlling failure of the test specimen may have a quite different dependence upon the stress state, strain rate and temperature than do those controlling plastic flow. However, from an empirical point of view, it is common practice to employ the same form of stress criteria for failure as for yielding.

The relative change from brittle to ductile behavior with stress orientation for both beryllium and titanium has previously not been well demonstrated because of the lack of biaxial stress testing. Uniaxial tests

along principal material axes alone may not be sufficient to predict the amount of plasticity or ductility available under combined stress. For the materials tested, the condition of biaxial tension would appear to be the most critical from the standpoint of reduced ductility. This should be taken into account in structural applications where some ductility is required.

The present tests also confirm the transition from brittle to ductile behavior with increasing temperature. Increasing the strain rate has the effect of shifting the transition to higher temperatures as has previously been noted for beryllium and other metals.

SECTION VI.

CONCLUSIONS

The work presented may be summarized by a few general conclusions.

1. The equipment and techniques developed make possible controlled multiaxial stress testing at temperatures up to 2000°F and strain rates to 1 sec^{-1}. Much higher uniaxial strain rates can be achieved.

2. The yield surface for S-200E, hot-pressed block beryllium can be described by an isotropic Mises yield criteria. The yield surface contracts isotropically with increasing temperature. The failure surface at 70°F is anisotropic but can be described by a single quadratic expression in the three stress components of the type proposed by Hoffman.

3. The S-200E extruded beryllium is essentially brittle in the σ_L, σ_T plane and ductile in the σ_L, σ_{LT} plane at 70°F. The fracture stress in the σ_L, σ_T plane is described by the St. Venant maximum normal strain criteria for brittle materials. Yield and failure in the σ_L, σ_{LT} plane can be described by anisotropic quadratic expressions in stress. At elevated temperature there appears to be a greater reduction in strength in the longitudinal direction than in shear. The effect of increasing strain rate is an isotropic increase in the size of the yield surface.

4. The ductility of both forms of beryllium and of the 6Al -4V titanium was found to be highly dependent upon the orientation of the stress at 70°F. In comparison with the uniaxial tensile ductility, increased ductility was found in torsion and in the stress direction of equal biaxial tension and compression ($\sigma_T/\sigma_L = -1$). On the other hand, reduced ductility (as measured by total elongation at fracture) was found in the tension-tension quadrant.

5. The ductility of beryllium increased greatly with increasing temperature, although at slow rates a ductility maximum is observed around 700°F. As the testing speed is increased the brittle to ductile transition is shifted in the direction of higher temperatures.

6. At temperatures up to 600°F, the highly anisotropic extruded beryllium fractured simultaneously on two cleavage surfaces oriented at $\pm$ 62° to the longitudinal tensile axis. These fractures are assumed to be parallel to $\{11\bar{2}0\}$ plane positions with the extrusion having $\langle 10\bar{1}0 \rangle$ texture with the basal planes oriented parallel to the surface. The fractures in the hot-pressed block were oriented in a direction normal to the maximum principal tensile stress.

SECTION VII.

REFERENCES

1. U. S. Lindholm, L. M. Yeakley and R. L. Bessey, "An Investigation of the Behavior of Materials Under High Rates of Deformation" AFML-TR-68-194, (1968).

2. R. G. Kumble, F. L. Schierloh, S. G. Babcock, "Mechanical Properties of Beryllium at High Strain Rates", SAMSO TR-68-71 Vol. VI. (1968).

3. F. L. Schierloh and S. G. Babcock, "Tensile Properties of Beryllium at High Strain Rates and Temperatures" AFML-TR-69-273 (1969).

4. U. S. Lindholm and L. M. Yeakley, "A Dynamic Biaxial Testing Machine", Exp. Mechs. 7, 1, (1967).

5. U. S. Lindholm "Some Experiments in Dynamic Plasticity Under Combined Stress" in MECHANICAL BEHAVIOR OF MATERIALS UNDER DYNAMIC LOADS, Springer-Verlag New York, Inc. (1968).

6. B. King "Mechanical Properties" Chapter 7 in BERYLLIUM: ITS METALLURGY AND PROPERTIES, H. Hausner, Ed., U. Cal. Press (1965).

7. G. L. Tauer and A. R. Kaufmann, "Ductility of Beryllium as Related to Single Crystal Deformation and Fracture" THE METAL BERYLLIUM, D. W. White and J. E. Burke, Eds., ASM (1965).

8. R. Hill, PLASTICITY, Oxford University Press, 1956.

9. O. Hoffman "The Brittle Strength of Orthotropic Materials" J. Composite Materials, 1, 200 (1967).

10. R. W. Fenn, D. D. Crooks and W. C. Kinder, "Test Methods for Evaluating the Properties of Anisotropic Materials (Beryllium)" AFML-TR-68-373 (1969).

11. D. W. Lillie "The Physical and Mechanical Properties of Beryllium Metal" in THE METAL BERYLLIUM, D. W. White and J. E. Burke , Eds., ASM (1965).

12. B. Paul "Macroscopic Criteria for Plastic Flow and Brittle Fracture" in FRACTURE, Vol. II, H. Liebowitz, Ed., Academic Press (1968).

13. J. J. Blass and W. N. Findley, "Short Time Biaxial Creep of an Aluminum Alloy With Abrupt Changes of Temperature and State of Stress" J. Appl. Mechs. (to appear).

14. S. Smith and B. O. Almroth, "An Experimental Investigation of Plastic Flow Under Biaxial Stress" Exp. Mechs., 10, 217, (1970).

15. J. Klepaczko "Generalized Conditions for Stability in Tension Tests" Int. J. Mech. Sci., 10, 297, (1968).

16. J. D. Campbell "Plastic Instability in Rate-Dependent Materials" J. Mech. Phys. Solids, 15, 359, (1967).

APPENDIX A

STRESS-STRAIN CURVES
(Uniaxial Button-Head Specimens)

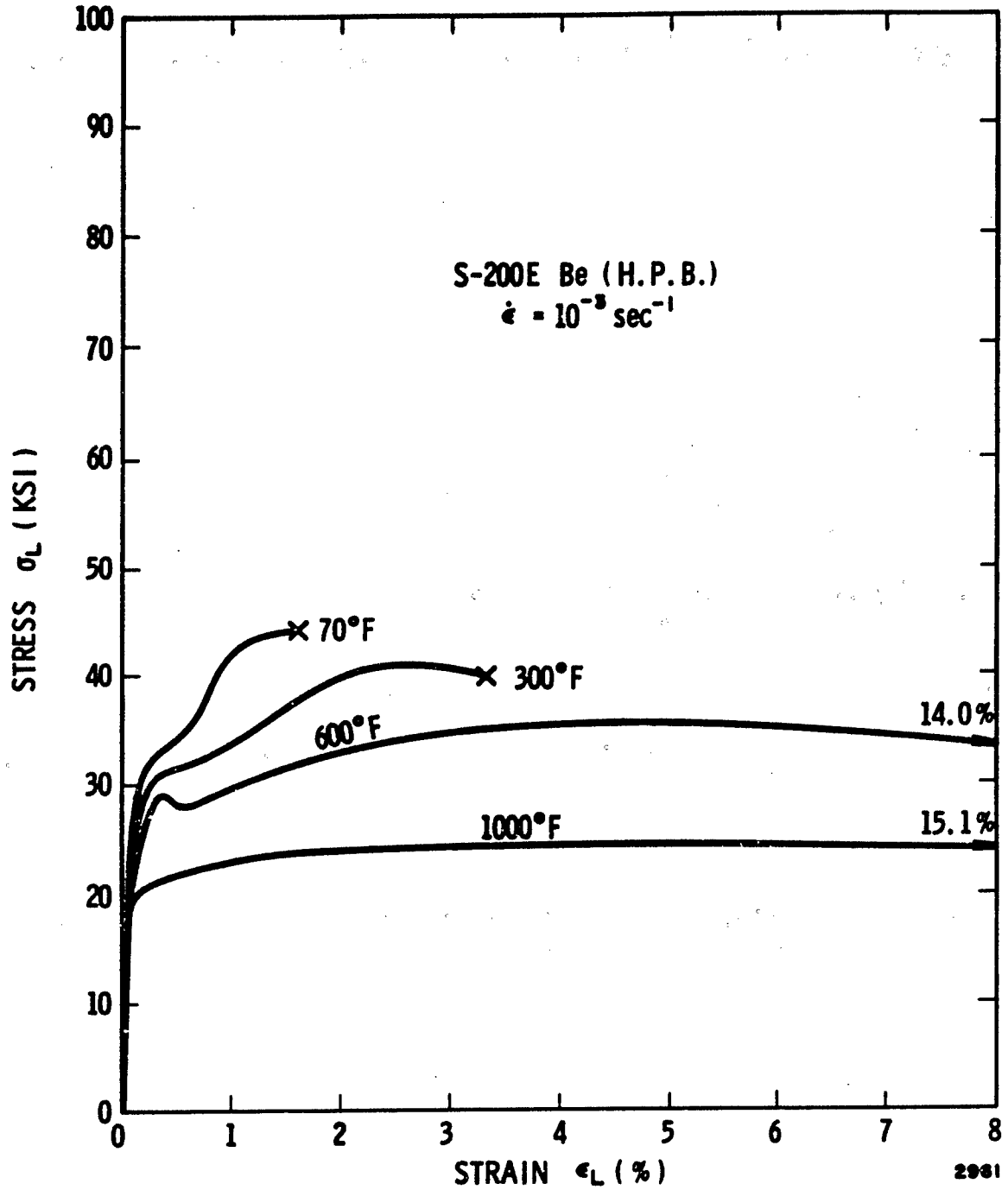

FIGURE 38. TENSION TESTS OF HOT-PRESSED BLOCK BERYLLIUM, LONGITUDINAL DIRECTION AT 10^{-3} SEC^{-1}

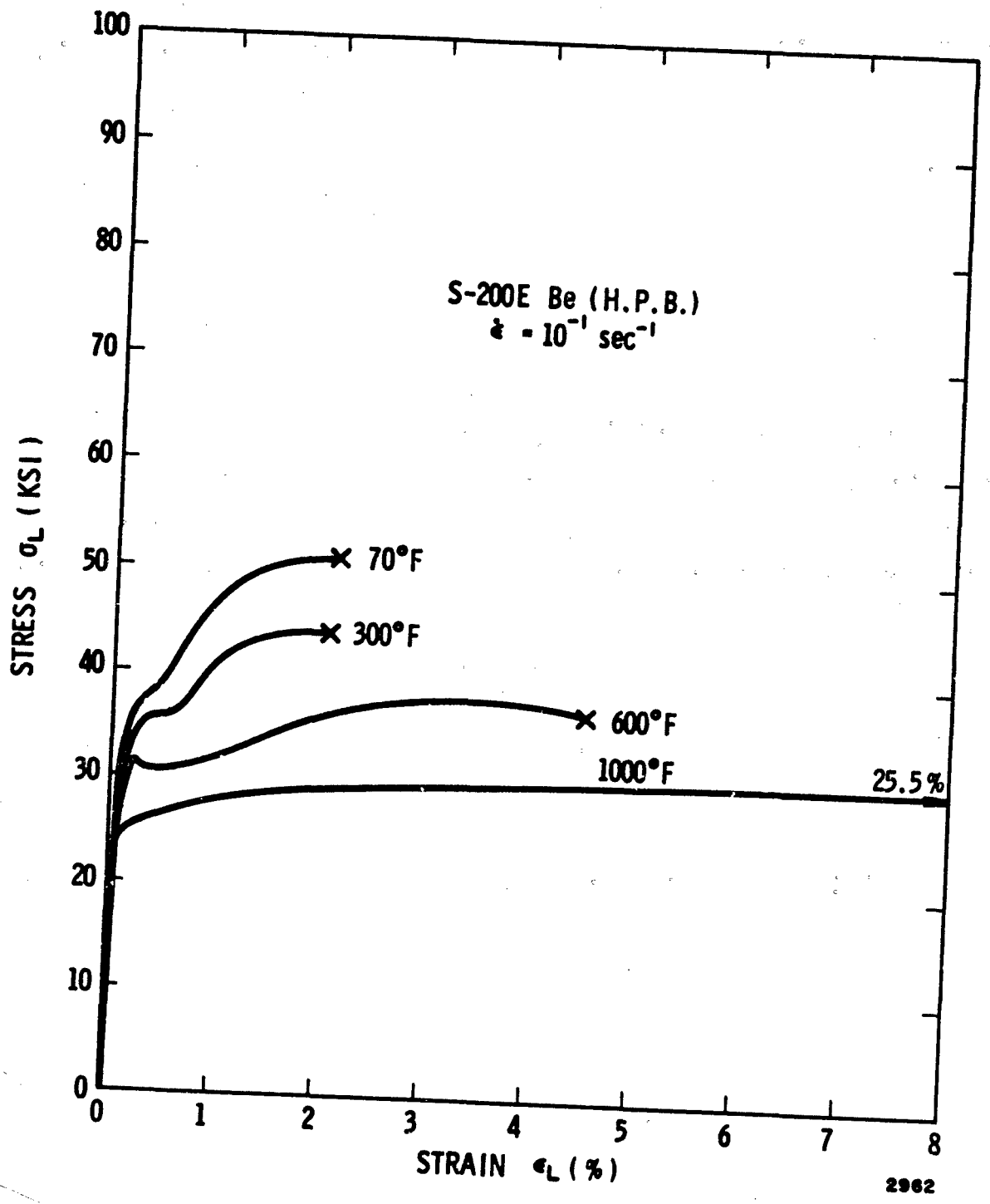

FIGURE 39. TENSION TESTS OF HOT-PRESSED BLOCK BERYLLIUM, LONGITUDINAL DIRECTION AT 10^{-1} SEC^{-1}

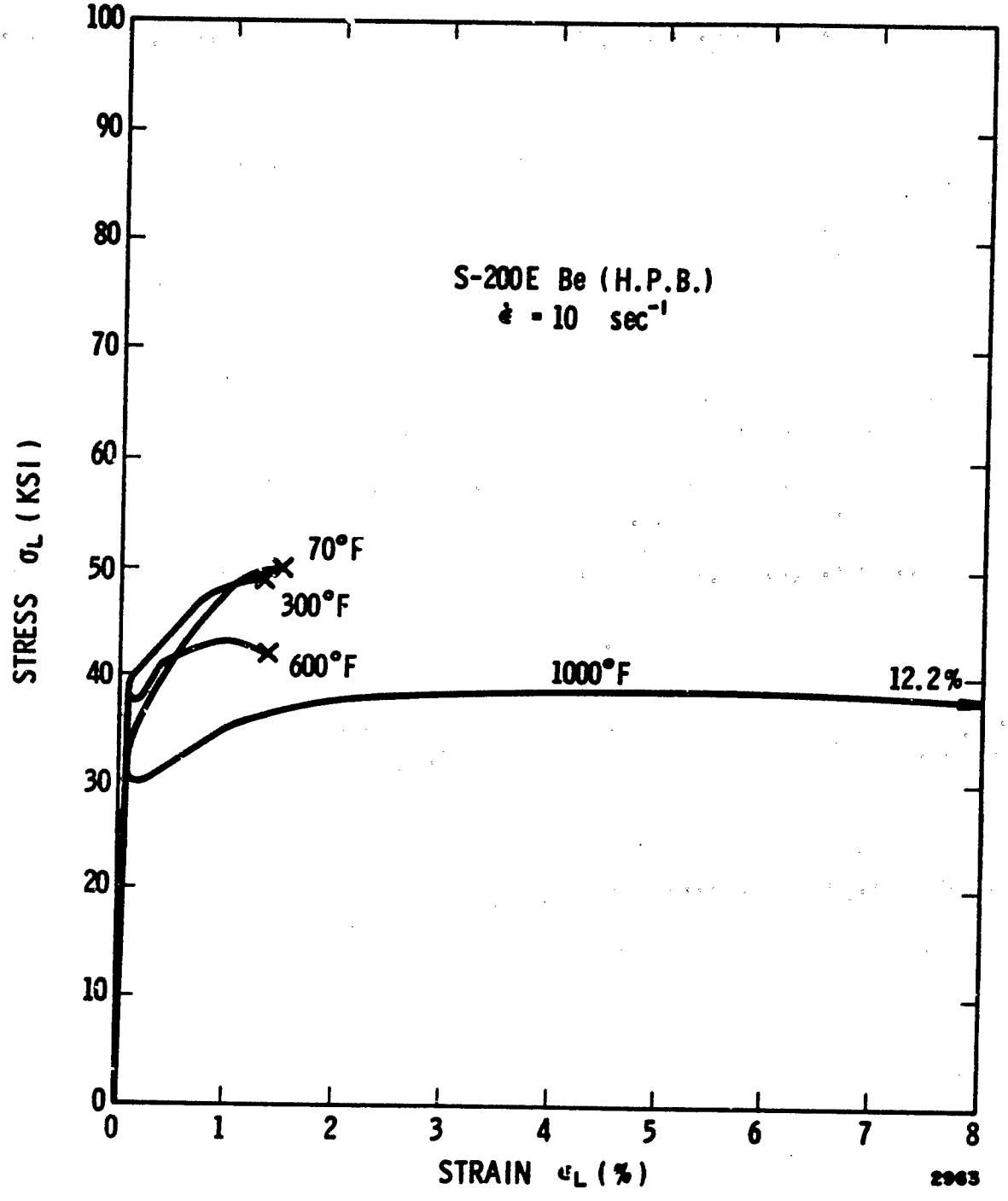

FIGURE 40. TENSION TESTS OF HOT-PRESSED BLOCK BERYLLIUM, LONGITUDINAL DIRECTION AT 10 SEC^{-1}

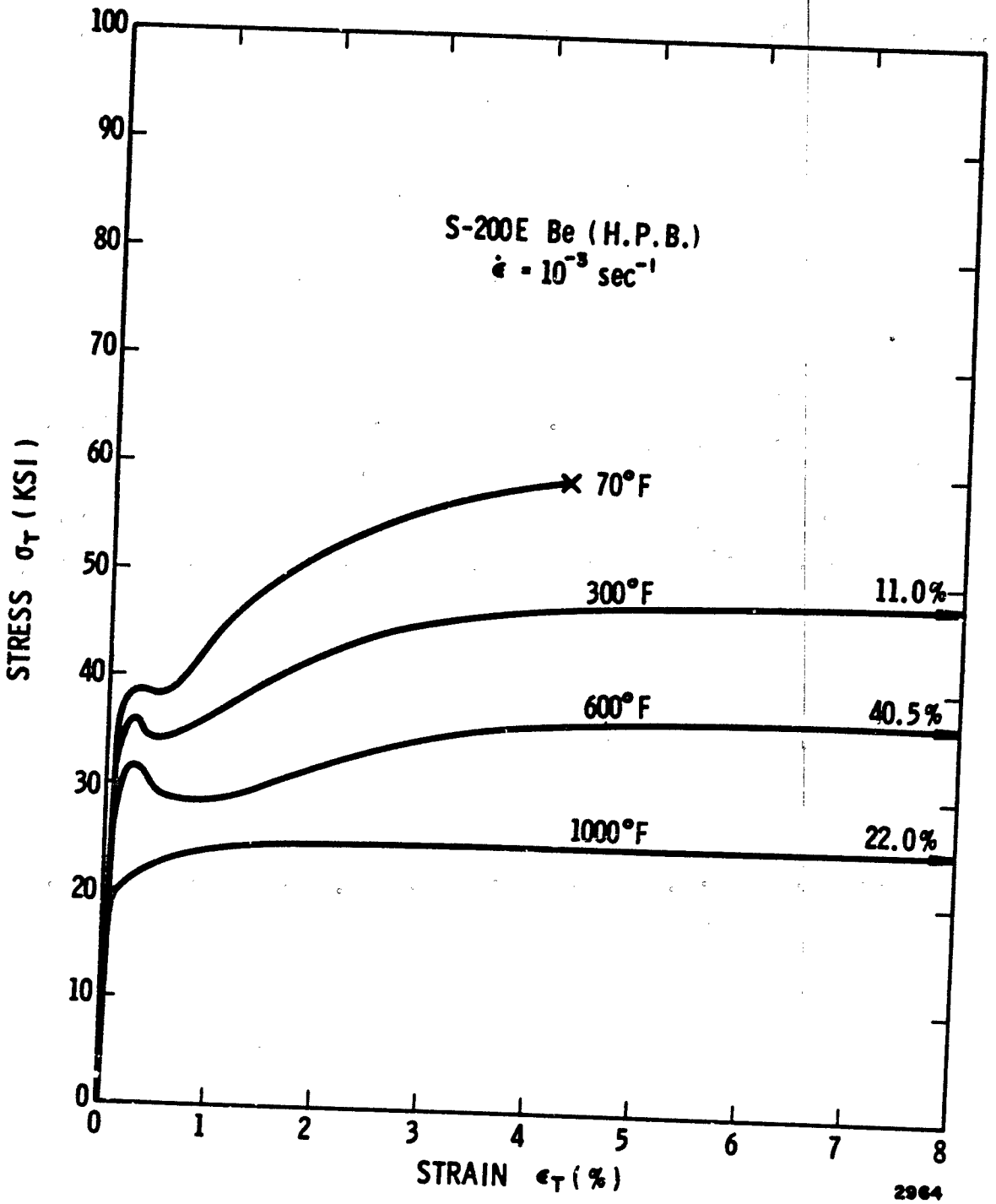

FIGURE 41. TENSION TESTS OF HOT-PRESSED BLOCK BERYLLIUM, TRANSVERSE DIRECTION AT 10^{-3} SEC^{-1}

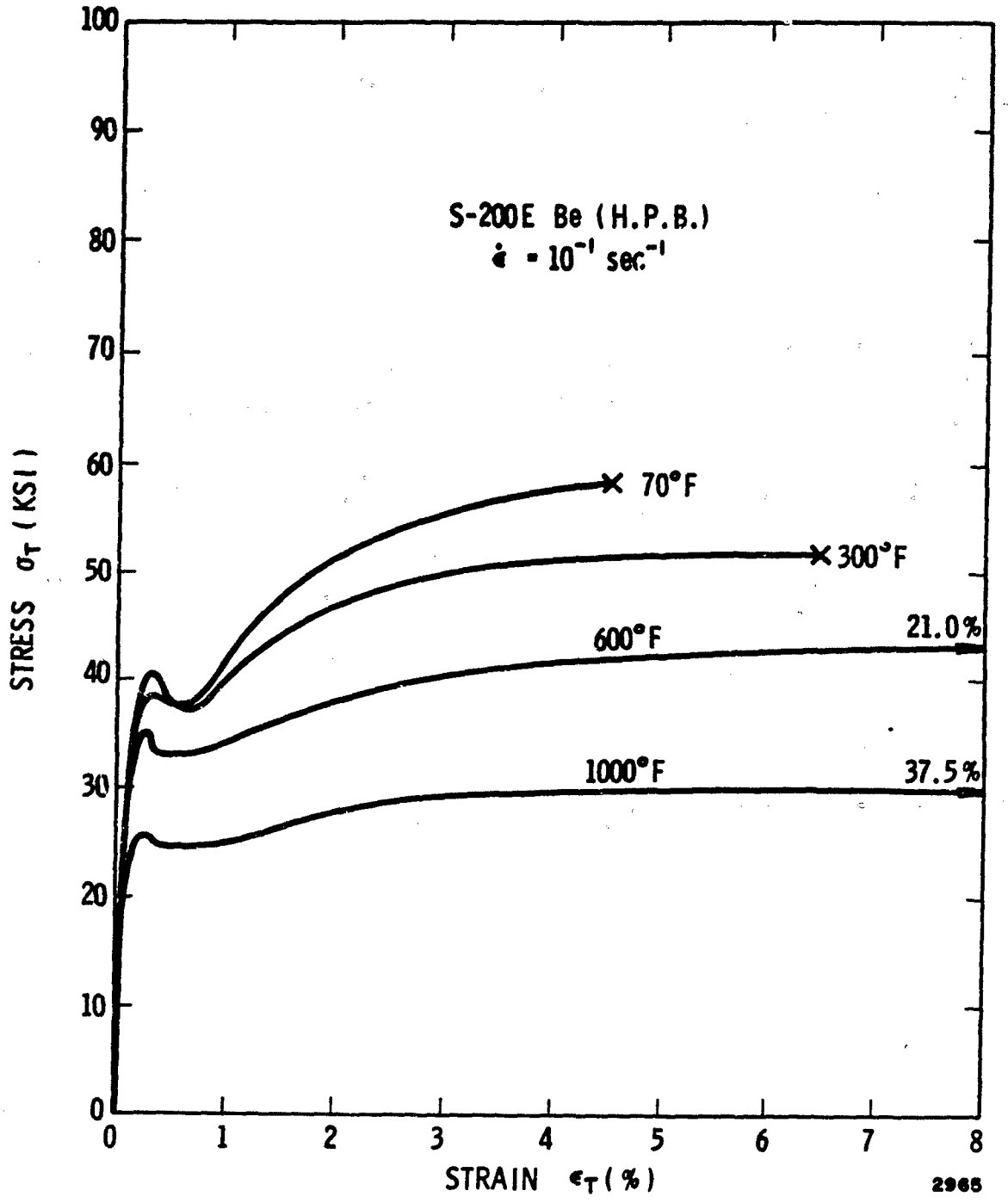

FIGURE 42. TENSION TESTS OF HOT-PRESSED BLOCK BERYLLIUM, TRANSVERSE DIRECTION AT 10^{-1} SEC^{-1}

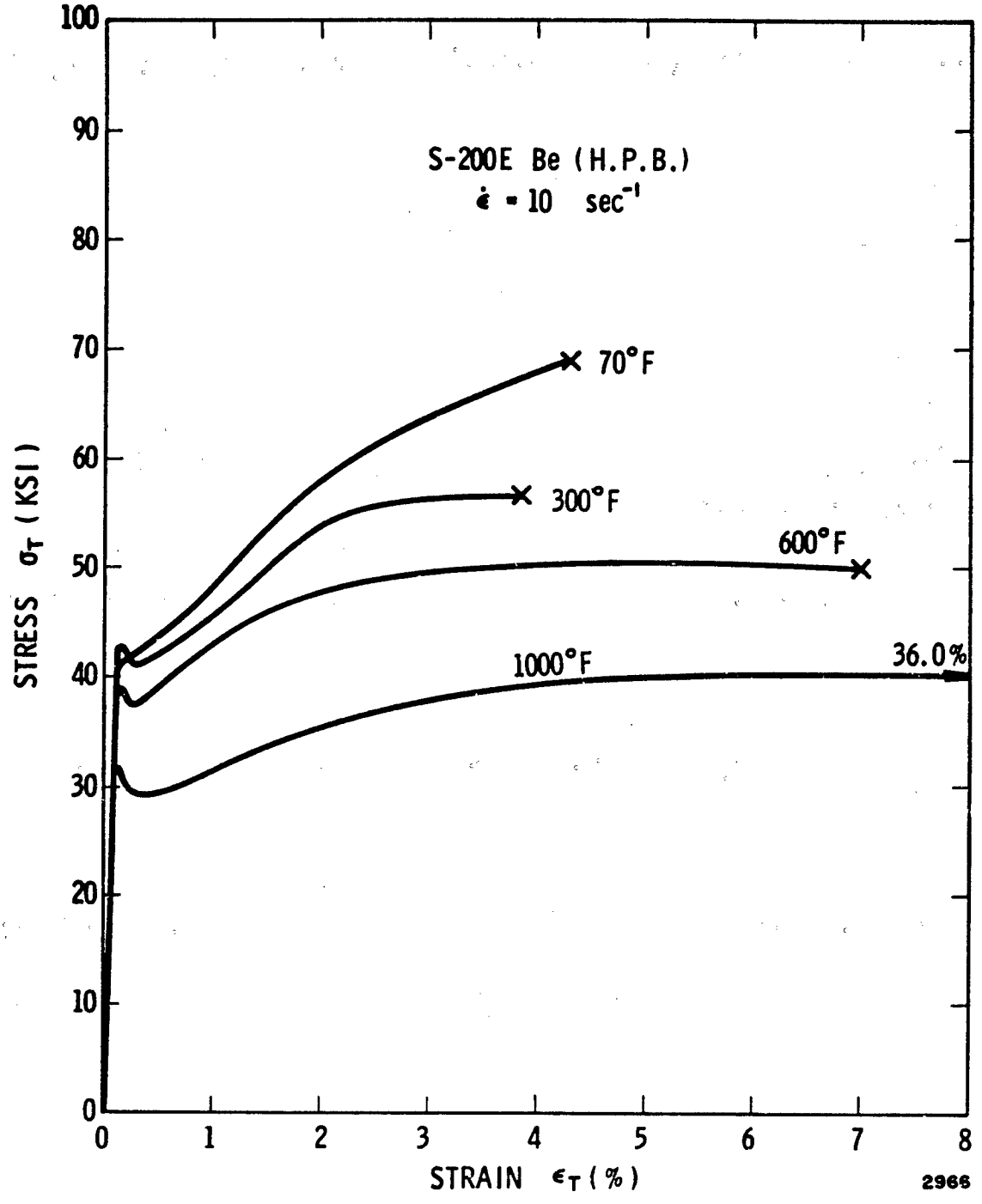

FIGURE 43. TENSION TESTS OF HOT-PRESSED BLOCK BERYLLIUM, TRANSVERSE DIRECTION AT 10 SEC^{-1}

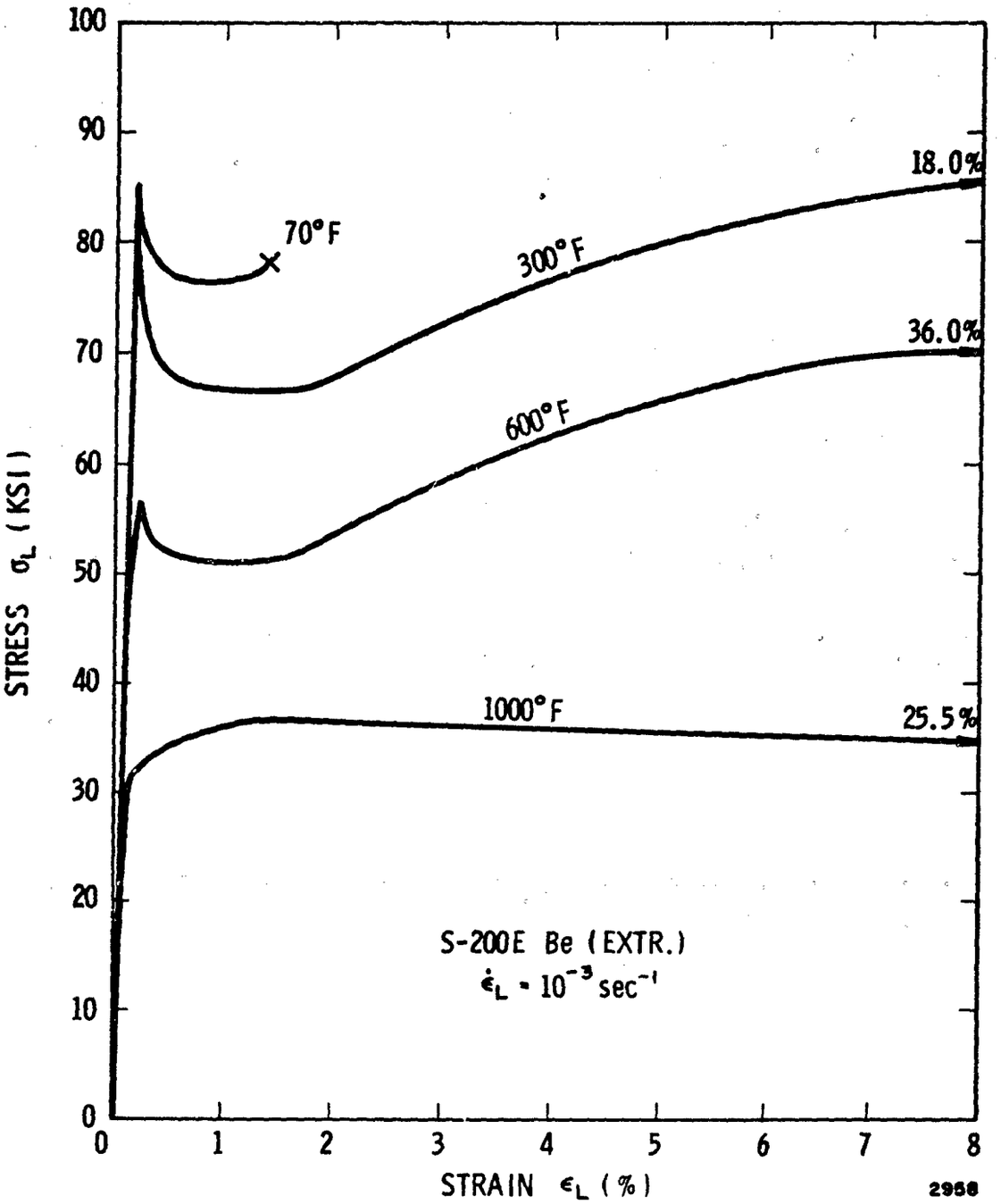

FIGURE 44. TENSION TESTS OF EXTRUDED BERYLLIUM AT 10^{-3} SEC^{-1}

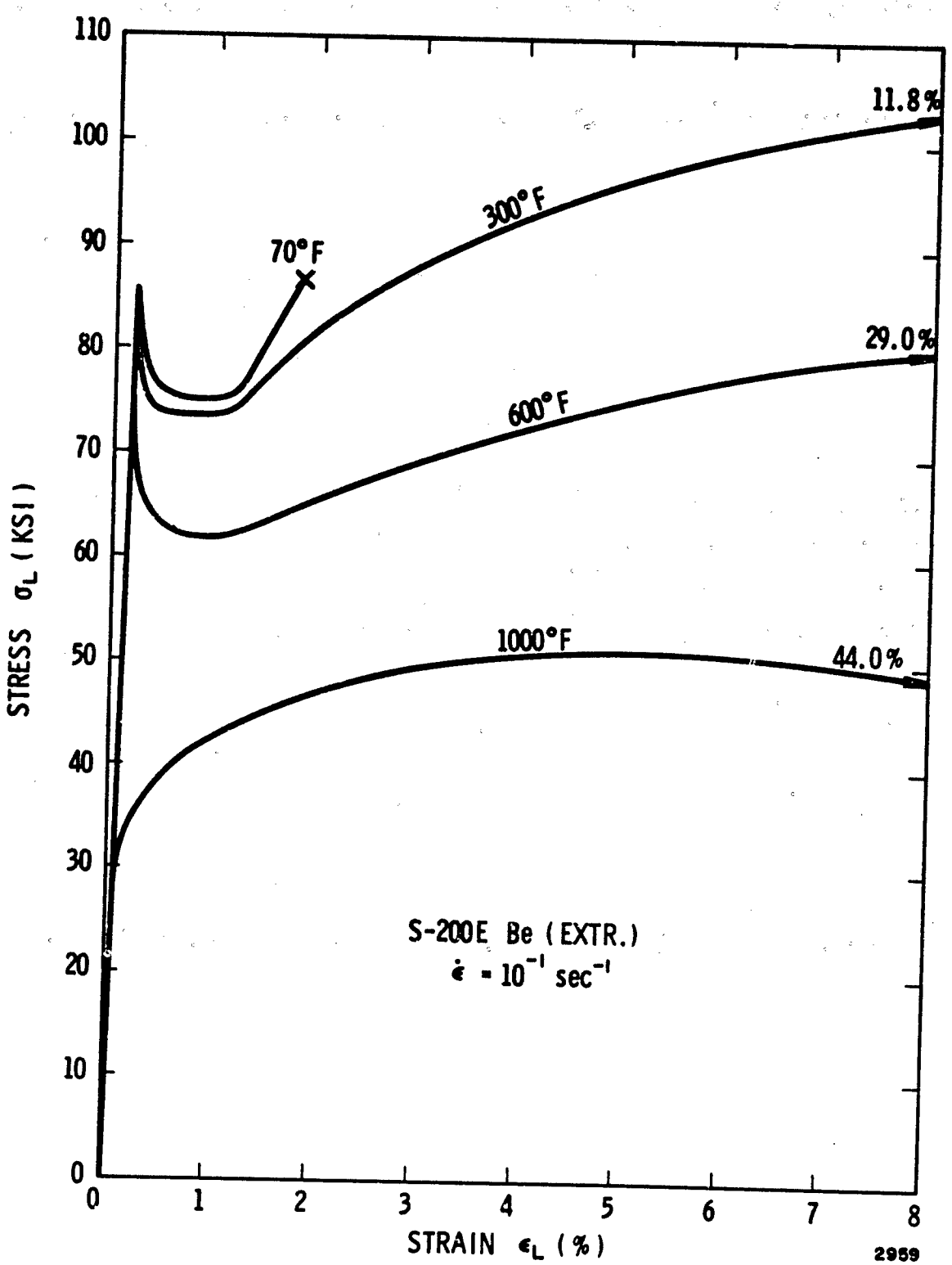

FIGURE 45. TENSION TESTS OF EXTRUDED BERYLLIUM AT 10^{-1} SEC^{-1}

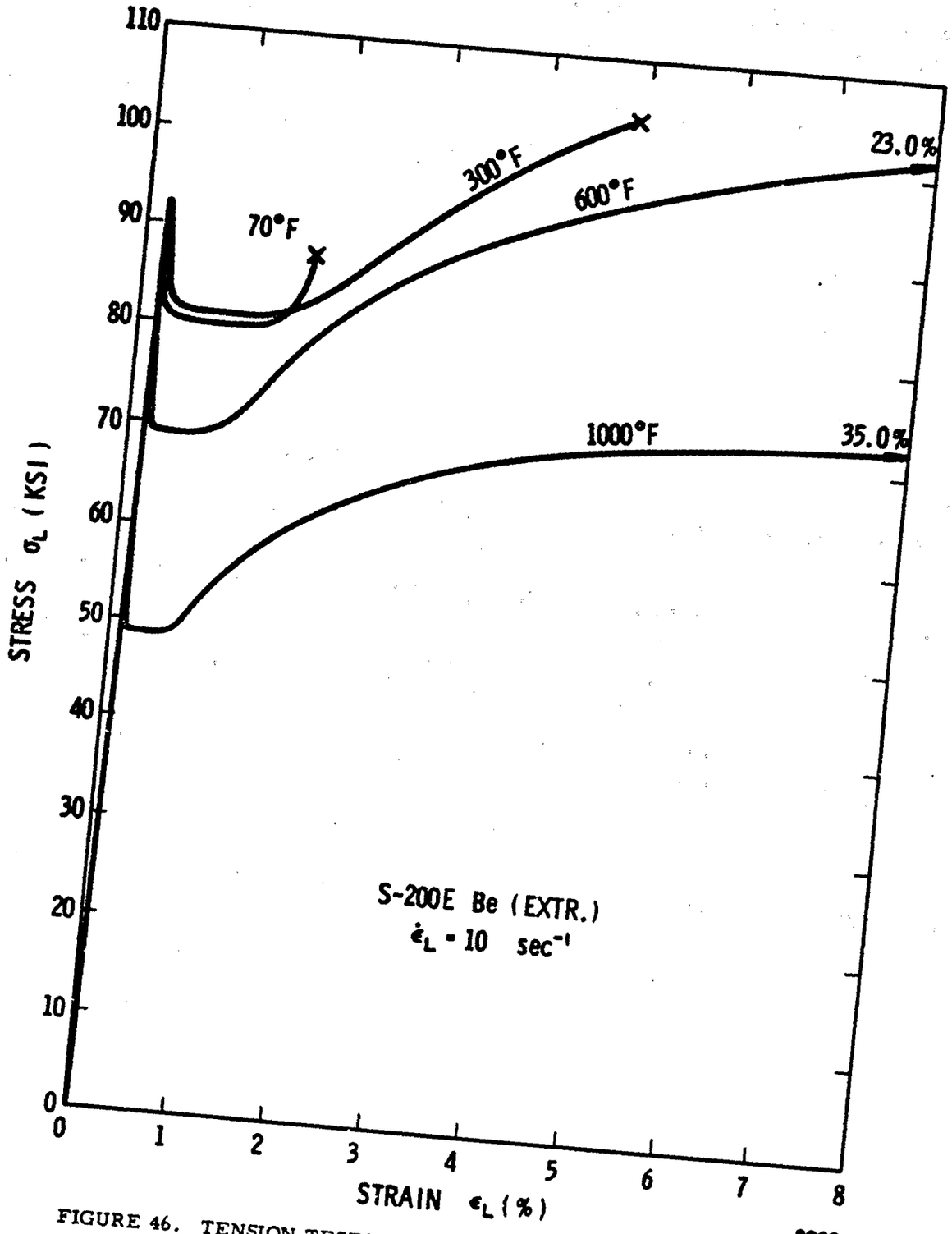

FIGURE 46. TENSION TESTS OF EXTRUDED BERYLLIUM AT 10 SEC^{-1}

APPENDIX B

STRESS-STRAIN CURVES
(Biaxial Tube Specimens)

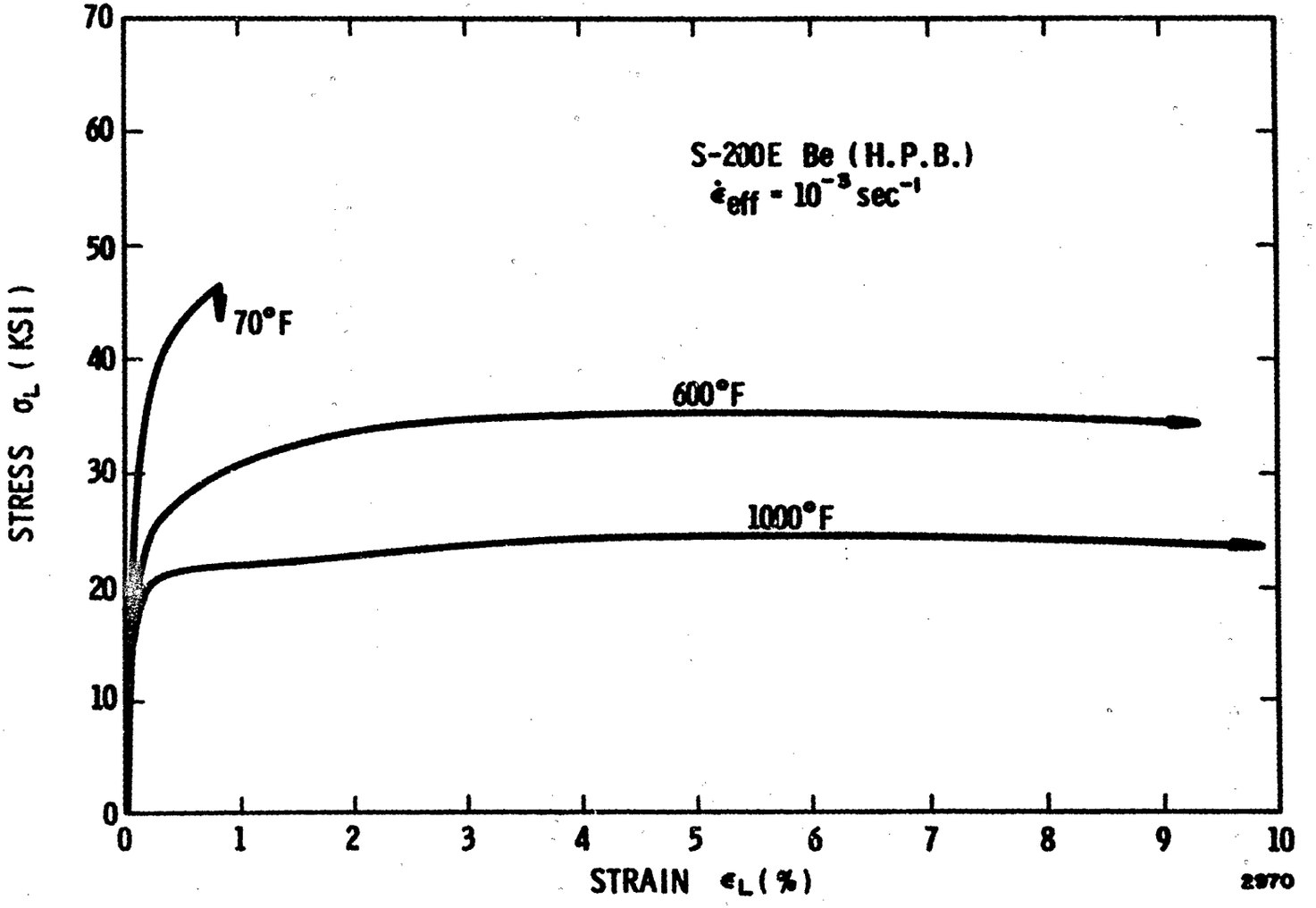

FIGURE 47. TENSION TESTS OF HOT-PRESSED BLOCK BERYLLIUM SPECIMENS AT 10^{-3} SEC^{-1} (TUBES)

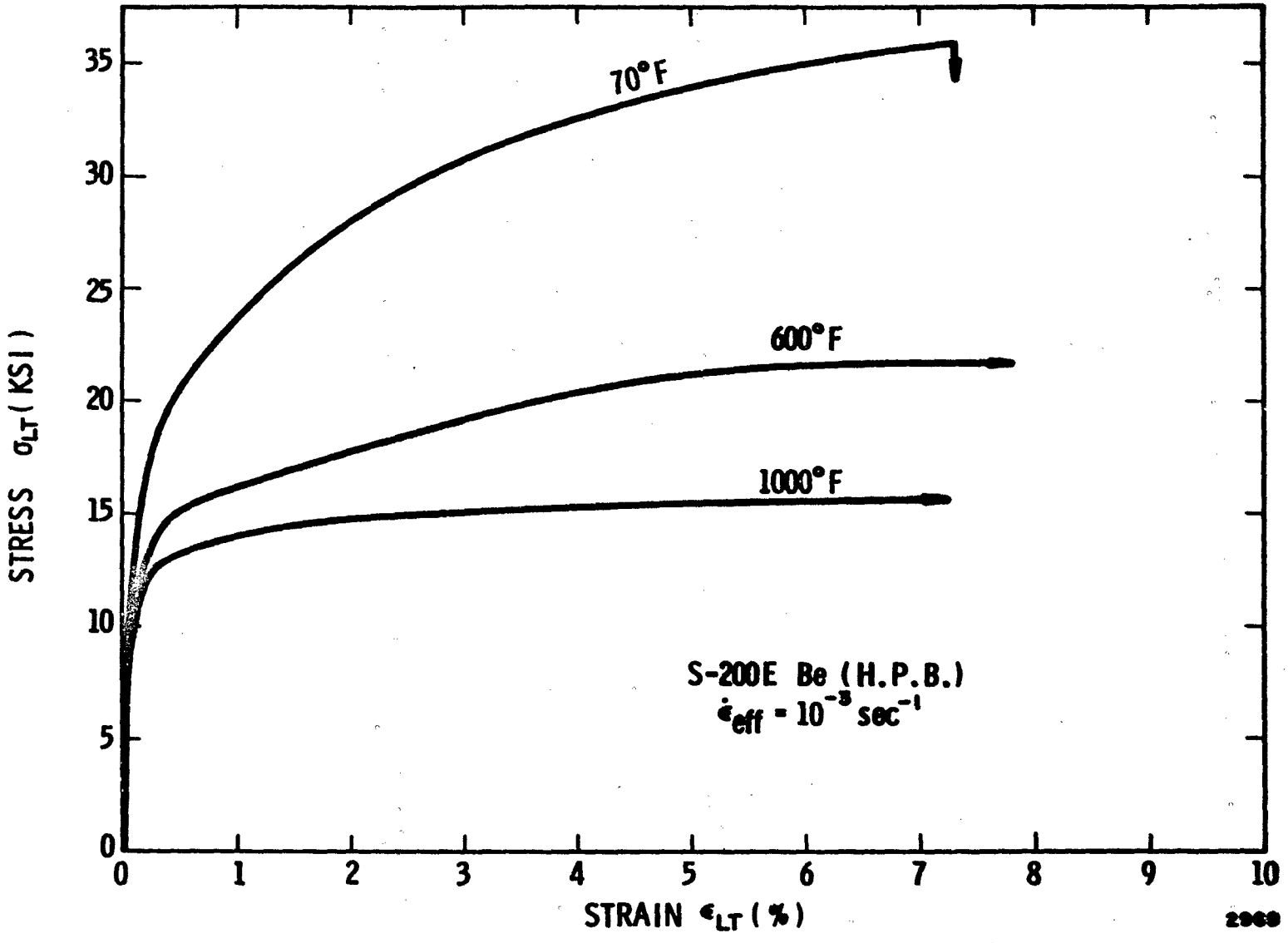

FIGURE 48. TORSION TESTS OF HOT-PRESSED BLOCK BERYLLIUM SPECIMENS AT 10^{-3} SEC^{-1} (TUBES)

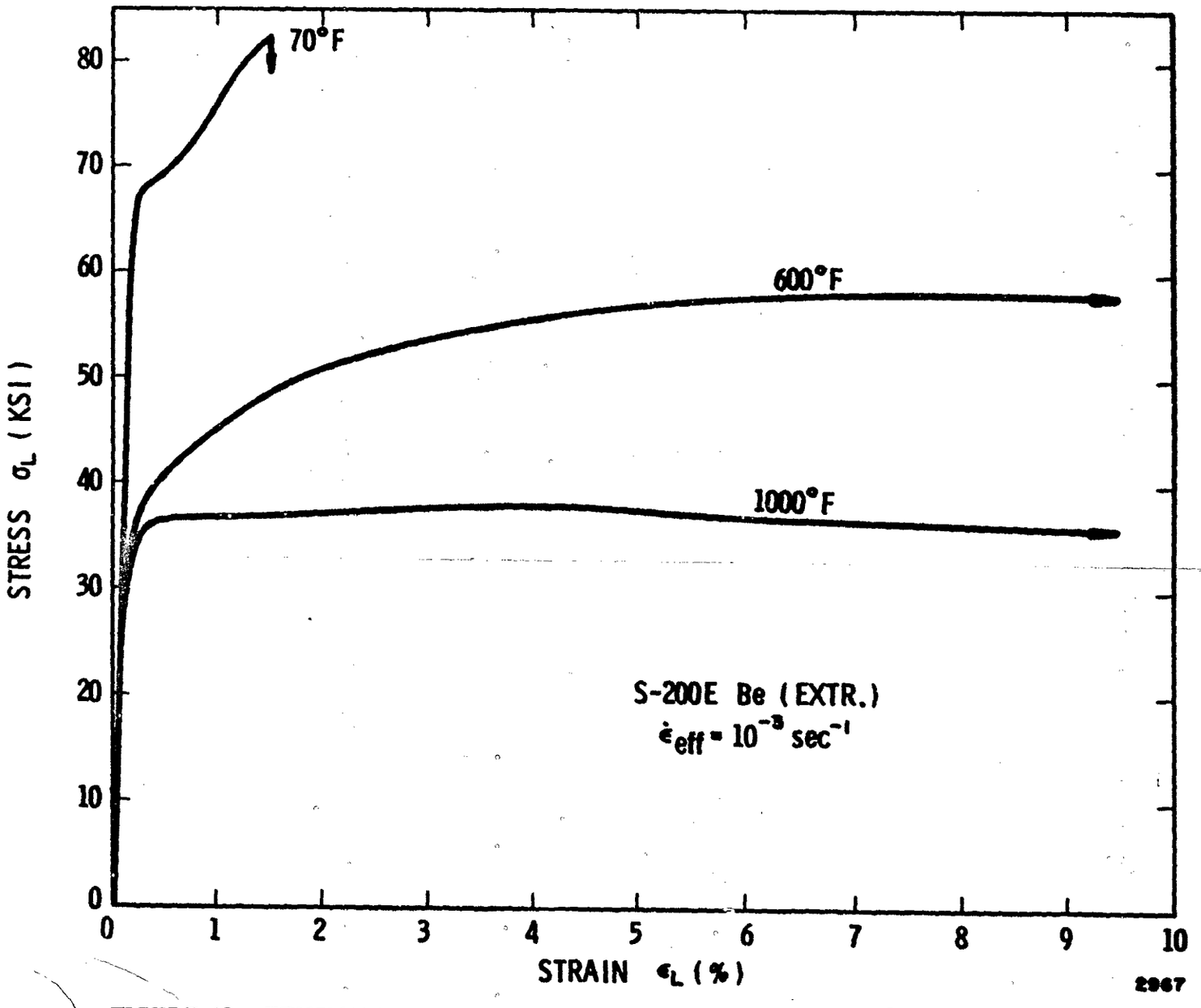

FIGURE 49. TENSION TESTS OF EXTRUDED BERYLLIUM AT 10^{-3} SEC^{-1} (TUBES)

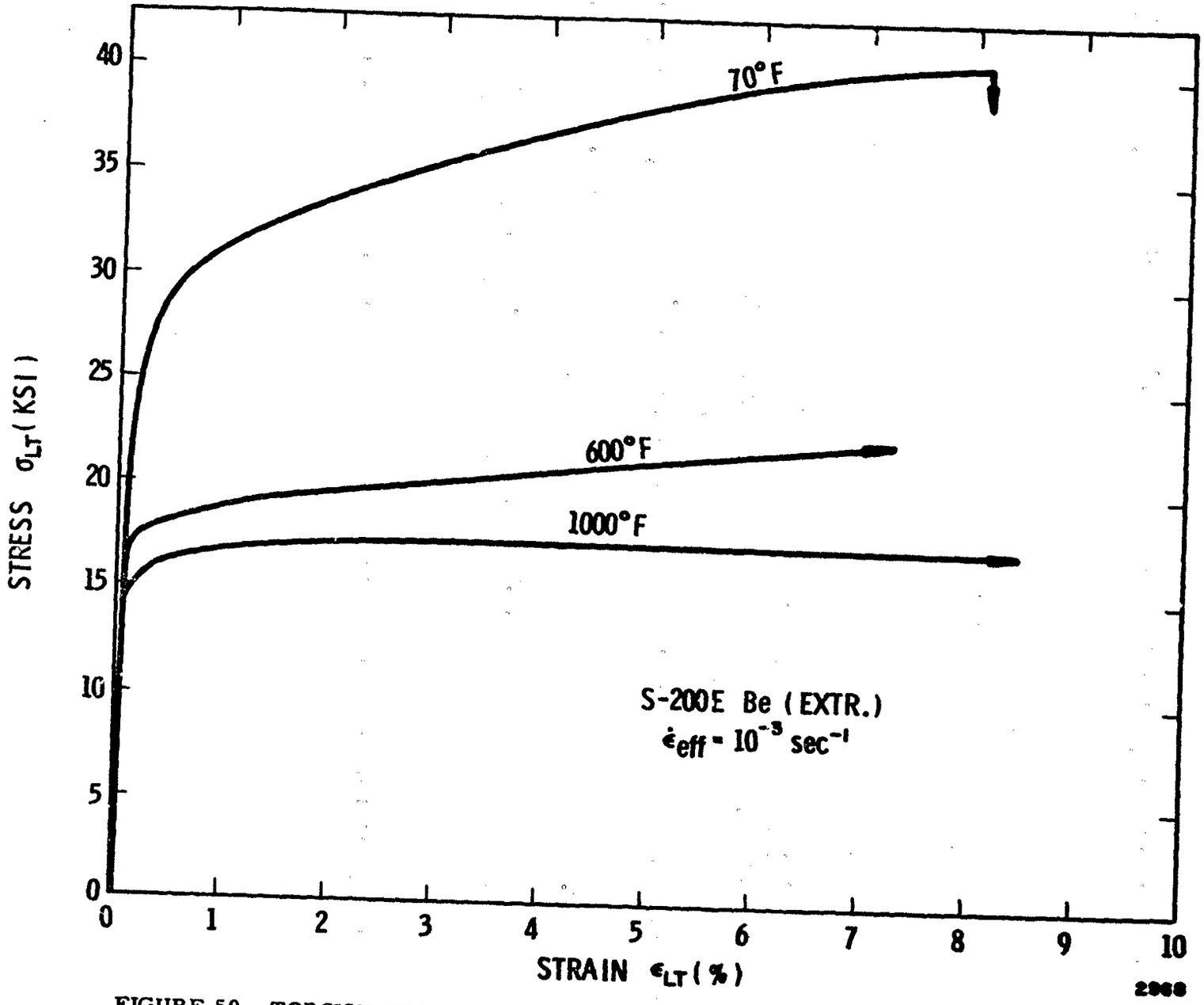

FIGURE 50. TORSION TESTS OF EXTRUDED BERYLLIUM AT 10^{-3} SEC (TUBES)